POLITECNICO DI TORINO

Corso di Laurea in
Ingegneria Aerospaziale

Tesi di Laurea Magistrale

Dynamic analysis of Carbon Nanotube-Reinforced Piezoelectric Composite for Active Control of Smart Structures

Supervisors:
prof. Fiorenzo Fazzolari
prof. Erasmo Carrera

Candidate:
Lorenzo Violi

Acknowledgements

I would like to thank Prof. Carrera who gave me the opportunity to carry out this research project abroad. I would like to say thank you to Prof. Fazzolari who provided me his consistent support for this work and for the willingness he has showed me during these months. A special thank you goes to Lorenzo Chianchiano who I had the pleasure to live with for 6 months and has always helped me when I was in trouble. I would like to thank my family who have always supported my choices these years. Last but not least, I'd like to thank my friends who have always been close to me.

Contents

List of Figures

List of Tables

Summary

Smart structures have a wide range of potential applications in aerospace engineering, such as vibration and noise suppression, shape adaption and aeroelastic control of lifting surfaces. Piezoelectric materials are largely used as smart materials due to the their capability to perform both as sensors and actuators. Composite structures embedded with piezoelectric materials confer the low density, superior mechanical and thermal properties of composite materials along with sensing and vibration control.
The aim of this thesis is the study of the dynamic behaviour and vibration attenuation of carbon nanotube reinforced composite (CNT-RC) plates, integrated with piezoelectric layers at the bottom and top surfaces. Distribution of CNTs reinforcement may be uniformly distributed (UD) or functionally graded (FG) according to linear functions of the thickness direction. The material properties of both matrix and CNTs are obtained through a modified rule of mixtures approach. Plate is modeled acccording with the method of the power series expansion of the displacement components and the electric potential. Primary variable's expansion order is considered as a free parameter of the model. Hamilton's principle is employed to derive the governing equations in their weak form. The latter are written in terms of fundamental nuclei which are mathematically invariant with respect to both the expansion order and the kinematic description of the unknows. The free vibration analysis is carried out considering the full coupling between the electrical and mechanical fields. The approximated solution is obtained by using Ritz method based on highly stable trigonometric trial functions. Forced response is obtained through the Newmark method considering various dynamic load cases. The response of the plate is controlled through the dynamic velocity feedback control algorithm and a closed loop. The upper piezoelectric layer acts as actuators, while the lower one acts as sensors.
Corvengence and accurancy of the proposed formulation is investigated comparing results with those available in literature. The effect of significant parameters such as volume fraction, CNTs distribution and boundary conditions, on the natural frequencies and both uncontrolled and controlled response, is discussed.

Chapter 1

Introduction

1.1 Composite structures and their applications

In the last few decades the development of composite materials in structural applications has dramatically risen. Composite materials consist of a combination of two or more materials that are mixed together in order to reach specific structural properties or give a new set of charateristics that neigther single costituents could achieve on their own. Laminated composites, that show anisotropic properties, have completely changed the methodology of design and made possible a wide range of new possibilities as materials for construction. Composites have become especially attractive in the aerospace and aircraft sectors because of their outstanding strength and stiffness-to-density ratios, corrosion resistance and superior physical properties compared to traditional isotropic materials. In fact, Fibre reinforced plastics (CFRP) can and will in the future contribute more than 50% of the structural mass of an aircraft [1]. As well as traditional composites, the so-called smart structures has been developed in the last years, due to their potential applications in aerospace industry, such as: monitoring of composites, suppression of structural vibration, noise suppression, and surface morphing. An overview of several structures and their appications, that are the aim of study in this thesis, is described in this chapter.

1.1.1 Multilayered structures

The most common composite structure is made of a fibrous material embedded in a resin matrix. For istance, Carbon fiber-reinforced plastic (CFRP) is a typical composite for structural applications in aerospace and automotive industries. Fibers are the primary load carrying elements, and the matrix material has the function of keeping the fibers together, acting as a load-transfer medium between fibers, and protecting fibers from the external environment. The composite material is strong and stiff only in the direction of the fibers. Geometrically, fibers have near crystal-sized diameter and a very high length-todiameter ratio. Constituents used in composites are either metallic or non-metallic. Fibers are commonly made of organic materials such as glass, boron, and graphite. Fiber-reinforced composites for structural applications are often made in the form of a thin layer, called lamina. A multilayerd plate is obtained by stacking uni-directional laminae until specific mechanical properties are reached. The stacking sequence describes the distribution of ply orientations through the laminate thickness. The lamination scheme and material properties of individual lamina provide an added flexibility to designers to tailor the stiffness and strength of the laminate to match the structural stiffness and strength requirements [2].

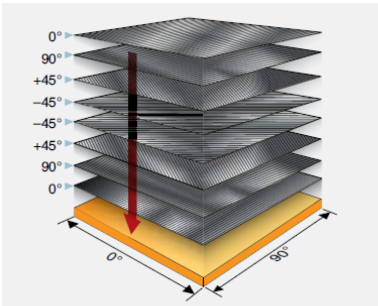

Figure 1.1: Typical Multilayered structure

1.1.2 Sandwich structures

A Sandwich structure is a special class of composite, obtained by bonding two thin and stiff face sheets to a lightweight and tick core. This kind of composite is especially suitable in order to develop a lightweight structure with high in-plane and flexural stiffness. Sandwich structures are used for producing boat hulls, car hoods and other body part, aircraft panels ecc. The core supports the faces against buckling and resists out-of-plane shear loads, while the skins carry all the bending and in-plane loads. Commonly used materials for facings are composite laminates and metals, while cores are made of metallic and non-metallic honeycombs, cellular foams, balsa wood and trusses. The overall performance of sandwich structures depends on the material properties of the constituents (facings, adhesive and core), geometric dimensions and type of loading.

1.1.3 Functionally Graded Materials

While laminated composite materials provide the design flexibility to achieve desirable stiffness and strength through the choice of lamination scheme, the anisotropic constitution of laminated composite structures often results in stress concentrations near material and geometric discontinuities that can lead to damage in the

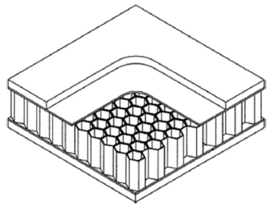

Figure 1.2: Typical Sandwich structure

form of delamination, matrix cracking, and adhesive bond separation. Functionally graded materials are a class of composite, consisting of two or more different constituents, designed to have a gradually varying spatial composition profile with a corresponding continuous change in macroscopic properties [7]. The continuous variation in properties of the material reduces thermal stresses, residual stresses, and stress concentration factors. The gradual variation results in a very efficient material tailored to suit the needs of the structure. FGMs are mainly constructed to operate in high-temperature environments such as ultra-light and temperature-resistant materials for space vehicles [9]. They are typically manufactured from isotropic components such as metals and ceramics as they are mainly used as thermal barrier structures in environments with severe thermal gradients [8]. The concept of functionally graded materials was introducted first in Japan in the 80s during a space project, in order to construct a thermal barrier capable of withstanding a surface temperature of 2000 K and a temperature gradient of 1000 K across a 10 mm section. Due to the high thermal stress, conventional thermal barrier coating can easily peel off at the phase boundary. FGM offers an advantage since the thermal stress distribution is smooth. The application of this new material is increased over the years in the aerospace industry. Most aerospace equipment and structures are made of functionally graded materials. These include, for istance, the rocket engine components, the turbine wheels and the turbine blade coatings.

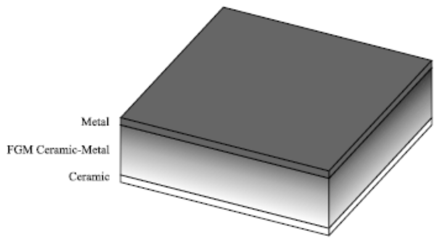

Figure 1.3: Multilayered plate embedding a FGM layer

1.1.4 Carbon-Nanotubes

Carbon nanotubes (CNTs) are allotropes of carbon with a cylindrical nanostructure. Nanotubes have been constructed as hollows with length-to-diameter ratio of up to 132 million, significantly larger than any other material. These cylindrical carbon molecules have unusual properties that are valuable for nanotechnology, electronics, optics, and structural applications. They are derived from the grapheme sheets which are rolled at specific and discrete chiral angles. The combination of the rolling angle and radius affect the nanotube properties. Carbon-nanotubes exhibit outstanding mechanical, thermal and electrical properties and they can be considered as a valid alternative to classical fiber reinforced composites. They have low density, high stiffness and strength aspect ratios [5]. It has been shown that CNTs are very strong in the axial direction: Young's modulus on the order of 270-950 GPa and tensile strength of 11-63 GPa [6]. Dispersion of low weight of graphene (0.02 wt.%) results in significant increases in compressive and flexural mechanical properties of polymeric nanocomposites. Referring to their electronic structure, they exhibit semiconducting, as well as metallic behavior and thus cover the full range of properties important for technology.

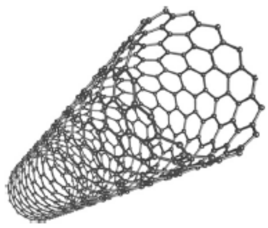

Figure 1.4: Single-walled Carbon nanotube

1.1.5 Piezoelectric materials

Research on piezoelectricity started in 1880 when Jaques and Pierre Curie discovered that some kind of crystals were able to generate electric charges under mechanical loads. A charge is generated when molecular electrical dipoles are caused by a mechanical loading: this is called the direct effect (sensor configuration). Conversely, when an electric charge is applied, a slight change occurs in the shape of the structure: that is called the inverse effect (actuator configuration). Thus, piezoelectric materials can be used at the same time as actuators and sensors, obtaining the so-called *self-sensing piezoelectric actuator* [3]. The most common piezoelectric materials are the piezoceramic barium titanate ($BaTiO_3$) and piezo lead zirconate titanate (PZT). The crystal lattice of piezoelectric materials is the face-centered cubic (FCC). Metallic atoms are located at the vertex of the cube, while oxygen atoms are located at the center of the faces. Due to the slightly shift of an havier atom to positions with less energy, the crystal lattice undergoes deformation. On the other hand, when an elctric field is applied to the structure, the central atom can exceed the potential energy and move to a lower energy configuration. The rupture of symmetry causes the generation of an electric dipole as shown in Figure 1.5.

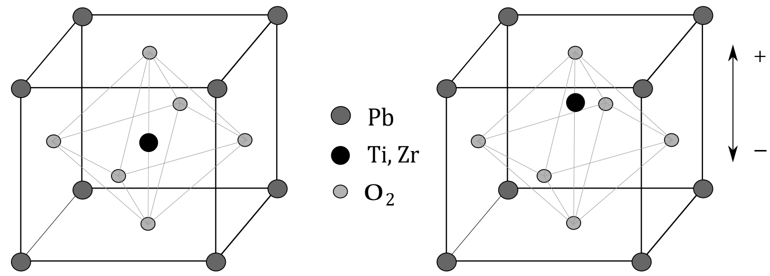

Figure 1.5: Piezoceramic cell before and after polarization

This phenomenon occurs only when piezoeletric material has a temperature lower than the so called *Curie temperature*. In fact, due to high thermal agitation the piezoelectric effect disappears. To obtain the piezoelectric effect, piezoceramic material must be subjected to a poling process: It is heated above the Curie temperature and then subjected to an intense electric field during thermal cooling. So all the dipoles are oriented in the same direction and the material obtains a permanent polarization. An Hysteresis curve for polarization of piezoelectric material is shown in Figure 1.6. The piezoelectric layers considered in this work are polarized through the thickness-direction.

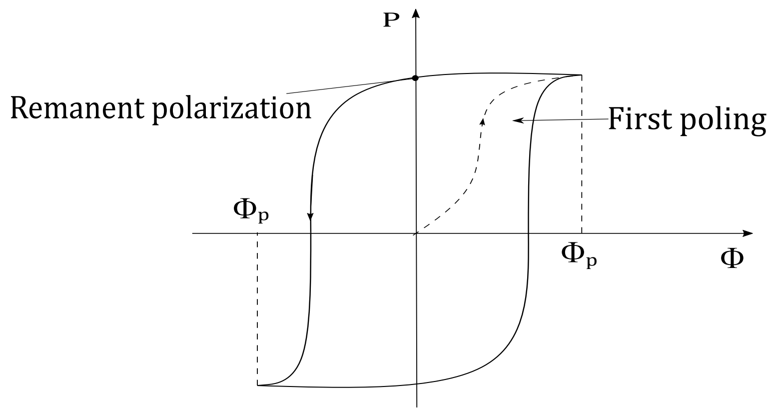

Figure 1.6: Poling of piezoelectric materials: Hysteresis of polarization P

Applications of smart structures

Piezoelectric materials are of great interest when designing *smart structures*, which are systems that are able to sense and react to their environment, through the integration of various elements, such as sensors and actuators. Smart structures that use discrete piezoelectric patches or layers to control the response of a structure have been of considerable interest in recent years. Thanks to the improvement of modern software, it is possible to model coupled thermo-mechanical-electrical systems and to obtain mutual relations between piezoelectric actuator voltages and system response. So by integrating these models into a closed-loop control system, active control can be achieved. Main current and potential applications of smart structure are mentioned:

Structural health monitoring

By embedding sensors in some critical locations of a structural system, it is possible to measure the strain field in order to identify potential damage and mantain structural safety and reliability. *Self-diagnostic* plays a crucial role in the aeronautical and space industry, where sensing the strain field of some relevant structural subcomponents helps in the conduction of an appropriate maintenance program and in avoiding crack propagation. Self-diagnostic is particular relevant for composites whose the failure prediction is still a challenging task. The monitoring process is performed by measuring the dynamic response from an array of sensors, properly located on the structural system. The measurements are recorded and by a statistical analysis it is possible to extract damage-sensitive features to determine the current state of system health. This concept is widely applied in civil engineering to various forms of infrastructures, ranging from bridges to skyscrapers. The most well-known examples refer to the remote monitoring of bridge deflections, mode shapes, and the corresponding frequencies [3].

Vibration control

Piezoelectric sensors and actuators are employed for vibration damping, attenuation and suppression. They are used to reduce noise and improve the comfort of vehicles, such as cars, trucks, and helicopters. Piezoelectric materials are also effective in passive damping: a part of the mechanical energy introduced into the structural system is converted into electrical energy, according to the piezoelectric effect. Piezoelectric passive damping devices are commonly embedded in high-performance sports devices, such as tennis rackets, baseball bats, and skis. Due to their high strain sensitivity (Sirohi and Chopra 2000), piezoelectric sensors and actuators are easily employed for vibration damping/attenuation/suppression (Inman et al. 2001). The same technique is often employed in spacecraft carrying equipment in a pure operational dynamic environment. Active vibration control is usually applied in engineering practice in order to suppress dangerous vibrations over a certain range of frequencies, as in the case of helicopter blades (Chopra 2000).

Shape morphing

In the aeronautics field, *shape morphing* has been used to identify those aircraft wings that undergo certain geometrical changes to enhance or adapt to their mission profiles [4]. In fact, commercial aircraft have to satisfy increasing efficiency requirements and reduce emissions. The means that can be employed to vary the shape of the wing are quite challenging and can vary in complexity, depending on which properties have to be modified: sweep angle, profile, aspect ratio, etc. A smart flexible wing that would be able to perform proper shape changes, without movable rigid parts as flaps, slats, ailerons, and spoilers, would lead to a reduction in drag, weight, and overall system complexity.

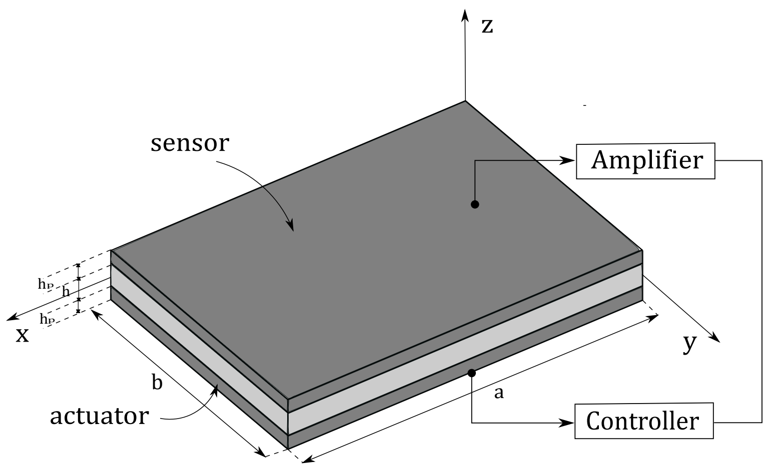

Figure 1.7: Sensor-Actuator network for a plate

1.2 Overview on free vibration analysis and control of composite piezoelectric plates

A brief literature review on free vibration analysis and control of composite piezoelectric plates is reported. Fayaz R. Rofooei and Ali Nikkhoo derived the governing differential equation of motion for an un-damped thin rectangular plate with a number of bonded piezoelectric patches on its surface and arbitrary boundary conditions, by using Hamilton's principle [11]. F. Moleiroa, A.L. Araújoa and J.N. Reddy provided a new Benchmark 3D exact free vibration solutions for two different piezoelectric multilayered plates, using piezoelectric polymer polyvinylidene fluoride (PVDF) as material and considering three sets of electrical boundary conditions and three different aspect ratios [12]. Zhu Su, Guoyong Jin and Tiangui Ye investigated the dynamic characteristic of functionally graded piezoelectric plates with different boundary conditions through an unified approach on the basis of first order shear deformation theory. A modified Fourier series is employed in this work, to describe both diplacements and electric potential [13]. Farhad Abada and Jafar Rouzegar used the spectral element method (SEM) for free vibration analysis of FG plate with two piezoelectric layers embedded to the upper and lower surfaces. A first-order shear deformation theory is employed and governing equations are derived by Hamilton's principle and Maxwell's equation. One of the most interesting features is that the number of elements required for getting an acceptable accuracy of results is much lower than FEM [10]. B.A. Selim, L.W. Zhang and K.M. Liew used a novel element-free IMLS-Ritz model, based on Reddy's higher order shear deformation theory to study the free vibration and active control of FG-CNTRC plates with piezoelectric layers [14]. A. Robaldo, E. Carrera and A. Benjeddou presented new finite elements for the dynamic analysis of piezolaminated plates based on the principle of virtual displacement (PVD) and an unified formulation. The full coupling between electric and mechanical field is considered. Both equivalent single layer (ESL) and layer wise model are employed for displacement variables, while a layer wise description is assumed for the electric potential [15]. D.Ballhause, M.D'Ottavio, B.Kroplin and E. Carrera propose a unified formulation for the electro- mechanical analysis of multilayered plates embedding piezo-layers to assess multilayered theories for piezoelectric plates [16]. Chih-Ping, Wu and Hong-Ru Lin developed a unified formulation of finite layer methods based on the Reissner's mixed variational theorem for the dynamic analysis of simply supported, functionally graded carbon nanotube-reinforced composite plates embedded with piezoelectric layers, considering closed and open-circuit surface conditions. The elastic displacement, transverse shear and normal stress, electric potential, and normal electric displacement components are considered as primary variables of the formulation [17]. Y. Kiani analyzed free vibration behavior of carbon nanotube reinforced composite, embedded with two piezoelectric layers at the bottom and top surfaces. The displacement field is apporximated according to the first order shear deformation plate theory and the electric potential across the piezoelectric thickness is emplyed to be linear. Distribution of CNTs through the thickness of the plate may be functionally graded (FG) or uniformly distributed (UD). The complete set of motion and Maxwell equations of the system are obtained according to the Ritz formulation suitable for arbitrary in-plane and out-of-plane boundary conditions. Close circuit and open circuit boundary conditions on the free surfaces of piezoelectric layers are studied. Chebyshev polynomials are assumed as trial functions in Ritz approximation. frequencies and mode shapes are obtained by solving the eigenvalue system. It is shown that, fundamental frequency of a closed circuit plate is always higher than a plate with open circuit boundary conditions [18]. K. Nguyen-Quang, T. Vo-Duy, H. Dang-Trung and T. Nguyen-Thoi proposed an isogeometric approach for the dynamic response of carbon nanotube reinforced composite (CNTRC) plates integrated with piezoelectric layers. The displacement field is approximated to the higher-order shear deformation theory (HSDT) using the formulation based on Non-Uniform Rational B-Spline (NURBS) basis functions, while a linear function through the thickness of each piezoelectric sub-layer is employed for the electric potential. The single-walled carbon nanotubes (SWCNTs) are assumed to be uniformly distributed (UD) or functionally graded (FG) distributed along the thickness direction. The active control of the plate is based on a velocity feedback control algorithm through a closed-loop control with piezoelectric sensors and actuators [19]. S. Y. Wang, S. T. Quek and K. K. Ang investigated the effect of the stretching-bending coupling of the piezoelectric sensor/actuator pairs on the system stability of smart composite plates. An isoparametric finite element is formulated and the classical negative velocity feedback control method is assumed for the active vibration control analysis of composie plates embedded with distribuited piezoelectric sensors and actuators [20]. X.Q. He, T.Y. Ng, S. Sivashanker and K.M. Liew developed a finite element formulation basend on the classical laminated plate thoery for the shape and vibration control of FGM plates integrated with piezoelectric sensors and actuators. A constant velocity feedback control algorithm is used for the active control of the dynamic response of the FGM plate through closed loop control. Both static and dynamic response are analyzed for an FGM plate of aluminum oxide/Ti-6A1-4V material composition. The effect of the volume fractions and the influence of feedback control gain are examined for static and dynamic responses of the plates [21].

Chapter 2

Constitutive equations

2.1 Equations of Elasticity

2.1.1 Laminate Reference system

The reference system adopted for the plate has the x and y axes which identifies the plate mid-surface Ω and the z axis is orthogonal at both as shown in the figure 2.1.

2.1.2 Generalized Hooke's law

The linear constitutive model for infinitesimal deformation is referred to as the generalized Hooke's law. Stress components are assumed to be linear functions of the strain components and the material coefficients that specify the constitutive relationship between the stress and strain components are assumed to be constant during the deformation. The most general form of the constitutive equations for an elastic material, which does not have a residual stress state σ_0, is given as [25]

$$\begin{bmatrix}\sigma_{11}\\ \sigma_{22}\\ \sigma_{33}\\ \tau_{23}\\ \tau_{13}\\ \tau_{33}\end{bmatrix} = \begin{bmatrix} C_{11} & C_{12} & C_{13} & C_{14} & C_{15} & C_{16}\\ C_{21} & C_{22} & C_{23} & C_{24} & C_{25} & C_{26}\\ C_{31} & C_{32} & C_{33} & C_{34} & C_{35} & C_{36}\\ C_{41} & C_{42} & C_{43} & C_{44} & C_{45} & C_{46}\\ C_{51} & C_{52} & C_{53} & C_{54} & C_{55} & C_{56}\\ C_{61} & C_{62} & C_{63} & C_{64} & C_{65} & C_{66}\end{bmatrix} \begin{bmatrix}\epsilon_{11}\\ \epsilon_{22}\\ \epsilon_{33}\\ \gamma_{23}\\ \gamma_{13}\\ \gamma_{12}\end{bmatrix} \tag{2.1}$$

where C_{ij} are the elastic coefficients, σ_i are the 6 indipendent components of the stress tensor and ϵ_j are the 6 indipendent components of the strain tensor expressed in the the engineering notation. The elastic matrix $[C]$ must be symmetric by virtue of the assumption that the material is hyperelastic. Thus, there are 21 independent stiffness coefficients for the most general anisotropic material.

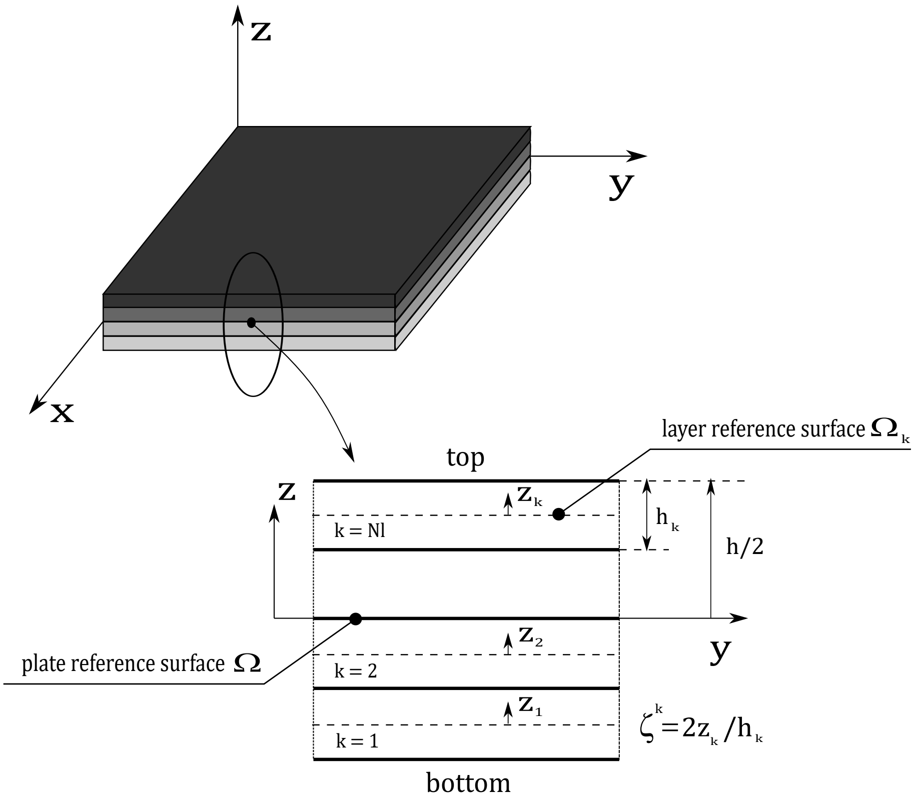

Figure 2.1: Coordinate system of a plate

Isotropic materials

When there exist no preferred direction in the materials (i.e., the material has infinite number of planes of material symmetry), the number of independent elastic coefficients reduces to 2. Such materials are called *isotropic*. For isotropic material we have that the stress-strain relations take the following form [2]

$$\begin{bmatrix} \sigma_{xx} \\ \sigma_{yy} \\ \sigma_{xy} \\ \tau_{xz} \\ \tau_{yz} \\ \tau_{zz} \end{bmatrix} = \begin{bmatrix} C_{11} & C_{12} & 0 & 0 & C_{13} & C_{23} \\ C_{12} & C_{22} & 0 & 0 & 0 & 0 \\ 0 & 0 & C_{66} & 0 & 0 & 0 \\ 0 & 0 & 0 & C_{44} & 0 & 0 \\ 0 & 0 & 0 & 0 & C_{55} & 0 \\ C_{13} & C_{23} & 0 & 0 & 0 & C_{33} \end{bmatrix} \begin{bmatrix} \epsilon_{xx} \\ \epsilon_{yy} \\ \gamma_{xy} \\ \gamma_{xz} \\ \gamma_{yz} \\ \epsilon_{zz} \end{bmatrix} \tag{2.2}$$

with

$$\begin{aligned} C_{11} &= C_{22} = C_{33} = \lambda + 2\mu \\ C_{12} &= C_{23} = C_{13} = \lambda \\ C_{44} &= C_{55} = C_{66} = \mu \end{aligned} \tag{2.3}$$

and

$$\mu = G = \frac{E}{2(1+\nu)}$$
$$\lambda = \frac{E\nu}{(1+\nu)(1-2\nu)} \tag{2.4}$$

μ and λ are referred to as *Lamé constants*, E indicates the *Young's modulus*, G is the transverse *shear modulus* and ν the Poisson's ratio.

Orthotropic materials

When three mutually orthogonal planes of material symmetry exist, the number of elastic coefficients is reduced to 9 and such materials are called *orthotropic*. The stress-strain relations for an orthotropic material takes the form [25]

$$\begin{bmatrix} \sigma_{11} \\ \sigma_{22} \\ \sigma_{12} \\ \tau_{13} \\ \tau_{23} \\ \tau_{33} \end{bmatrix} = \begin{bmatrix} C_{11} & C_{12} & 0 & 0 & C_{13} & C_{23} \\ C_{12} & C_{22} & 0 & 0 & 0 & 0 \\ 0 & 0 & C_{66} & 0 & 0 & 0 \\ 0 & 0 & 0 & C_{44} & 0 & 0 \\ 0 & 0 & 0 & 0 & C_{55} & 0 \\ C_{13} & C_{23} & 0 & 0 & 0 & C_{33} \end{bmatrix} \begin{bmatrix} \epsilon_{11} \\ \epsilon_{22} \\ \epsilon_{12} \\ \gamma_{13} \\ \gamma_{23} \\ \gamma_{33} \end{bmatrix} \tag{2.5}$$

with

$$\begin{aligned}
&C_{11} = E_1 \frac{1-\nu_{23}\nu_{32}}{\Delta} \; , \; C_{12} = E_1 \frac{\nu_{21}-\nu_{31}\nu_{23}}{\Delta} = E_2 \frac{\nu_{12}+\nu_{32}\nu_{13}}{\Delta} \\
&C_{22} = E_2 \frac{1-\nu_{13}\nu_{31}}{\Delta} \; , \; C_{13} = E_1 \frac{\nu_{31}-\nu_{21}\nu_{32}}{\Delta} = E_3 \frac{\nu_{13}+\nu_{12}\nu_{23}}{\Delta} \\
&C_{33} = E_3 \frac{1-\nu_{12}\nu_{21}}{\Delta} \; , \; C_{23} = E_1 \frac{\nu_{32}-\nu_{12}\nu_{31}}{\Delta} = E_3 \frac{\nu_{23}+\nu_{21}\nu_{13}}{\Delta} \\
&C_{44} = G_{23} \; , \; C_{55} = G_{13} \; , \; C_{66} = G_{12} \\
&\Delta = 1 - \nu_{12}\nu_{21} - \nu_{23}\nu_{32} - \nu_{31}\nu_{13} - 2\nu_{12}\nu_{32}\nu_{13}
\end{aligned} \tag{2.6}$$

The nine independent material coefficients for an orthotropic material are

$$E_1, E_2, E_3, G_{12}, G_{13}, G_{23}, \nu_{12}, \nu_{13}, \nu_{23} \tag{2.7}$$

where E_1, E_2, E_3 are Young's moduli in 1, 2 and 3 material direction respectively, ν_{ij} is Poisson's ratio, defined as the ratio of transverse strain in the jth direction to the axial strain in the ith direction when stressed in the ith direction, and G_{23}, G_{13}, G_{12} are shear moduli in the 2–3, 1–3, and 1–2 planes, respectively.

2.1.3 Characterization of a Unidirectional Lamina

A unidirectional fiber-reinforced lamina is considered as an orthotropic material whose material symmetry planes are parallel and transverse to the fiber direction. The material coordinate axis l is taken to be parallel to the fiber, the 2-axis transverse to the fiber direction in the plane of the lamina, and the 3-axis is perpendicular to the plane of the lamina. The orthotropic material properties of a lamina are determined either by suitable laboratory tests or through the theoretical approach, called *micromechanics approach*. The moduli and Poisson's ratio of a fiber-reinforced material can be expressed in terms of the moduli, Poisson's ratios, and volume fractions of the constituents [2]

$$\begin{aligned} &E_1 = E_f v_f + E_m v_m \ , \quad \nu_{12} = \nu_f\, v_f + \nu_m\, v_m \\ &E_2 = \frac{E_f E_m}{E_f\, v_m + E_m\, v_f} \ , \quad G_{12} = \frac{G_f G_m}{G_f v_m + G_m v_f} \end{aligned} \tag{2.8}$$

where the subscripts m and f indicate matrix and fiber rispectively. E_1 is the longitudinal modulus, E_2 is transverse modulus, ν_{12} is the major Poisson's ratio, and G_{12} is the shear modulus.

Coordinate Transformations

The constitutive relations for an orthotropic material were written in terms of the stress and strain components that are referred to a coordinate system that coincides with the principal material coordinate system. In general the coordinate system used in the problem formulation, does not coincide with the principal material coordinate system. Furthermore, composite laminates have several layers, each with different orientation of their material coordinates with respect to the laminate coordinates. Thus, there is a need to establish transformation relations among stresses and strains in one coordinate system to the corresponding quantities in other coordinate system. These relations can be used to transform constitutive equations from the material coordinates of each layer to the coordinate used in the problem description. Beginning from the stress and strain vector written in both coordinate systems

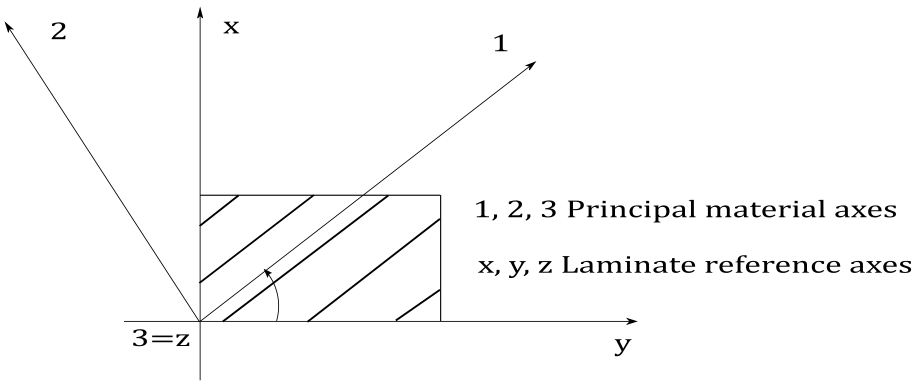

Figure 2.2: Reference system

$$\boldsymbol{\sigma}_m = \begin{bmatrix} \sigma_{11} \\ \sigma_{22} \\ \sigma_{12} \\ \sigma_{13} \\ \sigma_{23} \\ \sigma_{33} \end{bmatrix}, \quad \boldsymbol{\epsilon}_m = \begin{bmatrix} \epsilon_{11} \\ \epsilon_{22} \\ \gamma_{12} \\ \gamma_{13} \\ \gamma_{23} \\ \epsilon_{33} \end{bmatrix}, \quad \boldsymbol{\sigma} = \begin{bmatrix} \sigma_{xx} \\ \sigma_{yy} \\ \sigma_{xy} \\ \sigma_{xz} \\ \sigma_{yz} \\ \sigma_{zz} \end{bmatrix}, \quad \boldsymbol{\epsilon} = \begin{bmatrix} \epsilon_{xx} \\ \epsilon_{yy} \\ \gamma_{xy} \\ \gamma_{xz} \\ \gamma_{yz} \\ \epsilon_{zz} \end{bmatrix} \tag{2.9}$$

the relation that links stress and strain components in the two different reference systems can be written as

$$\begin{aligned} \boldsymbol{\sigma} &= \mathbf{T}\boldsymbol{\sigma}_m \\ \boldsymbol{\epsilon}_m &= \mathbf{T}^T\boldsymbol{\epsilon} \end{aligned} \tag{2.10}$$

where the rotation matrix T is given as

$$\mathbf{T} = \begin{bmatrix} \cos(\theta)^2 & \sin(\theta)^2 & -\sin(2\theta) & 0 & 0 & 0 \\ \cos(\theta)^2 & \sin(\theta)^2 & \sin(2\theta) & 0 & 0 & 0 \\ \sin(\theta)\cos(\theta) & -\sin(\theta)\cos(\theta) & \cos(\theta)^2 - \sin(\theta)^2 & 0 & 0 & 0 \\ 0 & 0 & 0 & \cos(\theta) & -\sin(\theta) & 0 \\ 0 & 0 & 0 & \sin(\theta) & \cos(\theta) & 0 \\ 0 & 0 & 0 & 0 & 0 & 1 \end{bmatrix} \tag{2.11}$$

Thus, by substituting Eq. (2.5) in Eq.(2.10) the constitutive equation, referred to the (x,y,z) reference system, are obtained

$$\boldsymbol{\sigma} = \boldsymbol{T}\boldsymbol{\sigma}_m = \boldsymbol{T}\boldsymbol{C}_m\boldsymbol{\epsilon}_m = \boldsymbol{T}\boldsymbol{C}_m\boldsymbol{T}^T\boldsymbol{\epsilon} \tag{2.12}$$

Finally assuming

$$\tilde{C} = \boldsymbol{T}\boldsymbol{C}_m\boldsymbol{T}^T = \begin{bmatrix} \tilde{C}_{11} & \tilde{C}_{12} & 0 & 0 & \tilde{C}_{13} & \tilde{C}_{23} \\ \tilde{C}_{12} & \tilde{C}_{22} & 0 & 0 & 0 & 0 \\ 0 & 0 & \tilde{C}_{66} & 0 & 0 & 0 \\ 0 & 0 & 0 & \tilde{C}_{44} & 0 & 0 \\ 0 & 0 & 0 & 0 & \tilde{C}_{55} & 0 \\ \tilde{C}_{13} & \tilde{C}_{23} & 0 & 0 & 0 & \tilde{C}_{33} \end{bmatrix} \tag{2.13}$$

Hooke's law becomes

$$\boldsymbol{\sigma} = \tilde{\boldsymbol{C}}\boldsymbol{\epsilon} \tag{2.14}$$

2.2 Constitutive equations for FGMs

2.2.1 Material properties of FG-CNT reinforced composite plates

The FG-CNTRC plates are composed of a mixture of CNTs and the polymeric matrix. It is assumed that CNTs are (10,10) armchair single-walled carbon nanotubes (SWCNT) and the matrix is supposed to be isotropic and homogeneous. Four types of linear distributions of CNTs through the thickness are considered, including a uniformly distributed (UD) and three different functionally graded (FG), as shown in the Table 2.1

Table 2.1: Volume fraction of CNTs as a function of thickness coordinate

CNTs Distribution	$V_{CNT}(z)$
UD CNTRC	V^*_{CNT}
FG-V CNTRC	$V^*_{CNT}\left(1 + \frac{2z}{h}\right)$
FG-O CNTRC	$2V^*_{CNT}\left(1 - \frac{2\|z\|}{h}\right)$
FG-X CNTRC	$2V^*_{CNT}\frac{2\|z\|}{h}$

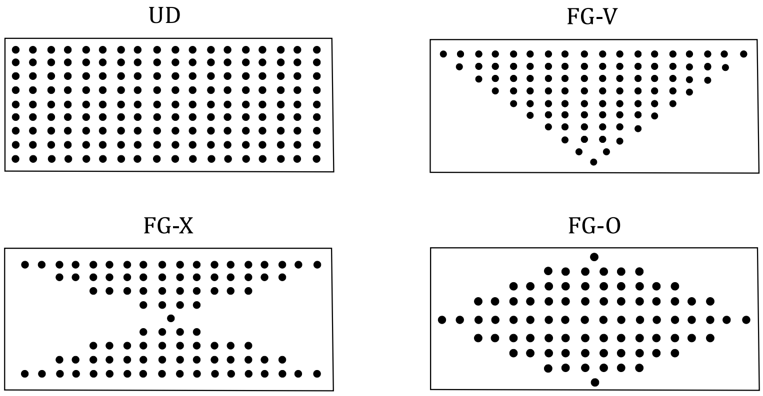

Figure 2.3: CNTs Distributions

where

$$V^*_{CNT} = \frac{w_{CNT}}{w_{CNT} + \frac{\rho_{CNT}}{\rho_m} - \frac{w_{CNT}\rho_{CNT}}{\rho_m}} \tag{2.15}$$

is the CNTs volume fraction, w_{CNT} is the mass fraction of the carbon nanotube in the composite plate, ρ_m and ρ_{CNT} are the densities of the matrix and carbon nanotube, respectively. The quantities V_{CNT} and V_m represent the volume fraction of the CNTs and the polymeric matrix, respectively, and they are related by the equation $V_{CNT}(z) + V_m(z) = 1$. The structure of the carbon nanotube strongly influences the overall properties of the composite. Several micromechanical models have been developed to predict the effective material properties of CNTRCs. They can be defined eighter by using the extended Voigt's rule of mixtures or Mori-Tanaka micromechanical model [23]. According to the rule of mixtures, the effective material properties can be expressed as follows [5]:

$$\begin{aligned}
&E_{11} = \eta_1 V_{CNT} E_{11}^{CNT} + V_m E_m \\
&\frac{\eta_2}{E_{22}} = \frac{V_{CNT}}{E_{22}^{CNT}} + \frac{V_m}{E_m} \\
&\frac{\eta_3}{G_{12}} = \frac{V_{CNT}}{G_{12}^{CNT}} + \frac{V_m}{G_m} \\
&\nu_{12} = V_{CNT}\nu_{12}^{CNT} + V_m \nu_m \\
&\rho = V_{CNT}\rho_{CNT} + V_m \rho_m
\end{aligned} \tag{2.16}$$

Where E_{11}^{CNT}, E_{22}^{CNT}, G_{12}^{CNT}, ν_{12}^{CNT} and ρ_{CNT} are the Young's modulii, the shear modulus, the Poisson's ratio and the density of the SWCNTs, respectively. E_m, G_m, ν_m and ρ_m are the material properties for the isotropic matrix. The efficiency parameters η_1, η_2 and η_3 are introduced in the equations to take into account the size dependent material properties of the plate. These parameters are chosen to equal the obtained values of Young modulus and shear modulus from the present modified rule of mixtures with the results obtained according to the molecular dynamics approach (MD).

Constitutive relations

The 3D constitutive equations for FG-CNT can be written as

$$\boldsymbol{\sigma} = \boldsymbol{C}(z)\boldsymbol{\epsilon} \tag{2.17}$$

Where C is the constitutive matrix

$$\boldsymbol{C}(z) = \begin{bmatrix} C_{11}(z) & C_{12}(z) & 0 & 0 & C_{13}(z) & C_{23}(z) \\ C_{12}(z) & C_{22}(z) & 0 & 0 & 0 & 0 \\ 0 & 0 & C_{66}(z) & 0 & 0 & 0 \\ 0 & 0 & 0 & C_{44}(z) & 0 & 0 \\ 0 & 0 & 0 & 0 & C_{55}(z) & 0 \\ C_{13}(z) & C_{23}(z) & 0 & 0 & 0 & C_{33}(z) \end{bmatrix} \tag{2.18}$$

2.3 Constitutive equations for piezoelectric materials

The general coupling between the mechanical, electric, and thermal fields can be established using thermodynamical principles and Maxwell's relations. For this purpose, it is necessary to define a *Gibbs free-energy function* G and a *thermopiezo-electric enthalpy density H*

$$\begin{aligned} G(\epsilon_{ij}, E_i, \theta) &= \sigma_{ij}\epsilon_{ij} - E_i D_i - \eta\theta \\ H(\epsilon_{ij}, E_i, \theta, \vartheta_i) &= G(\epsilon_{ij}, E_i, \theta) - F(\vartheta_i) \end{aligned} \tag{2.19}$$

where σ_{ij} and ϵ_{ij} are the stress and strain components,E_i is the electric field vector, D_i is the electric displacement vector, η is the variation in entropy per unit of volume, and θ is the temperature considered with respect to the reference temperature T_0. $F(\vartheta_i)$ is the dissipation function which depends on the spatial temperature gradient ϑ_i and in the most general case is given as:

$$F(\vartheta_i) = \frac{1}{2}\kappa_{ij}\vartheta_i\vartheta_j - \tau_0\dot{h}_i \tag{2.20}$$

where κ_{ij} is the symmetric, positive, semi-definite conductivity tensor, τ_0 is a thermal relaxation parameter and $\dot{h}_i$ is the temporal derivative of the heat flux h_i. The thermal relaxation parameter is usually omitted in the proposed multifield problems. The thermopiezoelectric enthalpy density H can be expanded in order to obtain a quadratic form for a linear interaction:

$$\begin{aligned} H(\epsilon_{ij}, E_i, \theta, \vartheta_i) = &\frac{1}{2}Q_{ijkl}\epsilon_{ij}\epsilon_{kl} - e_{ijk}\epsilon_{ij}E_k - \lambda_{ij}\epsilon_{ij}\theta \\ &- \frac{1}{2}\varepsilon_{kl}E_kE_l - p_kE_k\theta - \frac{1}{2}\chi\theta^2 - \frac{1}{2}\kappa_{ij}\vartheta_i\vartheta_j \end{aligned} \tag{2.21}$$

where Q_{ijkl} is the elastic coefficient tensor considered for an orthotropic material in the problem reference system. e_{ijk} are the piezoelectric coefficients and ϵ_{kl} are the permittivity coefficients.λ_{ij} are thermo-mechanical coupling coefficients, p_k are the pyroelectric coefficients, and $\chi = \rho C_v/T_0$, where ρ is the material mass density, C_v is the specific heat per unit mass, and T_0 is the reference temperature. For the piezoelectricity problems, the thermal contributions are not considered and the piezoelectric enthalpy density H coincides with the Gibbs free-energy function G. Hence, equation 2.21 can be rewritten as

$$H(\epsilon_{ij}, E_i, \theta, \vartheta_i) = \frac{1}{2}Q_{ijkl}\epsilon_{ij}\epsilon_{kl} - e_{ijk}\epsilon_{ij}E_k - \frac{1}{2}\varepsilon_{kl}E_kE_l \tag{2.22}$$

The constitutive equations are obtained by considering the following relations:

$$\sigma_{ij} = \frac{\partial H}{\partial \epsilon_{ij}}\ , \quad D_k = -\frac{\partial H}{\partial E_k} \tag{2.23}$$

The constitutive equations for the electromechanical problem are obtained by considering Eq.(2.22) and Eq. (2.23)

$$\begin{aligned} \sigma_{ij} &= Q_{ijkl}\epsilon_{kl} - e_{ijk}E_k \\ D_k &= e_{ijk}\epsilon_{ij} + \varepsilon_{kl}E_l \end{aligned} \tag{2.24}$$

Considering a generic multilayered structure, equations 2.24 can be written in their vectorial form in the reference system (x,y,z) as

$$\begin{aligned} \boldsymbol{\sigma}^k &= \boldsymbol{Q}^k\boldsymbol{\epsilon}^k - \boldsymbol{e}^{kT}\boldsymbol{E}^k \\ \boldsymbol{D}^k &= \boldsymbol{e}^k\boldsymbol{\epsilon}^k + \boldsymbol{\varepsilon}^k\boldsymbol{E}^k \end{aligned} \tag{2.25}$$

Where the strain and stress component vectors are

$$\boldsymbol{\sigma}^k = \begin{bmatrix} \sigma_{xx} \\ \sigma_{yy} \\ \sigma_{xy} \\ \sigma_{xz} \\ \sigma_{yz} \\ \sigma_{zz} \end{bmatrix}^k , \quad \boldsymbol{\epsilon}^k = \begin{bmatrix} \epsilon_{xx} \\ \epsilon_{yy} \\ \gamma_{xy} \\ \gamma_{xz} \\ \gamma_{yz} \\ \epsilon_{zz} \end{bmatrix}^k \tag{2.26}$$

The electric field $\boldsymbol{E}^k$ and electrical displacement $\mathbf{D}^k$ vectors are

$$\boldsymbol{E}^k = \begin{bmatrix} E_x \\ E_y \\ E_z \end{bmatrix}^k , \quad \boldsymbol{D}^k = \begin{bmatrix} D_x \\ D_y \\ D_z \end{bmatrix}^k \tag{2.27}$$

The elastic coefficients matrix $\boldsymbol{Q}^k$ of Hooke's law in the problem reference system for an orthotropic material is:

$$\boldsymbol{Q}^k = \begin{bmatrix} Q_{11} & Q_{12} & Q_{13} & 0 & 0 & Q_{16} \\ Q_{12} & Q_{22} & Q_{23} & 0 & 0 & Q_{26} \\ Q_{13} & Q_{23} & Q_{33} & 0 & 0 & Q_{36} \\ 0 & 0 & 0 & Q_{44} & Q_{45} & 0 \\ 0 & 0 & 0 & Q_{45} & Q_{55} & 0 \\ Q_{16} & Q_{26} & Q_{36} & 0 & 0 & Q_{66} \end{bmatrix}^k \tag{2.28}$$

The matrix $\boldsymbol{\varepsilon}^k$ of the permittivity coefficients has 3 × 3 dimensions:

$$\boldsymbol{\varepsilon}^k = \begin{bmatrix} \varepsilon_{11} & \varepsilon_{12} & 0 \\ \varepsilon_{12} & \varepsilon_{22} & 0 \\ 0 & 0 & \varepsilon_{33} \end{bmatrix}^k \tag{2.29}$$

The piezoelectric coefficients matrix $\boldsymbol{e}^k$ has 3 × 6 dimensions:

$$\boldsymbol{e}^k = \begin{bmatrix} 0 & 0 & 0 & e_{14} & e_{15} & 0 \\ 0 & 0 & 0 & e_{24} & e_{25} & 0 \\ e_{31} & e_{32} & e_{33} & 0 & 0 & e_{36} \end{bmatrix}^k \tag{2.30}$$

Chapter 3

Plate structural models

3.1 2D structural theories

The exact closed-form solution of the fundamental equations of continuum mechanics is generally available only for a few sets of geometries and boundary conditions. In most cases approximated solutions are required to solve the general 3D problem. This has brought, over the years, to the development of a large amount of structural theories in order to reduce the 3D problem to a 2D or 1D problem. The choice to reduce the 3D problem is strongly related to the geometric dimensions of structural element that has to be analyzed. There are two main approach to derive structural theories:

- *The asymptotic method*
- *The axiomatic method*

The *axiomatic method* is based on the establishment of a number of hypothesis that cannot be proved mathematically. Thus, it is possible to reduce the mathematical complexity of the 3D elasticity differential equations. This method provides a new set of governing equations that can be solve in a comfortable manner, and sometimes under specific iphotesis, the equations can be easily solved in the close-form. The *asymptotic method* introduced a geometric parameter in the governing equations that in the case of a 2D theory could be the ratio between the thickness and the length of a plate. One of the advantages by adopting this approch is that all the terms in the equations which multiply the geometric parameter by exponents that are lower or equal to n are preserved for a given value of the exponent. So all the terms have the same order of magnitude and th 2D solution approaches to the 3D solution when the parameter tends to zero. Despite this method provides a control on the effectiveness of each term in the equations, the development of asymptotic theories are generally more difficult than the axiomatic theories.

3.1.1 Plate reference system

Plates are defined as 2D structural elements with a small thickness h compared to the planar dimensions a and b. Due to this geometric assumption, it is possible to reduce 3D problem to a 2D one. The reference system assumed for the plate has the x and y axes which identify the plate mid-surface Ω and the z axis is orthogonal at both as shown in the figure 3.1.

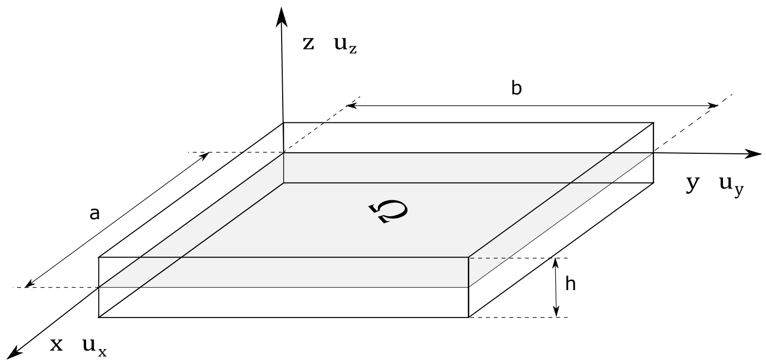

Figure 3.1: Coordinate system of a plate

3.1.2 The Unified approach for the displacement field

Dealing with a two-dimensional axiomatic theory, in the most general case the unknown displacements can be expressed as a series expansion through the tickhness coordinate. By the *Unified Formulation*, introduced by Carrera, the displacemnt field of a 2D structural problem can be expressed as [25]:

$$\boldsymbol{u} = F_\tau(z)\,\boldsymbol{u}_\tau(x,y) \quad \tau = 0,1,....,N \tag{3.1}$$

Where $F_\tau(z)$ are generic functions of the plate-thickness coordinate, $\mathbf{u}_\tau(x,y)$ is the vector of the unknow diplacements referred to the mid-surface of the plate Ω, and N is the order of expansion that can be arbitrarily chosen. Thus, by expanding the displacement field at any desired order, is possible to include a great number of 2D theories, from classical to advanced theories. For example, considering a Taylor-like polynomial expansion the displacement field assumes the following explicit form:

$$\begin{aligned} u_x(x,y,z) &= u_{x0}(x,y) + z\,u_{x1}(x,y) + z^2\,u_{x2}(x,y) + ... + z^N\,u_{xN}(x,y) \\ u_y(x,y,z) &= u_{y0}(x,y) + z\,u_{y1}(x,y) + z^2\,u_{y2}(x,y) + ... + z^N\,u_{yN}(x,y) \\ u_z(x,y,z) &= u_{z0}(x,y) + z\,u_{z1}(x,y) + z^2\,u_{z2}(x,y) + ... + z^N\,u_{zN}(x,y) \end{aligned} \tag{3.2}$$

3.2 Classical plate theories

Dealing with the displacement formulation, since the late 19th century many plate theories have been developed, such as those proposed by Kirchhoff and Reissner-Midlin, see [24]. A brief review of these classical models along with the complete linear expansion are described in this section.

3.2.1 Classical plate theory

In the framework of the Unified Formulation, the *Kirchhoff plate theory*, referred as *Classical Plate Theory* (CPT), can be considered as particular case of the N = 1 model by using a Taylor-like polynomial expansion. The displacement field is expressed as:

$$\begin{aligned} u_x(x,y,z) &= u_{x0}(x,y) + z\,u_{x1}(x,y) \\ u_y(x,y,z) &= u_{y0}(x,y) + z\,u_{y1}(x,y) \\ u_z(x,y,z) &= u_{z0}(x,y) \end{aligned} \tag{3.3}$$

The CPT is derived from the following a-priori assumptions:

1. segments normal to the mid-surface of the plate remain straight after deformation. Thus, the in-plane displacements are assumed to be linear along z as follows:

$$\begin{aligned} u_x(x,y,z) &= u_{x0}(x,y) + z\,u_{x1}(x,y) \\ u_y(x,y,z) &= u_{y0}(x,y) + z\,u_{y1}(x,y) \end{aligned} \tag{3.4}$$

2. segments normal to the mid-surface of the plate remain normal after deformation. This assumption implies that the shear deformations γ_{xz} and γ_{yz} are neglected:

$$\begin{aligned} \gamma_{xz} = u_{z,x} + u_{x,z} = u_{z0,x} + u_{x1} = 0 \Rightarrow u_{x1} = -u_{z0,x} \\ \gamma_{yz} = u_{z,y} + u_{y,z} = u_{z0,y} + u_{y1} = 0 \Rightarrow u_{y1} = -u_{z0,y} \end{aligned} \tag{3.5}$$

3. the tickness remains constant after deformation. The out-of-plane deformation ϵ_{zz} is neglected:

$$\epsilon_{zz} = u_{z,z} = 0 \tag{3.6}$$

Thus, the aforementioned ipothesis can be resumed in the following displacement model:

$$
\begin{aligned}
u_x(x, y, z) &= u_{x0}(x, y) - z\, u_{z0,x}(x, y) \\
u_y(x, y, z) &= u_{y0}(x, y) - z\, u_{z0,y}(x, y) \\
u_z(x, y, z) &= u_{z0}(x, y)
\end{aligned}
\tag{3.7}
$$

CPT presents three unknown variables (u_{x0}, u_{y0}, u_{z0}) and the relations amongst them have been derived from kinematic ipothesis. According to the kinematics hypotheses, CPT takes into account the in-plane strains only and neglects the cross-sectional shear deformation phenomena. Figure 3.4 shows the typical distribution of displacement components according to CPT: linear for u_x and u_y and constant for uz. The physical meaning of the derivatives of transversal displacement, $u_{z,x}$ and $u_{z,y}$, is also represented.

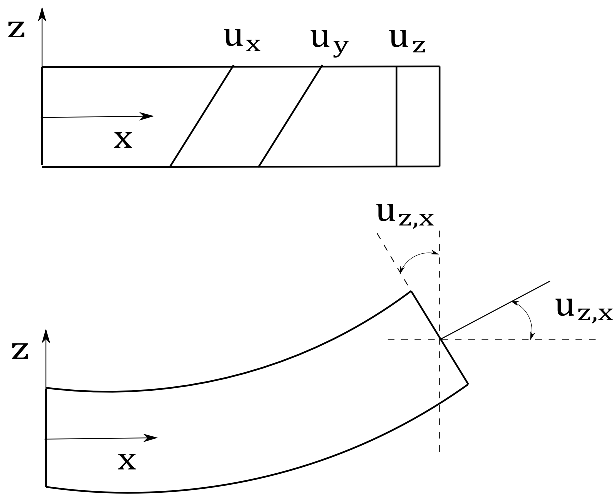

Figure 3.2: Kinematics of Kirchhoff plate model

3.2.2 First order shear deformation theory

The first order shear deformation theory (FSDT) is considered as an extesion of the classical plate theory and it is based on Reissner-Midlin ipothesis. The second assumption of Kirchhoff hypothesis is removed, thus the shear deformation is taken into account:

$$
\begin{aligned}
\gamma_{xz} &= u_{z,x} + u_{x,z} = u_{z0,x} + \phi_x \\
\gamma_{yz} &= u_{z,y} + u_{y,z} = u_{z0,y} + \phi_y
\end{aligned}
\tag{3.8}
$$

Where ϕ_x and ϕ_y are the rotation functions. According to Reissner-Midlin ipothesis, the displacement field can be resumed in the form:

$$\begin{aligned} u_x(x,y,z) &= u_{x0}(x,y) - z\,\phi_x(x,y) \\ u_y(x,y,z) &= u_{y0}(x,y) - z\,\phi_y(x,y) \\ u_z(x,y,z) &= u_{z0}(x,y) \end{aligned} \tag{3.9}$$

The unknows increase from to 3 to 5 (u_{x0}, u_{y0}, u_{z0}, ϕ_x, ϕ_y). Dealing with thin plates, when the in-plane characteristic dimension to thickness ratio is on the order 50 or greater the shear effect disappears and the rotation functions ϕ_x and ϕ_y approach the respective slopes of the transverse deflections $u_{z0,x}$ and $u_{z0,y}$. Figure 3.3 shows the typical distribution of displacement components according to FSDT. Also the physical meaning of the rotations, ϕ_x and ϕ_y, is represented.

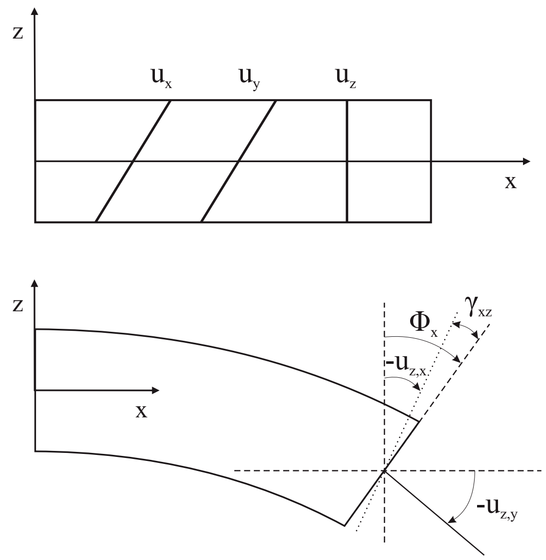

Figure 3.3: FSDT kinematics

3.2.3 The complete linear expansion case N=1

Considering the complete linear expansion case, the plate model has 6 displacement variables: three constant (N=0) and three linear (N=1). Thus, the displacement field assumes the following form:

$$\begin{aligned} u_x(x,y,z) &= u_{x0}(x,y) + z\,u_{x1}(x,y) \\ u_y(x,y,z) &= u_{y0}(x,y) + z\,u_{y1}(x,y) \\ u_z(x,y,z) &= u_{z0}(x,y) + z\,u_{z1}(x,y) \end{aligned} \tag{3.10}$$

Strain components are obtained by substituting the displacement field in the geometrical relations:

$$
\begin{aligned}
\epsilon_{xx} &= u_{x,x} = u_{x0,x} + z\, u_{x1,x} \\
\epsilon_{yy} &= u_{y,y} = u_{y0,y} + z\, u_{y1,y} \\
\epsilon_{zz} &= u_{z,z} = u_{z1} \\
\gamma_{xy} &= u_{x,y} + u_{y,x} = u_{x0,y} + u_{y0,x} + z\,(u_{x1,y} + u_{y1,x}) \\
\gamma xz &= u_{x,z} + u_{z,x} = u_{x1} + u_{z0,x} + z\, u_{z1,x} \\
\gamma yz &= u_{y,z} + u_{z,y} = u_{y1} + u_{z0,y} + z\, u_{z1,y}
\end{aligned}
\tag{3.11}
$$

The adoption of the complete linear expansion (N=1) is necessary to introduce the through-the-thickness stretching of the plate, given by ϵ_{zz}. This model leads to a constant distribution along the tickness of the strain component ϵ_{zz} and a linear distribution of other strain components. The thickness stretching cannot be neglected when the plate is relatively thick.

3.3 Higher order theories

The classical plate models are not able to account for many higher-order effects, such as the second-order out-of-plane deformations. The limitations of these models stimulated the development of higher order shear deformation theories (HSDT), to include the effect of cross sectional warping and to get the realistic variation of the transverse shear strains and stresses through the thickness of plate. Further refinements of FSDT are known as Higher-Order Theories (HOT). In general, higher-order theories are based on displacement models of the following type:

$$
u_i(x,y,z) = u_0(x,y) + z\, u_1(x,y) + z^2\, u_2(x,y) + ... + z^N\, u_N(x,y) \tag{3.12}
$$

3.3.1 Reddy's higher-order shear deformation theory

Reddy proposed a third-order plate theory based on the same assumptions as the classical and first-order plate theories, except that the assumption on the straightness and normality of a transverse normal after deformation is removed by expanding the displacements u_x, u_y as cubic functions of the thickness coordinate [26]. The displacement field is obtained by imposing traction-free boundary conditions on the top and bottom faces of the laminate ($\sigma_{yz}(x,y,\pm h/2) = \sigma_{xz}(x,y,\pm h/2) = 0$):

$$
\begin{aligned}
u_x(x,y,z) &= u_{x0}(x,y) + z\,\phi_x(x,y) - \frac{4}{3h^2} z^3 (\phi_x + u_{z0,x}) \\
u_y(x,y,z) &= u_{y0}(x,y) + z\,\phi_y(x,y) - \frac{4}{3h^2} z^3 (\phi_y + u_{z0,y}) \\
u_z(x,y,z) &= u_{z0}(x,y)
\end{aligned}
\tag{3.13}
$$

Where u_{x0}, u_{y0}, u_{z0}, ϕ_x and ϕ_y are the unknow variables.

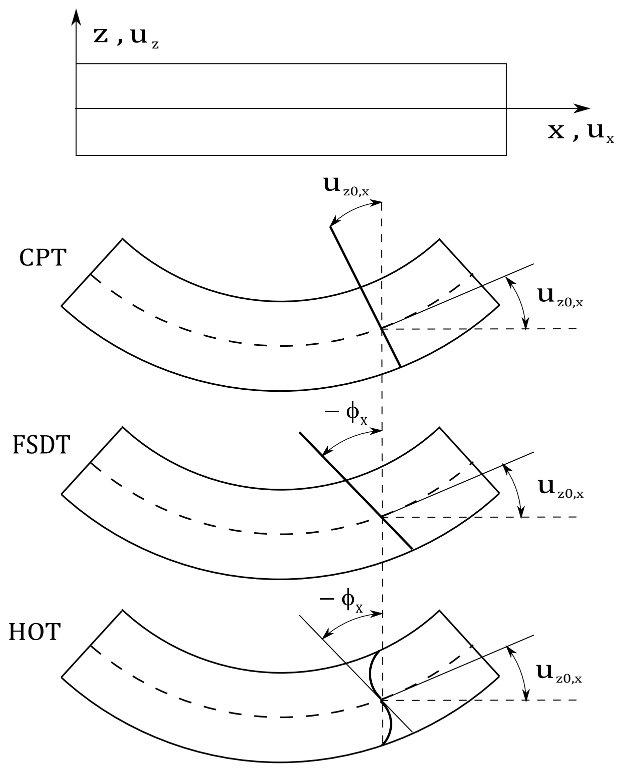

Figure 3.4: Deformation of a transverse normal according to the classical, first order, and third-order plate theories

3.4 Theories on Multylayered structures

Multilayered structures exhibit higher transverse shear and transverse normal flexibilities with respect to in-plane deformability along with a discontinuity of the mechanical properties in the thickness direction. These features require the displacement field and the transverse stresses to satisfy some conditions, summarized with the acronym C_z^0: the displacement field $\boldsymbol{u}$ should be able to describe sudden changes of slope in correspondence of layer interfaces. This is known as the *zig-zag* effect (ZZ). Although in-plane stresses $\boldsymbol{\sigma_p}$ can be discontinuos, the *Cauchy* theorem demands the continuity of the transverse stresses $\boldsymbol{\sigma_n}$. The fulfilment of the C_z^0-Requirements is a crucial point in the development of any theory suitable for multilayered structures.

3.4.1 ZZ theories

The extension of CLT, FSDT and HOT to multilayered plates doesn't permit the C_0^z-requirements to be fulfilled. Refined theories have therefore been introduced to resolve this problem. These types of theories are referred to as Zig-Zag theories. The idea behind zig-zag theories is that a certain displacement model is assumed in each layer and then compatibility and equilibrium conditions are used at the interface to reduce the number of unknown variables. Lekhnitskii was the first to propose a Zig-Zag theory, which was obtained by solving an elasticity problem involving a layered beam. An independent manner of formulating zig-zag plate/shell theories has been provided in the by Reissner. His formulation permits to satisfy, completely and a priori, the C_z^0-Requirements by assuming two indipendent fields for diplacements and transverse stresses [27].

3.4.2 ESL models

The theories mentioned in the previous sections consider a number of unknown variables that is independent of the number of constitutive layers Nl. These all are known as Equivalent Single Layer Models (ESL). Although these kinematic theories can describe transverse shear and normal strains, including transverse warping of the cross-section, their approach is kinematically homogeneous in the sense that the kinematics is insensitive to individual layers, unless zig-zag models are used. In the most general case, ESL models appear in the following form:

$$
\begin{aligned}
u_x(x,y,z) &= u_{x0}(x,y) + z\,u_{x1}(x,y) + z^2\,u_{x2}(x,y) + ... + z^N\,u_{xN}(x,y) \\
u_y(x,y,z) &= u_{y0}(x,y) + z\,u_{y1}(x,y) + z^2\,u_{y2}(x,y) + ... + z^N\,u_{yN}(x,y) \\
u_z(x,y,z) &= u_{z0}(x,y) + z\,u_{z1}(x,y) + z^2\,u_{z2}(x,y) + ... + z^N\,u_{zN}(x,y)
\end{aligned}
\tag{3.14}
$$

where N is the order of the Taylor-like polynomial expansion. These higher-order theories are denoted by acronyms ED1, ED2,ED3,...., EDN.

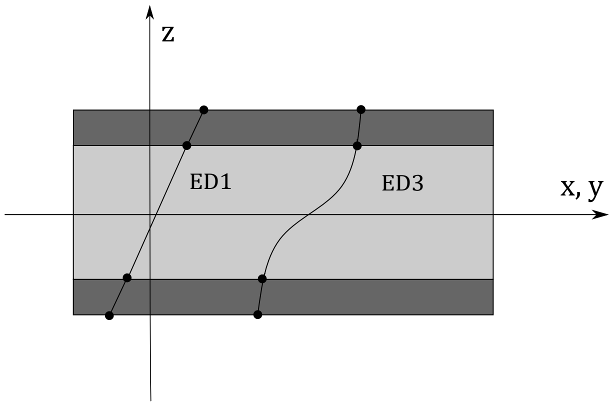

Figure 3.5: Linear and cubic Equivalent single layer expansions

3.4.3 Murakami's zig-zag function

For an ESL theory, the ZZ form of the displacements can be reproduced by introducing the Murakami's function which is able to describe the zig-zag effect [28]. He modified the FSDT theories according to the following model:

$$
\begin{aligned}
u_x(x,y,z) &= u_{x0}(x,y) + z\,u_{x1}(x,y) + (-1)^k \zeta_k u_{xZ} \\
u_y(x,y,z) &= u_{y0}(x,y) + z\,u_{y1}(x,y) + (-1)^k \zeta_k u_{yZ} \\
u_z(x,y,z) &= u_{z0}(x,y)
\end{aligned}
\tag{3.15}
$$

Where the subscript Z is referred to murakami's function and $\zeta_k = 2z_k/h_k$ is the non-dimensioned layer coordinate. The exponent k changes the sign of the zig-zag term in each layer. With the addition of the ZZ function, the discontinuity of the first derivative of the displacement variables can be reproduced through the thickness direction. Transverse normal strain/stress effects can be included in the displacement field, leading to:

$$
\begin{aligned}
u_x(x,y,z) &= u_{x0}(x,y) + z\,u_{x1}(x,y) + (-1)^k \zeta_k u_{xZ} \\
u_y(x,y,z) &= u_{y0}(x,y) + z\,u_{y1}(x,y) + (-1)^k \zeta_k u_{yZ} \\
u_z(x,y,z) &= u_{z0}(x,y) + z\,u_{z1}(x,y) + (-1)^k \zeta_k u_{zZ}
\end{aligned}
\tag{3.16}
$$

Where

$$
F_0 = 1, \;\; F_1 = z, \;\; F_2 = F_Z = (-1)^k \zeta_k, \quad \tau = 0{,}1{,}2 \tag{3.17}
$$

This model is denoted by the acronym EDZ1, in which Z is referred to the inclusion of murakami's function in the displacement field. Higher-order models take the following form:

$$
\begin{aligned}
u_x(x,y,z) &= u_{x0}(x,y) + z\,u_{x1}(x,y) + ... + z^N\,u_{xN}(x,y) + (-1)^k\zeta_k u_{xZ} \\
u_y(x,y,z) &= u_{y0}(x,y) + z\,u_{y1}(x,y) + ... + z^N\,u_{yN}(x,y) + (-1)^k\zeta_k u_{yZ} \\
u_z(x,y,z) &= u_{z0}(x,y) + z\,u_{z1}(x,y) + ... + z^N\,u_{zN}(x,y) + (-1)^k\zeta_k u_{zZ}
\end{aligned}
\tag{3.18}
$$

That in compact form can be written as:

$$
\boldsymbol{u} = \mathbf{u}_0 + (-1)^k\zeta_k\boldsymbol{u}_Z + z^r\,\boldsymbol{u}_r = F_\tau\boldsymbol{u}_\tau \quad \tau = 0,1,....,N,Z \tag{3.19}
$$

Where N is the order of expansion, thus:

$$
F_0 = 1,\;\; F_1 = z,\;\; F_2 = z^2....,F_N = z^N,\;\; F_Z = (-1)^k\zeta_k \tag{3.20}
$$

These higher-order theories are denoted by acronyms EDZ1,EDZ2, EDZ3,..., EDZN.

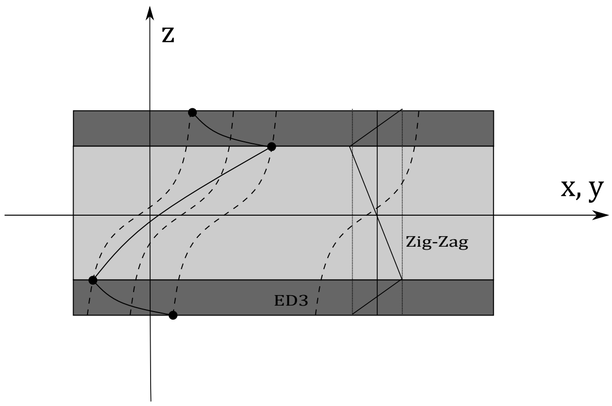

Figure 3.6: Cubic case of Murakami's zig-zag function

3.4.4 Layer Wise models

In all equivalent single-layer laminate theories, it is assumed that the displacements are continuous functions of the thickness coordinate. Hence, the transverse stresses at the interface of two layers, are discontinuous. For thin laminates the error introduced due to discontinuous interlaminar stresses can be negligible. However, for thick laminates, the ESL theories can give erroneous results for all stresses, requiring a more accurate approach to include the ZZ effect. By introducing the *Layer Wise* theories, is possible to obtain a detailed response of individual layer which is considered as an independent plate. The layer wise approach constists of the use of special higher-order theories at layer level which leads to an increase in the number of unknows in the solution process, and consequently to an higher computational cost of the analysis. The compatibility of the displacement components, corresponding to each interface, is then imposed as a constraint. The thickness variation of the displacement components in each layer can be defined eighter in terms of lagrangian interpolation functions [29] or, more preferred, in terms of Legendre polynomials. For the linear expansion case, the following displacement field is employed:

$$\begin{aligned} u_x^{(k)}(x,y,z) &= F_t(\zeta_k)u_{xt}^{(k)}(x,y) + F_b(\zeta_k)u_{xb}^{(k)}(x,y) \\ u_y^{(k)}(x,y,z) &= F_t(\zeta_k)u_{yt}^{(k)}(x,y) + F_b(\zeta_k)u_{yb}^{(k)}(x,y) \\ u_z^{(k)}(x,y,z) &= F_t(\zeta_k)u_{zt}^{(k)}(x,y) + F_b(\zeta_k)u_{zb}^{(k)}(x,y) \end{aligned} \tag{3.21}$$

The subscripts t and b denote values related to the top and bottom layer-surface, respectively. These two terms consist of the linear part of the expansion. The thickness functions $F_\tau(\zeta_k)$ have now been defined at the k-layer level:

$$F_t = \frac{P_0 + P_1}{2}, \;\; F_b = \frac{P_0 - P_1}{2} \tag{3.22}$$

Where $P_j = P_j(\zeta_k)$ is the Legendre polynomial of the j-order defined in the ζ_k-domain $-1 \le \zeta_k \le 1$. The first five Legendre polynomials are:

$$P_0 = 1\,,\; P_1 = \zeta_k\,,\; P_2 = \frac{3\zeta_k^2 - 1}{2}\,,\; P_3 = \frac{5\zeta_k^3}{2}\,,\; P_4 = \frac{35\zeta_k^4}{8} - \frac{15\zeta_k^2}{4} + \frac{3}{8} \tag{3.23}$$

The chosen functions have the following interesting properties:

$$\zeta_k = \begin{cases} 1 \;:\;\; F_t = 1;\; F_b = 0;\; F_r = 0; \\ -1 \;:\; F_t = 1;\; F_b = 0;\; F_r = 0; \end{cases} \tag{3.24}$$

That permits to have interface values as unknown variables, avoiding therefore the inclusion of constraint equations to impose C_0^z-requirements. Higher-order layer-wise theories are written by adding higher-order terms:

$$\begin{aligned} u_x^{(k)}(x,y,z) &= F_t u_{xt}^{(k)} + F_b u_{xb}^{(k)} + F_2 u_{x2}^{(k)} + .. + F_N u_{xN}^{(k)} \\ u_y^{(k)}(x,y,z) &= F_t u_{yt}^{(k)} + F_b u_{yb}^{(k)} + F_2 u_{y2}^{(k)} + .. + F_N u_{yN}^{(k)} \\ u_z^{(k)}(x,y,z) &= F_t u_{zt}^{(k)} + F_b u_{zb}^{(k)} + F_2 u_{z2}^{(k)} + .. + F_N u_{zN}^{(k)} \end{aligned} \tag{3.25}$$

Where

$$F_r = P_r - P_{r-2}, \quad r = 2{,}3, ..., N \tag{3.26}$$

In a compact form the displacement field is given as follows:

$$\mathbf{u}^{(k)} = F_t \mathbf{u}_t^{(k)} + F_b \mathbf{u}_b^{(k)} + F_r \mathbf{u}_r^{(k)} = F_\tau \mathbf{u}_\tau^{(k)}, \quad \tau = t, b, r, \;\; r = 2{,}3, .., N \tag{3.27}$$

These higher-order expansions have been denoted by the acronyms LD2,LD3,...,LDN.

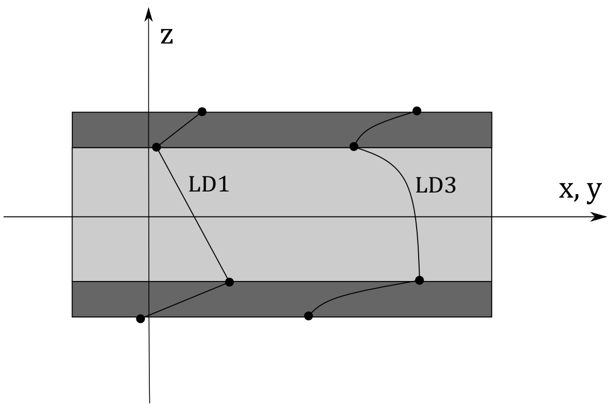

Figure 3.7: Linear and cubic Layer-wise expansions

Chapter 4

Theoretical Formulation

4.1 Geometric and constitutive relations in electro-mechanical problems

The features of multilayered composite plates geometry are shown in the figure 4.1. In the most general case the plate is composed of N_l layers which can be made of any kind of materials (piezoelectric or purely elastic). The integer k, used as superscript or subscript, identifies the layer number which starts from the bottom of the plate. The plate middle surface Ω coordinates are indicated by x and y while z is the thickness coordinate. Ω_k denotes the k-layer surface domain. z_k denotes the local thickness coordinate of each layer. According to the classical nomenclature used in literature, the length of the plate in the x and y direction is indicated by a and b, respectively, while h and h_k denote the plate and layer thicknesses. ζ_k is the dimensionless local layer-coordinate. A_k denotes the k-layer thickness domain. Symbols without the k subscript or superscripts refer to the whole plate.

The notation for the displacement and electric field vectors $\boldsymbol{u}^k$ and $\boldsymbol{E}^k$ are given as

$$\boldsymbol{u}^k = \begin{bmatrix} u_x \\ u_y \\ u_z \end{bmatrix}^k , \quad \boldsymbol{E}^k = \begin{bmatrix} E_x \\ E_y \\ E_z \end{bmatrix}^k \tag{4.1}$$

Consistently to the reference coordinate system the stress and strain vectors $\boldsymbol{\sigma}^k$ and $\boldsymbol{\epsilon}^k$ are indicated as follows

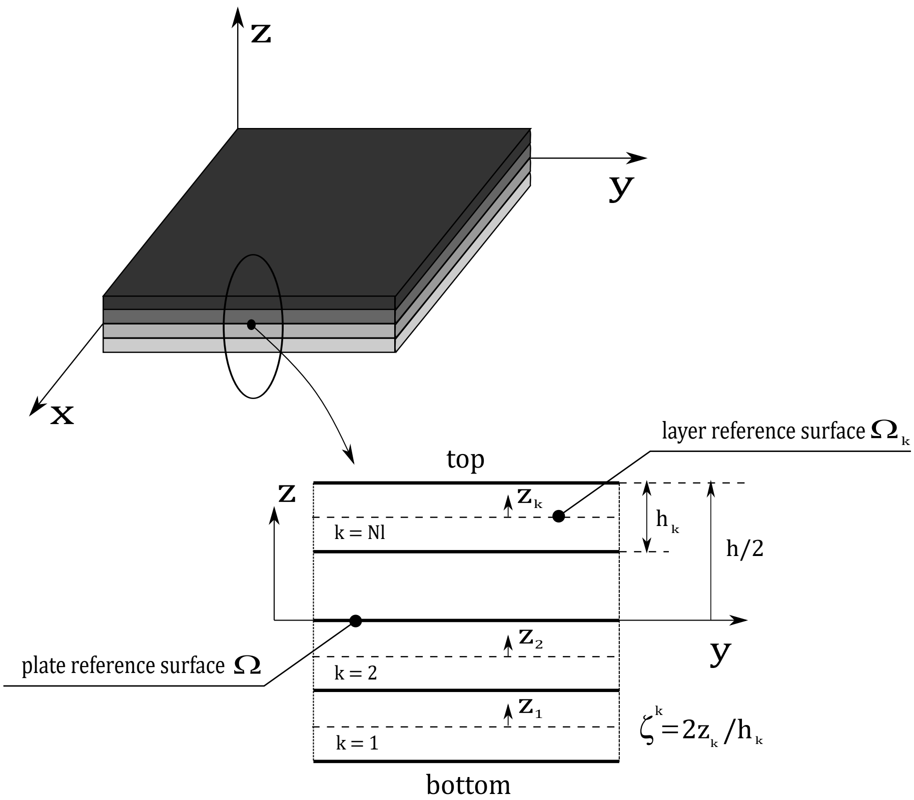

Figure 4.1: Multilayered composite plate geometry

$$\boldsymbol{\sigma}^k = \begin{bmatrix} \sigma_{xx} \\ \sigma_{yy} \\ \sigma_{xy} \\ \sigma_{xz} \\ \sigma_{yz} \\ \sigma_{zz} \end{bmatrix}^k , \quad \boldsymbol{\epsilon}^k = \begin{bmatrix} \epsilon_{xx} \\ \epsilon_{yy} \\ \gamma_{xy} \\ \gamma_{xz} \\ \gamma_{yz} \\ \epsilon_{zz} \end{bmatrix}^k \tag{4.2}$$

The strain-displacement relations are

$$\boldsymbol{\epsilon}^k = \boldsymbol{D}\boldsymbol{u}^k \tag{4.3}$$

where $\boldsymbol{D}$ is a differential matrix operator, defined as follows

$$\boldsymbol{D} = \begin{bmatrix} \frac{\partial}{\partial x} & 0 & 0 \\ 0 & \frac{\partial}{\partial y} & 0 \\ \frac{\partial}{\partial x} & \frac{\partial}{\partial y} & 0 \\ \frac{\partial}{\partial z} & 0 & \frac{\partial}{\partial x} \\ 0 & \frac{\partial}{\partial z} & \frac{\partial}{\partial y} \\ 0 & 0 & \frac{\partial}{\partial z} \end{bmatrix} \tag{4.4}$$

The electric field $\boldsymbol{E}^k$ is defined as the gradient of the electric potential Φ^k

$$\boldsymbol{E}^k = -\begin{bmatrix} \frac{\partial}{\partial x} \\ \frac{\partial}{\partial y} \\ \frac{\partial}{\partial z} \end{bmatrix} \Phi^k = \boldsymbol{D}_{pe}\Phi^k \tag{4.5}$$

In the laminate reference system, the constitutive equations for the kth layer take the following form

$$\begin{aligned} \boldsymbol{\sigma}^k &= \boldsymbol{C}^k \boldsymbol{\epsilon}^k - \boldsymbol{e}^{k^T} \boldsymbol{E}^k \\ \boldsymbol{D}^k &= \boldsymbol{e}^k \boldsymbol{\epsilon}^k + \boldsymbol{\varepsilon}^k \boldsymbol{E}^k \end{aligned} \tag{4.6}$$

where $\boldsymbol{\sigma}^k$ is the stress tensor, $\boldsymbol{\epsilon}^k$ is the linear strain tensor, $\boldsymbol{C}^k$ is the matrix of the elastic moduli and is given as

$$\boldsymbol{C}^k = \begin{bmatrix} C_{11} & C_{12} & C_{16} & 0 & 0 & C_{13} \\ C_{12} & C_{22} & C_{26} & 0 & 0 & C_{23} \\ C_{16} & C_{26} & C_{66} & 0 & 0 & C_{36} \\ 0 & 0 & 0 & C_{44} & C_{45} & 0 \\ 0 & 0 & 0 & C_{45} & C_{55} & 0 \\ C_{13} & C_{23} & C_{36} & 0 & 0 & C_{33} \end{bmatrix}^k \tag{4.7}$$

$\boldsymbol{e}^k$ is the matrix of the piezoelectric constants and assumes the following form

$$\boldsymbol{e}^k = \begin{bmatrix} 0 & 0 & 0 & e_{14} & e_{15} & 0 \\ 0 & 0 & 0 & e_{24} & e_{25} & 0 \\ e_{31} & e_{32} & e_{33} & 0 & 0 & e_{36} \end{bmatrix}^k \tag{4.8}$$

$\boldsymbol{D}^k$ is the vector of the electric displacement and $\boldsymbol{\varepsilon}^k$ is the permittivity matrix and is given as

$$\boldsymbol{\varepsilon}^k = \begin{bmatrix} \varepsilon_{11} & \varepsilon_{12} & 0 \\ \varepsilon_{12} & \varepsilon_{22} & 0 \\ 0 & 0 & \varepsilon_{33} \end{bmatrix}^k \tag{4.9}$$

4.2 Approximations of the mechanical displacement field and electric potential

As mentioned in Section 3.4 the unknown variables $\boldsymbol{u}^k$ and Φ^k can be expressed as a set of thickness functions that only depend on the thickness coordinate z and the associated variable depending on the in-plane coordinate x and y. The displacement field is assumed by using a generalized expansion that allows to develop both equivalent single layer and layer-wise analyses. Instead the approximation of the potential is restricted only to layer-wise formulation. In fact, due to the significant differences of the electric properties of each layer, the ESL description for the potential is not appropriate to cover these high gradients [16]. The most general displacement field and electric potential assume the following explicit form [5]

$$\begin{aligned}
u_x^k(x,y,z,t) &= \sum_{\tau_{u_x}=1}^{N_{u_x}} F_{\tau_{u_x}}(z)\, u^k_{x\tau_{u_x}}(x,y,t) \\
u_y^k(x,y,z,t) &= \sum_{\tau_{u_y}=1}^{N_{u_y}} F_{\tau_{u_y}}(z)\, u^k_{y\tau_{u_y}}(x,y,t) \\
u_z^k(x,y,z,t) &= \sum_{\tau_{u_z}=1}^{N_{u_z}} F_{\tau_{u_z}}(z)\, u^k_{y\tau_{u_z}}(x,y,t) \\
\Phi^k(x,y,z,t) &= \sum_{\tau_{\phi}=1}^{N_{\phi}} F_{\tau_{\phi}}(z)\, \Phi^k_{\tau_{\phi}}(x,y,t)
\end{aligned} \tag{4.10}$$

where $F_{\tau_{u_x}}$, $F_{\tau_{u_y}}$, $F_{\tau_{u_z}}$ and F_{τ_ϕ} are the thickness functions. According to this approach, the governing differential equations can be written in terms of fundamental nuclei, which are mathematically invariant with respect to both the expansion order and the kinematic description of the unknows. The expansion order of the potential N_ϕ is totally indipendent from the expansion of the displacement N_u, even if the two orders can be the same. In this case the superscript N_ϕ is omitted in the analysis.

4.3 Hamilton's principle

Hamilton's principle (HP) is assumed to derive the governing equations of the electro-mechanical problem in their weak form [33]. The approximated solution is then obtained by using the Hierarchical Trigonometric Ritz Formulation (HTRF) [31]. In its most general form HP can be written as

$$\int_{t_1}^{t_2} \delta\mathcal{L}^k \, dt = 0 \tag{4.11}$$

where δ is the variational operator, t_1 and t_2 are the initial and the generic instant of time. $\mathcal{L}^k$ is the Lagrangian for the kth layer and assumes the following form [30]

$$\mathcal{L}^k = T^k - \Pi^k \tag{4.12}$$

where T^k is the kinetic energy and Π^k is the total potential energy which includes strain energy, dielectric energy and the external work by point-loads.

$$\begin{gathered} T^k = \frac{1}{2}\int_{V^k} \rho^k \, \dot{\boldsymbol{u}}^{k^T} \dot{\boldsymbol{u}}^k \, dV^k \\ \Pi^k = U_{el}^k + U_d^k + V^k = \frac{1}{2}\int_{V^k} \boldsymbol{\epsilon}^{k^T} \boldsymbol{\sigma}^k \, dV^k - \frac{1}{2}\int_{V^k} \boldsymbol{E}^{k^T} \boldsymbol{D}^k \, dV^k - \sum_{p=1}^{P} \boldsymbol{u}_p^{k^T} \boldsymbol{F}_{\boldsymbol{p}}^k \end{gathered} \tag{4.13}$$

Substituting Eq. (4.12) in Eq. (4.11), HP becomes:

$$\delta\int_{t_1}^{t_2} \Pi^k \, dt - \delta\int_{t_1}^{t_2} T^k \, dt = 0 \tag{4.14}$$

where the variational form of the kinetic and potential energy can be rearranged as

$$\begin{gathered} \delta\int_{t_1}^{t_2} T^k \, dt = -\int_{t_1}^{t_2}\int_{V^k} \rho^k \delta\boldsymbol{u}^{k^T} \ddot{\boldsymbol{u}}^k \, dV^k dt \\ \delta\int_{t_1}^{t_2} \Pi^k \, dt = \int_{t_1}^{t_2}\int_{V^k} \delta\boldsymbol{\epsilon}^{k^T} \boldsymbol{\sigma}^k \, dV^k dt - \int_{t_1}^{t_2}\int_{V^k} \delta\boldsymbol{E}^{k^T} \boldsymbol{D}^k \, dV^k dt - \sum_{p=1}^{P} \delta\boldsymbol{u}_p^{k^T} \boldsymbol{F}_{\boldsymbol{p}}^k \end{gathered} \tag{4.15}$$

By coupling (4.6) in Eq. (4.14) HP becomes

$$
\begin{aligned}
&\int_{t_1}^{t_2}\int_{V^k}(\delta\boldsymbol{\epsilon}^{k^T}\boldsymbol{C}^k\boldsymbol{\epsilon}^k-\delta\boldsymbol{\epsilon}^{k^T}\boldsymbol{e}^{k^T}\boldsymbol{E}^k-\delta\boldsymbol{E}^{k^T}\boldsymbol{e}^k\boldsymbol{\epsilon}^k-\delta\boldsymbol{E}^{k^T}\boldsymbol{\varepsilon}^k\boldsymbol{E}^k)\;dV^k dt\\
&-\sum_{p=1}^{P}\delta\boldsymbol{u}_p^{k^T}\boldsymbol{F}_{\boldsymbol{p}}^k+\int_{t_1}^{t_2}\int_{V^k}(\rho^k\delta\boldsymbol{u}^{k^T}\ddot{\boldsymbol{u}}^k)\;dV^k dt=0
\end{aligned}
\tag{4.16}
$$

subtituting Eq. (4.3), (4.5) in Eq. (4.16) the variational form of Eq. (4.11) can be expressed in terms of the unknown variables $\boldsymbol{u}^k$ and Φ^k

$$
\begin{aligned}
&\int_{t_1}^{t_2}\int_{V^k}(\delta\boldsymbol{u}^{k^T}\boldsymbol{D}^T\boldsymbol{C}^k\boldsymbol{D}\boldsymbol{u}^k-\delta\boldsymbol{u}^{k^T}\boldsymbol{D}^T\boldsymbol{e}^{k^T}\boldsymbol{D}_{pe}\Phi^k-\delta\Phi^k\boldsymbol{D}_{pe}^T\boldsymbol{e}^k\boldsymbol{D}\boldsymbol{u}^k\\
&-\delta\Phi^k\boldsymbol{D}_{pe}^T\boldsymbol{\varepsilon}^k\boldsymbol{D}_{pe}\Phi^k)\;dV^k dt-\sum_{p=1}^{P}\delta\boldsymbol{u}_{p_i}^{k^T}\boldsymbol{F}_{\boldsymbol{p_i}}^k+\int_{t_1}^{t_2}\int_{V^k}(\rho^k\delta\boldsymbol{u}^{k^T}\ddot{\boldsymbol{u}}^k)\;dV^k dt=0
\end{aligned}
\tag{4.17}
$$

4.3.1 The Hierarchical Ritz Formulation

In the variational form of (4.17), the mechanical displacement field and electric potential field are unknown functions. To solve these unknowns numerically, it is necessary to use efficient numerical methods to approximate the mechanical displacement field and electric potential field. In this work the Hierarchical Trigonometric Ritz Formulation (HTRF) [34] is employed to derive the GDEs in their weak form. In the Ritz method the displacement vector $\boldsymbol{u}^k$ and the potential Φ^k are expressed in series expansion and assume the following explicit form [32].

$$
\begin{aligned}
u_x^k(x,y,z,t)&=\sum_{i=1}^{\mathcal{N}}\sum_{\tau_{u_x}=1}^{N_{u_x}}U_{x\tau_{u_x}i}^k(t)\,F_{\tau_{u_x}}(z)\,\psi_{x_i}(x,y)\\
u_y^k(x,y,z,t)&=\sum_{i=1}^{\mathcal{N}}\sum_{\tau_{u_y}=1}^{N_{u_y}}U_{y\tau_{u_y}i}^k(t)\,F_{\tau_{u_y}}(z)\,\psi_{y_i}(x,y)\\
u_z^k(x,y,z,t)&=\sum_{i=1}^{\mathcal{N}}\sum_{\tau_{u_z}=1}^{N_{u_z}}U_{z\tau_{u_z}i}^k(t)\,F_{\tau_{u_z}}(z)\,\psi_{z_i}(x,y)\\
\Phi^k(x,y,z,t)&=\sum_{i=1}^{\mathcal{N}}\sum_{\tau_{\phi}=1}^{N_{\phi}}\Phi_{\tau_\phi i}^k(t)\,F_{\tau_{\phi}}(z)\,\psi_{\phi_i}(x,y)
\end{aligned}
\tag{4.18}
$$

where $\mathcal{N}$ indicates the order of expansion in the Ritz approximation, $U_{x\tau_{u_x}i}$, $U_{y\tau_{u_y}i}$, $U_{z\tau_{u_z}i}$, $\Phi_{\tau_\phi i}$ are the time-dependent unknown coefficients and ψ_{x_i}, ψ_{y_i}, ψ_{z_i}, ψ_{ϕ_i}

are the Ritz functions appropriately selected with respect to the features of the problem under investigation. Convergence to the exact solution is guaranteed if the Ritz functions are admissible functions in the used variational principle. Highly stable trigonometric functions are assumed as trial functions. The harmonic assumptions used for the displacements and the electric potential are

$$
\begin{aligned}
\psi_{x_{mn}} &= \sum_{m=1}^{M}\sum_{n=1}^{N} \cos\left(\frac{m\pi x}{a}\right)\sin\left(\frac{n\pi y}{b}\right) \\
\psi_{y_{mn}} &= \sum_{m=1}^{M}\sum_{n=1}^{N} \sin\left(\frac{m\pi x}{a}\right)\cos\left(\frac{n\pi y}{b}\right) \\
\psi_{z_{mn}} &= \sum_{m=1}^{M}\sum_{n=1}^{N} \sin\left(\frac{m\pi x}{a}\right)\sin\left(\frac{n\pi y}{b}\right) \\
\psi_{\phi_{mn}} &= \sum_{m=1}^{M}\sum_{n=1}^{N} \sin\left(\frac{m\pi x}{a}\right)\sin\left(\frac{n\pi y}{b}\right)
\end{aligned}
\tag{4.19}
$$

It is known that in Ritz family methods, adoption of a shape function depends only on the essential boundary conditions. In this case on each edge of the plate either electric potential and the displacements should be equal to zero to satisfy simply supported condition and grounded condition, respectively. The armonic displacement and potential field of Eq. (4.18) can be expressed in a compact way as

$$
\begin{aligned}
\boldsymbol{u}^k &= \boldsymbol{F}_\tau \boldsymbol{\Psi}_{u_i} \boldsymbol{U}^k_{\tau i} \\
\Phi^k &= F_{\tau_\phi} \psi_{\phi_i} \Phi^k_{\tau_\phi i}
\end{aligned}
\tag{4.20}
$$

Where:

$$
\boldsymbol{U}^k_{\tau i} = \begin{bmatrix} U^k_{x\tau_{u_x} i} \\ U^k_{y\tau_{u_y} i} \\ U^k_{z\tau_{u_z} i} \end{bmatrix}, \boldsymbol{\Psi}_{u_i} = \begin{bmatrix} \psi_{x_i} & 0 & 0 \\ 0 & \psi_{y_i} & 0 \\ 0 & 0 & \psi_{z_i} \end{bmatrix}, \boldsymbol{F}_\tau = \begin{bmatrix} F_{\tau_{u_x}} & 0 & 0 \\ 0 & F_{\tau_{u_y}} & 0 \\ 0 & 0 & F_{\tau_{u_z}} \end{bmatrix}
\tag{4.21}
$$

4.3.2 Fundamental Nuclei

Substituting Eq. (4.20) in Eq. (4.17), the variational form of the total potential energy and the kinetic energy become

$$
\begin{aligned}
\delta\Pi^k = {} & \delta \boldsymbol{U}_{\tau i}^{k^T} \int_{\Omega_k}\int_{A_k} [\boldsymbol{D}(\boldsymbol{F}_\tau \boldsymbol{\Psi}_{u_i})]^T \boldsymbol{C}^k \boldsymbol{D}\boldsymbol{F}_\tau \boldsymbol{\Psi}_{u_i}\, dA_k d\Omega_k \boldsymbol{U}_{sj}^k \\
& - \delta \boldsymbol{U}_{\tau i}^{k^T} \int_{\Omega_k}\int_{A_k} [\boldsymbol{D}(\boldsymbol{F}_\tau \boldsymbol{\Psi}_{u_i})]^T \boldsymbol{e}^{k^T} \boldsymbol{D}_{pe} F_{s_\phi}\psi_{\phi_j}\, dA_k d\Omega_k \Phi_{s_\phi j}^k \\
& - \delta \Phi_{\tau_\psi i}^{k^T} \int_{\Omega_k}\int_{A_k} [\boldsymbol{D}_{pe} F_{\tau_\phi}\psi_{\phi_i}]^T \boldsymbol{e}^k \boldsymbol{D}\boldsymbol{F}_s \boldsymbol{\Psi}_{u_j}\, dA_k d\Omega_k \boldsymbol{U}_{sj}^k \\
& - \delta \Phi_{\tau_\psi i}^{k^T} \int_{\Omega_k}\int_{A_k} [\boldsymbol{D}_{pe} F_{\tau_\phi}\psi_{\phi_i}]^T \boldsymbol{\varepsilon}^k \boldsymbol{D}_{pe} F_{s_\phi}\psi_{\phi_j}\, dA_k d\Omega_k \Phi_{s_\phi}^k \\
& - \delta \boldsymbol{U}_{\tau i}^{k^T} \sum_{p=1}^{P} \boldsymbol{F_{\tau p}} \boldsymbol{\Psi_{u_i p}} \boldsymbol{F}_p
\end{aligned}
\tag{4.22}
$$

$$
\delta T^k = -\delta \boldsymbol{U}_{\tau i}^{k^T} \int_{\Omega_k}\int_{A_k} [\rho^k (\boldsymbol{F}_\tau \boldsymbol{\Psi}_{u_i})^T (\boldsymbol{F}_s \boldsymbol{\Psi}_{u_j})]\, dA_k d\Omega_k \ddot{\boldsymbol{U}}_{sj}^k
$$

The compact form of Eq. (4.22) is

$$
\begin{aligned}
\delta\Pi^k = {} & \delta \boldsymbol{U}_{\tau i}^{k^T} \boldsymbol{K}_{uu}^{k\tau sij} \boldsymbol{U}_{sj}^k + \delta \boldsymbol{U}_{\tau i}^{k^T} \boldsymbol{K}_{u\phi}^{k\tau sij} \Phi_{s_\phi j}^k \\
& + \delta \Phi_{\tau_\psi i}^{k^T} \boldsymbol{K}_{\phi u}^{k\tau sij} \boldsymbol{U}_{sj}^k + \delta \Phi_{\tau_\psi i}^{k^T} \boldsymbol{K}_{\phi\phi}^{k\tau sij} \Phi_{s_\phi j}^k - \delta \boldsymbol{U}_{\tau i}^{k^T} \boldsymbol{F}_{sj} \\
\delta T^k = {} & -\delta \boldsymbol{U}_{\tau i}^{k^T} \boldsymbol{M}^{k\tau sij} \ddot{\boldsymbol{U}}_{sj}^k
\end{aligned}
\tag{4.23}
$$

the Ritz primary fundamental nuclei are obtained:

$$
\begin{aligned}
\boldsymbol{K}_{uu}^{k\tau sij} &= \int_{\Omega_k}\int_{A_k} [\boldsymbol{D}(\boldsymbol{F}_\tau \boldsymbol{\Psi}_{u_i})]^T \boldsymbol{C}^k \boldsymbol{D}\boldsymbol{F}_\tau \boldsymbol{\Psi}_{u_i}\, dA_k d\Omega_k \\
\boldsymbol{K}_{u\phi}^{k\tau sij} &= -\int_{\Omega_k}\int_{A_k} [\boldsymbol{D}(\boldsymbol{F}_\tau \boldsymbol{\Psi}_{u_i})]^T \boldsymbol{e}^{k^T} \boldsymbol{D}_{pe} F_{s_\phi}\psi_{\phi_j}\, dA_k d\Omega_k \\
\boldsymbol{K}_{\phi u}^{k\tau sij} &= -\int_{\Omega_k}\int_{A_k} [\boldsymbol{D}_{pe} F_{\tau_\phi}\psi_{\phi_i}]^T \boldsymbol{e}^k \boldsymbol{D}\boldsymbol{F}_s \boldsymbol{\Psi}_{u_j}\, dA_k d\Omega_k \\
\boldsymbol{K}_{\phi\phi}^{k\tau sij} &= -\int_{\Omega_k}\int_{A_k} [\boldsymbol{D}_{pe} F_{\tau_\phi}\psi_{\phi_i}]^T \boldsymbol{\varepsilon}^k \boldsymbol{D}_{pe} F_{s_\phi}\psi_{\phi_j}\, dA_k d\Omega_k \\
\boldsymbol{M}^{k\tau sij} &= \int_{\Omega_k}\int_{A_k} [\rho^k (\boldsymbol{F}_\tau \boldsymbol{\Psi}_{u_i})^T (\boldsymbol{F}_s \boldsymbol{\Psi}_{u_j})]\, dA_k d\Omega_k
\end{aligned}
\tag{4.24}
$$

where $\boldsymbol{M}^{k\tau sij}$ is the mass fundamental nucleus, $\boldsymbol{K}_{uu}^{k\tau sij}$ is the stiffness fundamental nucleus, $\boldsymbol{K}_{u\phi}^{k\tau sij}$ and $\boldsymbol{K}_{\phi\phi}^{k\tau sij}$ are the piezoelectric and permettivity fundamental nuclei respectively.

Table 4.1: Dimensions of the fundamental nuclei

Fundamental Nucleus	Dimension
$\boldsymbol{K}_{uu}^{k\tau sij}$	$[3 \times 3]$
$\boldsymbol{K}_{u\phi}^{k\tau sij}$	$[3 \times 1]$
$\boldsymbol{K}_{\phi u}^{k\tau sij}$	$[1 \times 3]$
$\boldsymbol{K}_{\phi\phi}^{k\tau sij}$	$[1 \times 1]$
$\boldsymbol{M}^{k\tau sij}$	$[3 \times 3]$

The explicit forms of the secondary stiffness, piezoelectric, permettivity and mass fundamental nuclei are following reported:

$$
\begin{aligned}
\boldsymbol{K}_{u_x u_x}^{\tau_{u_x} s_{u_x}} = C_{11}^k & \left[\int_{A_k} (F_{\tau_{u_x}} F_{s_{u_x}})\, dz\right]\left[\int_{\Omega_k} (\psi_{x_i,x}\psi_{x_j,x})\, d\Omega_k\right] \\
& + C_{16}^k \left[\int_{A_k} (F_{\tau_{u_x}} F_{s_{u_x}})\, dz\right]\left[\int_{\Omega_k} (\psi_{x_i,x}\psi_{x_j,y})\, d\Omega_k\right] \\
& + C_{16}^k \left[\int_{A_k} (F_{\tau_{u_x}} F_{s_{u_x}})\, dz\right]\left[\int_{\Omega_k} (\psi_{x_i,y}\psi_{x_j,x})\, d\Omega_k\right] \\
& + C_{66}^k \left[\int_{A_k} (F_{\tau_{u_x}} F_{s_{u_x}})\, dz\right]\left[\int_{\Omega_k} (\psi_{x_i,y}\psi_{x_j,y})\, d\Omega_k\right] \\
& + C_{55}^k \left[\int_{A_k} (F_{\tau_{u_x},z} F_{s_{u_x},z})\, dz\right]\left[\int_{\Omega_k} (\psi_{x_i}\psi_{x_j})\, d\Omega_k\right]
\end{aligned}
$$

$$
\begin{aligned}
\boldsymbol{K}_{u_x u_y}^{\tau_{u_x} s_{u_y}} &= C_{16}^k \left[\int_{A_k} (F_{\tau_{u_x}} F_{s_{u_y}})\, dz \right] \left[\int_{\Omega_k} (\psi_{x_i,x} \psi_{y_j,x})\, d\Omega_k \right] \\
&+ C_{12}^k \left[\int_{A_k} (F_{\tau_{u_x}} F_{s_{u_y}})\, dz \right] \left[\int_{\Omega_k} (\psi_{x_i,x} \psi_{y_j,y})\, d\Omega_k \right] \\
&+ C_{66}^k \left[\int_{A_k} (F_{\tau_{u_x}} F_{s_{u_y}})\, dz \right] \left[\int_{\Omega_k} (\psi_{x_i,y} \psi_{y_j,x})\, d\Omega_k \right] \\
&+ C_{26}^k \left[\int_{A_k} (F_{\tau_{u_x}} F_{s_{u_y}})\, dz \right] \left[\int_{\Omega_k} (\psi_{x_i,y} \psi_{y_j,y})\, d\Omega_k \right] \\
&+ C_{45}^k \left[\int_{A_k} (F_{\tau_{u_x},z} F_{s_{u_y},z})\, dz \right] \left[\int_{\Omega_k} (\psi_{x_i} \psi_{y_j})\, d\Omega_k \right]
\end{aligned}
$$

$$
\begin{aligned}
\boldsymbol{K}_{u_x u_z}^{\tau_{u_x} s_{u_z}} &= C_{55}^k \left[\int_{A_k} (F_{\tau_{u_x},z} F_{s_{u_z}})\, dz \right] \left[\int_{\Omega_k} (\psi_{x_i} \psi_{z_j,x})\, d\Omega_k \right] \\
&+ C_{45}^k \left[\int_{A_k} (F_{\tau_{u_x},z} F_{s_{u_z}})\, dz \right] \left[\int_{\Omega_k} (\psi_{x_i} \psi_{z_j,y})\, d\Omega_k \right] \\
&+ C_{13}^k \left[\int_{A_k} (F_{\tau_{u_x}} F_{s_{u_z},z})\, dz \right] \left[\int_{\Omega_k} (\psi_{x_i,x} \psi_{z_j})\, d\Omega_k \right] \\
&+ C_{36}^k \left[\int_{A_k} (F_{\tau_{u_x}} F_{s_{u_z},z})\, dz \right] \left[\int_{\Omega_k} (\psi_{x_i,y} \psi_{z_j})\, d\Omega_k \right]
\end{aligned}
$$

$$
\begin{aligned}
\boldsymbol{K}_{u_y u_x}^{\tau_{u_y} s_{u_x}} &= C_{16}^k \left[\int_{A_k} (F_{\tau_{u_y}} F_{s_{u_x}})\, dz \right] \left[\int_{\Omega_k} (\psi_{y_i,x} \psi_{x_j,x})\, d\Omega_k \right] \\
&+ C_{12}^k \left[\int_{A_k} (F_{\tau_{u_y}} F_{s_{u_x}})\, dz \right] \left[\int_{\Omega_k} (\psi_{y_i,y} \psi_{x_j,x})\, d\Omega_k \right] \\
&+ C_{66}^k \left[\int_{A_k} (F_{\tau_{u_y}} F_{s_{u_x}})\, dz \right] \left[\int_{\Omega_k} (\psi_{y_i,x} \psi_{x_j,y})\, d\Omega_k \right] \\
&+ C_{26}^k \left[\int_{A_k} (F_{\tau_{u_y}} F_{s_{u_x}})\, dz \right] \left[\int_{\Omega_k} (\psi_{y_i,y} \psi_{x_j,y})\, d\Omega_k \right] \\
&+ C_{45}^k \left[\int_{A_k} (F_{\tau_{u_y},z} F_{s_{u_x},z})\, dz \right] \left[\int_{\Omega_k} (\psi_{y_i} \psi_{x_j})\, d\Omega_k \right]
\end{aligned}
$$

$$
\begin{aligned}
\boldsymbol{K}_{u_y u_y}^{\tau_{u_y} s_{u_y}} &= C_{26}^k \left[\int_{A_k} (F_{\tau_{u_y}} F_{s_{u_y}})\, dz \right] \left[\int_{\Omega_k} (\psi_{y_i,y} \psi_{y_j,x})\, d\Omega_k \right] \\
&+ C_{22}^k \left[\int_{A_k} (F_{\tau_{u_y}} F_{s_{u_y}})\, dz \right] \left[\int_{\Omega_k} (\psi_{y_i,y} \psi_{y_j,y})\, d\Omega_k \right] \\
&+ C_{66}^k \left[\int_{A_k} (F_{\tau_{u_y}} F_{s_{u_y}})\, dz \right] \left[\int_{\Omega_k} (\psi_{y_i,y} \psi_{y_j,x})\, d\Omega_k \right] \\
&+ C_{26}^k \left[\int_{A_k} (F_{\tau_{u_y}} F_{s_{u_y}})\, dz \right] \left[\int_{\Omega_k} (\psi_{y_i,y} \psi_{y_j,y})\, d\Omega_k \right] \\
&+ C_{44}^k \left[\int_{A_k} (F_{\tau_{u_y},z} F_{s_{u_y},z})\, dz \right] \left[\int_{\Omega_k} (\psi_{y_i} \psi_{y_j})\, d\Omega_k \right]
\end{aligned}
$$

$$
\begin{aligned}
\boldsymbol{K}_{u_y u_z}^{\tau_{u_y} s_{u_z}} &= C_{45}^k \left[\int_{A_k} (F_{\tau_{u_y},z} F_{s_{u_z}})\, dz \right] \left[\int_{\Omega_k} (\psi_{y_i} \psi_{z_j,x})\, d\Omega_k \right] \\
&+ C_{44}^k \left[\int_{A_k} (F_{\tau_{u_y},z} F_{s_{u_z}})\, dz \right] \left[\int_{\Omega_k} (\psi_{y_i} \psi_{z_j,y})\, d\Omega_k \right] \\
&+ C_{36}^k \left[\int_{A_k} (F_{\tau_{u_y}} F_{s_{u_z},z})\, dz \right] \left[\int_{\Omega_k} (\psi_{y_i,x} \psi_{z_j})\, d\Omega_k \right] \\
&+ C_{23}^k \left[\int_{A_k} (F_{\tau_{u_y}} F_{s_{u_z},z})\, dz \right] \left[\int_{\Omega_k} (\psi_{y_i,y} \psi_{z_j})\, d\Omega_k \right]
\end{aligned}
$$

$$
\begin{aligned}
\boldsymbol{K}_{u_z u_x}^{\tau_{u_z} s_{u_x}} &= C_{55}^k \left[\int_{A_k} (F_{\tau_{u_z}} F_{s_{u_x},z})\, dz \right] \left[\int_{\Omega_k} (\psi_{z_i,x} \psi_{x_j})\, d\Omega_k \right] \\
&+ C_{45}^k \left[\int_{A_k} (F_{\tau_{u_z}} F_{s_{u_x},z})\, dz \right] \left[\int_{\Omega_k} (\psi_{z_i,y} \psi_{x_j})\, d\Omega_k \right] \\
&+ C_{13}^k \left[\int_{A_k} (F_{\tau_{u_z},z} F_{s_{u_x}})\, dz \right] \left[\int_{\Omega_k} (\psi_{z_i} \psi_{x_j,x})\, d\Omega_k \right] \\
&+ C_{36}^k \left[\int_{A_k} (F_{\tau_{u_z},z} F_{s_{u_x}})\, dz \right] \left[\int_{\Omega_k} (\psi_{z_i} \psi_{x_j,y})\, d\Omega_k \right]
\end{aligned}
$$

$$\boldsymbol{K}_{u_z u_y}^{\tau_{u_z} s_{u_y}} = C_{45}^k \left[\int_{A_k} (F_{\tau_{u_z}} F_{s_{u_y},z})\, dz \right] \left[\int_{\Omega_k} (\psi_{z_i,x} \psi_{y_j})\, d\Omega_k \right]$$
$$+ C_{44}^k \left[\int_{A_k} (F_{\tau_{u_z}} F_{s_{u_y},z})\, dz \right] \left[\int_{\Omega_k} (\psi_{z_i,y} \psi_{y_j})\, d\Omega_k \right]$$
$$+ C_{36}^k \left[\int_{A_k} (F_{\tau_{u_z},z} F_{s_{u_y}})\, dz \right] \left[\int_{\Omega_k} (\psi_{z_i} \psi_{y_j,x})\, d\Omega_k \right]$$
$$+ C_{23}^k \left[\int_{A_k} (F_{\tau_{u_z},z} F_{s_{u_y}})\, dz \right] \left[\int_{\Omega_k} (\psi_{z_i} \psi_{y_j,y})\, d\Omega_k \right]$$

$$\boldsymbol{K}_{u_z u_z}^{\tau_{u_z} s_{u_z}} = C_{45}^k \left[\int_{A_k} (F_{\tau_{u_z}} F_{s_{u_z}})\, dz \right] \left[\int_{\Omega_k} (\psi_{z_i,y} \psi_{z_j,x})\, d\Omega_k \right]$$
$$+ C_{44}^k \left[\int_{A_k} (F_{\tau_{u_z}} F_{s_{u_z}})\, dz \right] \left[\int_{\Omega_k} (\psi_{z_i,y} \psi_{z_j,y})\, d\Omega_k \right]$$
$$+ C_{55}^k \left[\int_{A_k} (F_{\tau_{u_z}} F_{s_{u_z}})\, dz \right] \left[\int_{\Omega_k} (\psi_{z_i,x} \psi_{z_j,x})\, d\Omega_k \right]$$
$$+ C_{45}^k \left[\int_{A_k} (F_{\tau_{u_z}} F_{s_{u_z}})\, dz \right] \left[\int_{\Omega_k} (\psi_{z_i,x} \psi_{z_j,y})\, d\Omega_k \right]$$
$$+ C_{33}^k \left[\int_{A_k} (F_{\tau_{u_z},z} F_{s_{u_z},z})\, dz \right] \left[\int_{\Omega_k} (\psi_{z_i} \psi_{z_j})\, d\Omega_k \right]$$

$$\boldsymbol{K}_{u_x \phi}^{\tau_{u_x} s_{\phi}} = e_{31}^k \left[\int_{A_k} (F_{\tau_{u_x}} F_{s_{\phi},z})\, dz \right] \left[\int_{\Omega_k} (\psi_{x_i,x} \psi_{\phi_j})\, d\Omega_k \right]$$
$$+ e_{36}^k \left[\int_{A_k} (F_{\tau_{u_x}} F_{s_{\phi},z})\, dz \right] \left[\int_{\Omega_k} (\psi_{x_i,y} \psi_{\phi_j})\, d\Omega_k \right]$$
$$+ e_{14}^k \left[\int_{A_k} (F_{\tau_{u_x},z} F_{s_{\phi}})\, dz \right] \left[\int_{\Omega_k} (\psi_{x_i} \psi_{\phi_j,x})\, d\Omega_k \right]$$
$$+ e_{24}^k \left[\int_{A_k} (F_{\tau_{u_x},z} F_{s_{\phi}})\, dz \right] \left[\int_{\Omega_k} (\psi_{x_i} \psi_{\phi_j,y})\, d\Omega_k \right]$$

$$\begin{aligned}
\boldsymbol{K}^{\tau_{u_y} s_\phi}_{u_y\phi} &= e^k_{32}\left[\int_{A_k}(F_{\tau_{u_y}}F_{s_\phi,z})\,dz\right]\left[\int_{\Omega_k}(\psi_{y_i,y}\psi_{\phi_j})\,d\Omega_k\right]\\
&+ e^k_{36}\left[\int_{A_k}(F_{\tau_{u_y}}F_{s_\phi,z})\,dz\right]\left[\int_{\Omega_k}(\psi_{y_i,x}\psi_{\phi_j})\,d\Omega_k\right]\\
&+ e^k_{15}\left[\int_{A_k}(F_{\tau_{u_y},z}F_{s_\phi})\,dz\right]\left[\int_{\Omega_k}(\psi_{y_i}\psi_{\phi_j,x})\,d\Omega_k\right]\\
&+ e^k_{25}\left[\int_{A_k}(F_{\tau_{u_y},z}F_{s_\phi})\,dz\right]\left[\int_{\Omega_k}(\psi_{y_i}\psi_{\phi_j,y})\,d\Omega_k\right]
\end{aligned}$$

$$\begin{aligned}
\boldsymbol{K}^{\tau_{u_z} s_\phi}_{u_z\phi} &= e^k_{14}\left[\int_{A_k}(F_{\tau_{u_z}}F_{s_\phi})\,dz\right]\left[\int_{\Omega_k}(\psi_{z_i,x}\psi_{\phi_j,x})\,d\Omega_k\right]\\
&+ e^k_{24}\left[\int_{A_k}(F_{\tau_{u_z}}F_{s_\phi})\,dz\right]\left[\int_{\Omega_k}(\psi_{z_i,x}\psi_{\phi_j,y})\,d\Omega_k\right]\\
&+ e^k_{15}\left[\int_{A_k}(F_{\tau_{u_z}}F_{s_\phi})\,dz\right]\left[\int_{\Omega_k}(\psi_{z_i,y}\psi_{\phi_j,x})\,d\Omega_k\right]\\
&+ e^k_{25}\left[\int_{A_k}(F_{\tau_{u_z}}F_{s_\phi})\,dz\right]\left[\int_{\Omega_k}(\psi_{z_i,y}\psi_{\phi_j,y})\,d\Omega_k\right]\\
&+ e^k_{33}\left[\int_{A_k}(F_{\tau_{u_z},z}F_{s_\phi,z})\,dz\right]\left[\int_{\Omega_k}(\psi_{z_i}\psi_{\phi_j})\,d\Omega_k\right]
\end{aligned}$$

$$\begin{aligned}
\boldsymbol{K}^{\tau_\phi s_\phi}_{\phi\phi} &= \varepsilon^k_{11}\left[\int_{A_k}(F_{\tau_\phi}F_{s_\phi})\,dz\right]\left[\int_{\Omega_k}(\psi_{\phi_i,x}\psi_{\phi_j,x})\,d\Omega_k\right]\\
&+ \varepsilon^k_{12}\left[\int_{A_k}(F_{\tau_\phi}F_{s_\phi})\,dz\right]\left[\int_{\Omega_k}(\psi_{\phi_i,x}\psi_{\phi_j,y})\,d\Omega_k\right]\\
&+ \varepsilon^k_{21}\left[\int_{A_k}(F_{\tau_\phi}F_{s_\phi})\,dz\right]\left[\int_{\Omega_k}(\psi_{\phi_i,y}\psi_{\phi_j,x})\,d\Omega_k\right]\\
&+ \varepsilon^k_{22}\left[\int_{A_k}(F_{\tau_\phi}F_{s_\phi})\,dz\right]\left[\int_{\Omega_k}(\psi_{\phi_i,y}\psi_{\phi_j,y})\,d\Omega_k\right]\\
&+ \varepsilon^k_{33}\left[\int_{A_k}(F_{\tau_\phi,z}F_{s_\phi,z})\,dz\right]\left[\int_{\Omega_k}(\psi_{\phi_i}\psi_{\phi_j})\,d\Omega_k\right]
\end{aligned}$$

$$
\begin{aligned}
\boldsymbol{M}_{u_x u_x}^{\tau_{u_x} s_{u_x}} &= \rho^k \left[\int_{A_k} (F_{\tau_{u_x}} F_{s_{u_x}})\, dz \right] \left[\int_{\Omega_k} (\psi_{x_i} \psi_{x_j})\, d\Omega_k \right] \\
\boldsymbol{M}_{u_y u_y}^{\tau_{u_y} s_{u_y}} &= \rho^k \left[\int_{A_k} (F_{\tau_{u_y}} F_{s_{u_y}})\, dz \right] \left[\int_{\Omega_k} (\psi_{y_i} \psi_{y_j})\, d\Omega_k \right] \\
\boldsymbol{M}_{u_z u_z}^{\tau_{u_z} s_{u_z}} &= \rho^k \left[\int_{A_k} (F_{\tau_{u_z}} F_{s_{u_z}})\, dz \right] \left[\int_{\Omega_k} (\psi_{z_i} \psi_{z_j})\, d\Omega_k \right]
\end{aligned}
\tag{4.25}
$$

4.3.3 Weak form of the governing equations

The minimization of the total energy of Eq. (4.14) leads to the equation:

$$\delta \Pi^k - \delta T^k = 0 \tag{4.26}$$

Now coupling Eq. (4.26) with Eq. (4.23) and considering that virtual variations are independent and arbitrary, the discrete form of two set of governing differential equations in terms of fundamental primary nuclei are obtained:

$$
\begin{aligned}
\delta \boldsymbol{U}_{\tau i}^{k^T} &: \quad \boldsymbol{M}^{k\tau s ij} \ddot{\boldsymbol{U}}_{sj}^k + \boldsymbol{K}_{uu}^{k\tau s ij} \boldsymbol{U}_{sj}^k + \boldsymbol{K}_{u\phi}^{k\tau s ij} \Phi_{s_\phi j}^k = \boldsymbol{F}_{sj} \\
\delta \Phi_{\tau i}^{k^T} &: \quad \boldsymbol{K}_{\phi u}^{k\tau s ij} \boldsymbol{U}_{sj}^k + \boldsymbol{K}_{\phi\phi}^{k\tau s ij} \Phi_{s_\phi j}^k = 0
\end{aligned}
\tag{4.27}
$$

Once the fundamental nuclei have been assembled at structure level as widely discussed in [32], the governing equations take the following form:

$$
\begin{aligned}
&\boldsymbol{M}\ddot{\boldsymbol{U}} + \boldsymbol{K}_{uu}\boldsymbol{U} + \boldsymbol{K}_{u\phi}\boldsymbol{\Phi} = \boldsymbol{F} \\
&\boldsymbol{K}_{\phi u}\boldsymbol{U} + \boldsymbol{K}_{\phi\phi}\boldsymbol{\Phi} = 0
\end{aligned}
\tag{4.28}
$$

where $\boldsymbol{U}$ and $\boldsymbol{\Phi}$ are the vectors of the unknown degrees of freedom related to the elctro-mechanical problem.

4.3.4 Free vibration problem

The free-vibration response of the multilayered plate, by assuming a simple armonic expansion of the variables in the time domain $\boldsymbol{U} = \hat{\boldsymbol{U}} e^{i\omega t}$, $\boldsymbol{\Phi} = \hat{\boldsymbol{\Phi}} e^{i\omega t}$, leads to the following eigenvalues problem:

$$(\boldsymbol{K}_{uu}^* - \omega^2 \boldsymbol{M}) \hat{\boldsymbol{U}} = 0 \tag{4.29}$$

where $\boldsymbol{K}_{uu}^*$ is the stiffness matrix, obtained applying the static condensation procedure [30]. This procedure requires to solve the second equation of the system in Eq. (4.27) which leads to the expression:

$$\boldsymbol{K}^{*}_{uu} = \boldsymbol{K}_{uu} - \boldsymbol{K}_{u\phi}\boldsymbol{K}^{-1}_{\phi\phi}\boldsymbol{K}_{\phi u} \tag{4.30}$$

The static condensation has been computed for different advanced theories. Eq. (4.29) is associated to the natural frequencies of an open circuit (OC) plate integrated with piezoelectric layers. On the other hand, dealing with a closed circuit condition (CC), it is assumed that piezoelectric layers are grounded and the electric potential at the free surfaces is identically zero. Therefore, for closed circuit condition, natural frequencies are obtained by set to zero the potential degrees of freedom at the top and bottom surfaces.

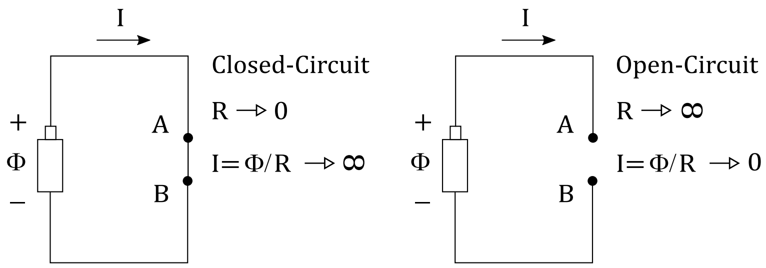

Figure 4.2: Electrical boundary conditions

4.4 Dynamic response and Active vibration control of CNT-RC plates with piezoelectric sensor and actuator layers

A laminated FG-CNTRC plate, embedded with piezoelectric layers at the bottom and top surfaces as shown in 4.4, is considered in this section. The top layer is a piezoelectric actuator denoted with subscript a and the bottom layer is a piezoelectric sensor labeled with subscript s.

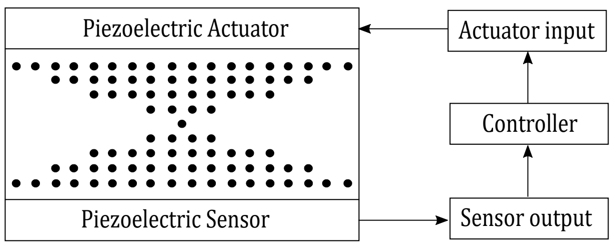

Figure 4.3: A schematic diagram of a FG-CNTRC plate with integrated piezoelectric sensors and actuators

4.4.1 Velocity feedback control algorithm

The distributed piezoelectric sensing layer monitors the structural oscillation due to the direct piezoelectric effect and the distributed actuator layer suppresses the oscillation via the converse piezoelectric effect. The velocity feedback control approach is employed for the active vibration control of each functionally graded CNTRC plate which can give a velocity component by using an appropriate electronic circuit [14]. When applying any external mechanical force, the composite plate undergoes deformation. Due to this deformation, a sensor output voltage is generated and is sent to the controller. The latter amplifies the sensor voltage and sends it to the actuator as input voltage. Due to the converse piezoelectric effect, stress and strains are generated. A resultant force, which actively suppresses and controls the vibration, is generated. The constant gain velocity feedback G_v is used to couple the input actuator voltage vector $\mathbf{\Phi}_a$ and the output sensor voltage as follows

$$\mathbf{\Phi}_a = G_v \dot{\mathbf{\Phi}}_s \tag{4.31}$$

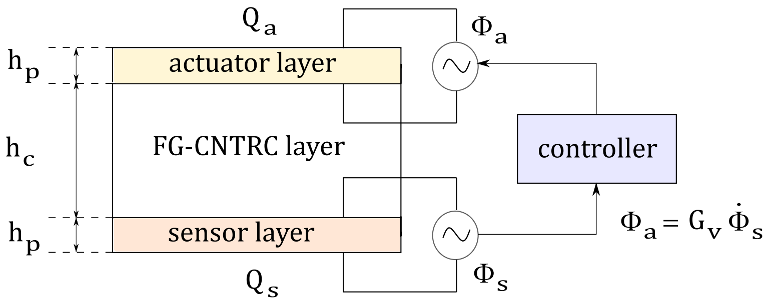

Figure 4.4: Close-loop control diagram

When there is no external charge $\boldsymbol{Q}$, the output voltage from the piezoelectric layer is obtained from the second equation of the system (4.28) as

$$\mathbf{\Phi}_s = -\boldsymbol{K}_{\phi\phi}^{s^{-1}} \boldsymbol{K}_{\phi u}^{s} \boldsymbol{U}_s \tag{4.32}$$

The sensor charge caused by deformation is given as

$$\boldsymbol{Q}_s = -\boldsymbol{K}_{\phi u}^{s} \boldsymbol{U}_s \tag{4.33}$$

When an electric charge $\boldsymbol{Q}$ occurs as external load, Eq. (4.28) become

$$\begin{aligned} \boldsymbol{M}\ddot{\boldsymbol{U}} + \boldsymbol{K}_{uu}\boldsymbol{U} + \boldsymbol{K}_{u\phi}\mathbf{\Phi} &= \boldsymbol{F} \\ \boldsymbol{K}_{\phi u}\boldsymbol{U} + \boldsymbol{K}_{\phi\phi}\mathbf{\Phi} &= \boldsymbol{Q} \end{aligned} \tag{4.34}$$

Eq. (4.34) can be rearranged by static condensation as

$$\boldsymbol{M}\ddot{\boldsymbol{U}} + \boldsymbol{K}_{uu}\boldsymbol{U} + \boldsymbol{K}_{u\phi}\boldsymbol{\Phi} = \boldsymbol{F} - \boldsymbol{K}_{u\phi}\boldsymbol{K}_{\phi\phi}^{-1}\boldsymbol{Q} \tag{4.35}$$

The actuator layer charge can be obtained by substituting Eqs. (4.31) and (4.32) in the second equation of the system (4.34)

$$\boldsymbol{Q}_a = \boldsymbol{K}_{\phi u}^a - G_v \boldsymbol{K}_{\phi\phi}^a \boldsymbol{K}_{\phi\phi}^{s^{-1}} \boldsymbol{K}_{\phi u}^s \dot{\boldsymbol{U}}_s \tag{4.36}$$

Now, substituting Eqs. (4.36) and (4.33) in Eq. (4.35), the equation of motion is obtained:

$$\boldsymbol{M}\ddot{\boldsymbol{U}} + \boldsymbol{C}\dot{\boldsymbol{U}} + \boldsymbol{K}_{uu}\boldsymbol{U} = \boldsymbol{F} \tag{4.37}$$

where $\boldsymbol{C}$ is the active damping matrix computed by

$$\boldsymbol{C} = \boldsymbol{K}_{u\phi}^a \boldsymbol{K}_{\phi\phi}^{s^{-1}} \boldsymbol{K}_{\phi u}^s \tag{4.38}$$

If the structural damping is considered in Eq. (4.37), it can be rearranged as

$$\boldsymbol{M}\ddot{\boldsymbol{U}} + (\boldsymbol{C} + \boldsymbol{C}_S)\dot{\boldsymbol{U}} + \boldsymbol{K}_{uu}\boldsymbol{U} = \boldsymbol{F} \tag{4.39}$$

in which $\boldsymbol{C}_S$ is the Rayleigh damping matrix which is computed assuming a linear combination of $\boldsymbol{M}$ and $\boldsymbol{K}_{uu}$ [35]

$$\boldsymbol{C}_S = a_S\boldsymbol{M} + b_S\boldsymbol{K}_{uu} \tag{4.40}$$

in which a_S and b_S are Rayleigh damping coefficients that can be determined from experiments.

4.4.2 Dynamic response

The equation of motion is solved by the iterative procedure of Newmark presented in [19]. When the current state of variables $(\boldsymbol{U}_i, \dot{\boldsymbol{U}}_i, \ddot{\boldsymbol{U}}_i)$ is known at $t = t_i$, a new state $(\boldsymbol{U}_{i+1}, \dot{\boldsymbol{U}}_{i+1}, \ddot{\boldsymbol{U}}_{i+1})$ at $t = t_i + \Delta t$ is computed from

$$\begin{aligned}
&\left(\frac{1}{\beta\Delta t^2}\boldsymbol{M} + \frac{\alpha}{\beta\Delta t}(\boldsymbol{C} + \boldsymbol{C}_S) + \boldsymbol{K}\right)\boldsymbol{U}_{i+1} = \boldsymbol{F}_{i+1} + \boldsymbol{M}\left[\frac{1}{\beta\Delta t^2}\boldsymbol{U}_i + \frac{1}{\beta\Delta t}\dot{\boldsymbol{U}}_i + \left(\frac{1}{2\beta} - 1\right)\ddot{\boldsymbol{U}}_i\right]\\
&\dot{\boldsymbol{U}}_{i+1} = \left(1 - \frac{\alpha}{\beta}\right)\dot{\boldsymbol{U}}_i + \left(1 - \frac{\alpha}{2\beta}\right)\Delta t\ddot{\boldsymbol{U}}_i + \frac{\alpha}{\beta\Delta t}(\boldsymbol{U}_{i+1} - \boldsymbol{U}_i)\\
&\ddot{\boldsymbol{U}}_{i+1} = \frac{1}{\beta\Delta t^2}(\boldsymbol{U}_{i+1} - \boldsymbol{U}_i) - \frac{1}{\beta\Delta t}\dot{\boldsymbol{U}}_i - \left(\frac{1}{2\beta} - 1\right)\ddot{\boldsymbol{U}}_i
\end{aligned} \tag{4.41}$$

where $\alpha = 0.5$ and $\beta = 0.25$.

Chapter 5

Numerical Results: Modal analysis

5.1 Laminated orthotropic plate

A laminated orthotropic piezoelectric plate is considered as first test-case of the formulation proposed in Chapter 4. The laminate is made of five layers which are perfectly bonded to each other. The top and bottom layers are made of PZT-4 piezoelectric material with the thickness of $h_p = 0.1h$ each. The three structural composite layers (graphite/epoxy) have equal thickness and have a cross-ply configuration [0/90/0]. The material properties are listed in Table 5.1. The plate is simply supported and short circuited $\Phi_t = \Phi_b = 0$. Firstly, in Tables 5.2-5.10 a stability model assessment is carried out by comparing the first six natural frequencies of the plate with the exact solutions provided in [16]. The free vibration analysis is performed with ED, EDZ and LD theories and the expansion order of the potential N_ϕ is consider totally indipendent from the expansion order of the displacements N_u in order to investigate how N_ϕ affects the convergence rate to the exact solutions. The length to thickness ratio is set to $a/h = 4$. Secondly, a convergence study on the first six natural frequencies is provided in Tables 5.14-5.15. Two different length to thickness ratios $a/h = 4, 50$ are considered. Tables 5.18-5.18 shows the first six natural frequencies of both mechanical and coupled case, computed with all the theories with a/h = 4,100. Δ denotes the natural frequency increment due to the electro-mechanical coupling and is defined as:

$$\Delta = \frac{\hat{\omega}_{coupled} - \hat{\omega}_{uncoupled}}{\hat{\omega}_{uncoupled}} \tag{5.1}$$

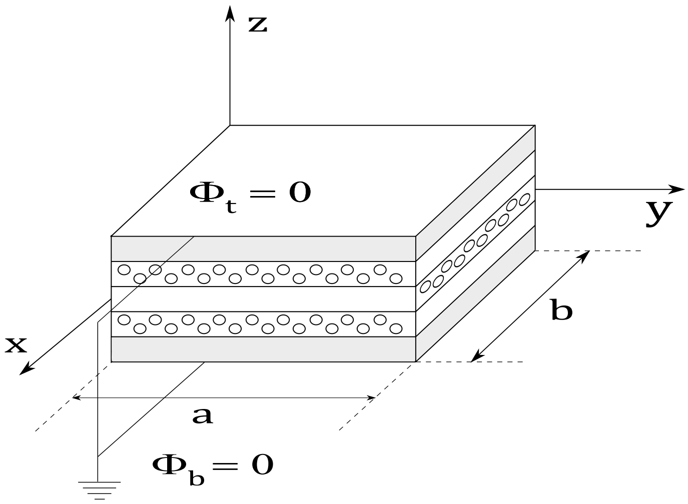

Figure 5.1: Hybrid sandwich plate [PZT-4/0/90/0/PZT-4]

Table 5.1: Elastic, piezoelectric and dielectric properties of used materials

Property	**PZT-4**	G_r/E_p	**SWCNT (300 K)**	**PmPV matrix**
E_1 (GPa)	81.3	132.38	5646.6	2.1
E_2 (GPa)	81.3	10.756	7080.0	2.1
E_3 (GPa)	64.5	10.756	7080.0	2.1
ν_{12}	0.329	0.24	0.175	0.34
ν_{13}	0.432	0.24	0.175	0.34
ν_{23}	0.432	0.49	0.175	0.34
G_{23} (GPa)	25.6	3.606	19944.5	0.7836
G_{13} (GPa)	25.6	5.6537	19944.5	0.7836
G_{12} (GPa)	30.6	5.6537	19944.5	0.7836
e_{14} (C/m^2)	12.72	0	0	0
e_{25} (C/m^2)	12.72	0	0	0
e_{31} (C/m^2)	- 5.20	0	0	0
e_{32} (C/m^2)	- 5.20	0	0	0
e_{33} (C/m^2)	15.08	0	0	0
$\varepsilon_{11}/\varepsilon_0$	1475	3.5	2000	10
$\varepsilon_{22}/\varepsilon_0$	1475	3.0	2000	10
$\varepsilon_{33}/\varepsilon_0$	1300	3.0	2000	10
ρ (Kg/m^3)	7600	1590	1400	1150

Table 5.2: Stability model assessment, first six natural frequencies $\hat{\omega} = \omega/100$ with ED theories for the simply-supported hybrid sandwich plate with $a/h = 4$ and $N_\phi = 1$

$N_\phi = 1$								
	$\hat{\omega}_1$	$\hat{\omega}_2$	$\hat{\omega}_3$	$\hat{\omega}_4$	$\hat{\omega}_5$	$\hat{\omega}_6$	Ave. Δ%	Max Δ%
Exact [16]	57074.5	191301	250769	274941	362492	381036		
ED^1_{111}	74105.8979	196021.3374	266337.1465	375608.2780	479222.7800	700380.4385	31.86	83.81
ED^1_{221}	74105.8979	195859.5510	262204.0352	375608.2780	479222.7800	698485.3556	31.49	83.31
ED^1_{331}	61473.4164	195859.5510	262204.0352	286259.4171	393505.0426	698485.3556	18.44	83.31
ED^1_{441}	61465.9329	194604.1491	258178.6509	286473.7018	393324.6765	503759.7573	9.55	32.21
ED^1_{112}	69390.2286	196021.3374	266337.1465	373493.0501	459959.1230	700380.4385	29.47	83.81
ED^1_{222}	69390.2286	195859.5510	262204.0352	373493.0501	459959.1230	698485.3556	29.09	83.31
ED^1_{332}	58804.8481	195859.5510	262204.0352	282239.2607	371896.3518	698485.3556	16.42	83.31
ED^1_{442}	58804.6861	194608.1421	258102.7118	282261.0536	371892.6234	503049.3156	7.49	32.02
ED^1_{113}	69390.2286	196019.6456	265905.0854	373493.0500	411310.6474	459959.1230	16.68	35.84
ED^1_{223}	69390.2286	195824.5147	259534.2033	373493.0501	391089.3177	459959.1230	15.31	35.84
ED^1_{333}	58804.8473	195824.5147	259534.2033	282197.1300	371915.8351	391089.3984	2.79	3.49
ED^1_{443}	58804.4266	194482.2290	253872.0648	282248.7388	371889.5555	388690.7592	2.20	3.03
ED^1_{114}	69361.4935	196019.6456	265905.0800	373492.5531	411309.3285	459562.1612	16.66	35.84
ED^1_{224}	69361.4300	195824.5147	259534.2035	373492.5533	391089.3920	459562.7920	15.29	35.84
ED^1_{334}	58676.0567	195824.5147	259534.2029	281814.7058	371233.0035	391089.4338	2.70	3.49
ED^1_{444}	58676.1119	194591.7321	254667.5525	281818.8233	371130.6017	389231.8893	2.19	2.81

$$\Delta\% = \left|\frac{\hat{\omega}_i - \hat{\omega}_{exact}}{\hat{\omega}_{exact}}\right| \times 100$$

Table 5.3: Stability model assessment, first six natural frequencies $\hat{\omega} = \omega/100$ with ED theories for the simply-supported hybrid sandwich plate with $a/h = 4$ and $N_\phi = 2$

$N_\phi = 2$								
	$\hat{\omega}_1$	$\hat{\omega}_2$	$\hat{\omega}_3$	$\hat{\omega}_4$	$\hat{\omega}_5$	$\hat{\omega}_6$	Ave. $\Delta\%$	Max $\Delta\%$
Exact [16]	57074.5	191301	250769	274941	362492	381036		
ED^2_{111}	74117.2610	196021.4357	266337.8019	375609.4464	479236.8287	700388.2754	31.86	83.81
ED^2_{221}	74117.2610	195859.5902	262204.0384	375609.4464	479236.8287	698489.6372	31.49	83.31
ED^2_{331}	61479.5963	195859.5902	262204.0384	286259.5305	393505.2063	698489.6372	18.44	83.31
ED^2_{441}	61471.9260	194604.1590	258178.7127	286474.2070	393323.3097	503760.3583	9.55	32.21
ED^2_{112}	69413.6740	196021.4357	266337.8019	373493.1294	459959.7518	700388.2754	29.47	83.81
ED^2_{222}	69413.6740	195859.5902	262204.0384	373493.1294	459959.7518	698489.6372	29.10	83.31
ED^2_{332}	58818.5754	195859.5902	262204.0384	282241.2919	371905.6785	698489.6372	16.43	83.31
ED^2_{442}	58818.4126	194609.2471	258097.2818	282263.6780	371901.9534	503049.5085	7.50	32.02
ED^2_{113}	69413.6740	196019.8645	265917.9142	373493.1294	413042.1563	459959.7518	16.77	35.84
ED^2_{223}	69413.6740	195825.4056	259586.0969	373493.1294	392800.6904	459959.7518	15.40	35.84
ED^2_{333}	58818.5754	195825.4056	259586.0970	282240.5711	371906.3240	392800.7731	2.88	3.52
ED^2_{443}	58818.1649	194478.4689	253956.9032	282251.1905	371898.9691	390380.6789	2.28	3.06
ED^2_{114}	69373.9451	196019.8645	265917.9088	373492.5645	413040.7813	459580.0338	16.74	35.84
ED^2_{224}	69373.8872	195825.4056	259586.0971	373492.5647	392800.7664	459580.5068	15.38	35.84
ED^2_{334}	58713.8342	195825.4056	259586.0965	281824.7197	371236.2657	392800.8091	2.79	3.52
ED^2_{444}	58713.9199	194592.2069	254768.4518	281830.2642	371143.8029	391069.1040	2.29	2.87

$\Delta\% = |\frac{\hat{\omega}_i - \hat{\omega}_{exact}}{\hat{\omega}_{exact}}| \times 100$

Table 5.4: Stability model assessment, first six natural frequencies $\hat{\omega} = \omega/100$ with ED theories for the simply-supported hybrid sandwich plate with $a/h = 4$ and $N_\phi = 3$

$N_\phi = 3$								
	$\hat{\omega}_1$	$\hat{\omega}_2$	$\hat{\omega}_3$	$\hat{\omega}_4$	$\hat{\omega}_5$	$\hat{\omega}_6$	Ave. $\Delta\%$	Max $\Delta\%$
Exact [16]	57074.5	191301	250769	274941	362492	381036		
ED^3_{111}	74117.2611	196021.4358	266337.8024	375609.4465	479236.8289	700388.2760	31.86	83.81
ED^3_{221}	74117.2611	195859.5904	262204.0404	375609.4465	479236.8289	698489.6390	31.49	83.31
ED^3_{331}	61479.6146	195859.5904	262204.0404	286259.1213	393505.6207	698489.6390	18.44	83.31
ED^3_{441}	61471.9611	194604.1729	258178.7170	286475.9281	393323.2446	503761.4767	9.55	32.21
ED^3_{112}	69413.6742	196021.4358	266337.8024	373493.1295	459959.7522	700388.2760	29.47	83.81
ED^3_{222}	69413.6742	195859.5904	262204.0404	373493.1295	459959.7522	698489.6390	29.10	83.31
ED^3_{332}	58818.5899	195859.5904	262204.0404	282241.3435	371905.8018	698489.6390	16.43	83.31
ED^3_{442}	58818.4292	194610.0679	258093.2206	282263.8187	371902.0685	503049.6747	7.50	32.02
ED^3_{113}	69413.6742	196019.8645	265917.9172	373493.1295	413043.4039	459959.7522	16.77	35.84
ED^3_{223}	69413.6742	195825.4056	259586.1198	373493.1295	392801.9334	459959.7522	15.40	35.84
ED^3_{333}	58818.5898	195825.4056	259586.1199	282244.1329	371905.1891	392802.0161	2.88	3.52
ED^3_{443}	58818.1469	194478.3788	253951.6203	282250.9981	371898.8807	390375.6033	2.28	3.05
ED^3_{114}	69373.9557	196019.8645	265917.9117	373492.5650	413042.0289	459580.2197	16.74	35.84
ED^3_{224}	69373.8799	195825.4056	259586.1200	373492.5653	392802.0094	459580.8401	15.37	35.84
ED^3_{334}	58713.8517	195825.4056	259586.1194	281825.2785	371253.9588	392802.0521	2.80	3.52
ED^3_{444}	58713.9162	194591.6096	254739.2456	281830.1418	371144.1310	390959.0008	2.29	2.87

$$\Delta\% = \left|\frac{\hat{\omega}_i - \hat{\omega}_{exact}}{\hat{\omega}_{exact}}\right| \times 100$$

Table 5.5: Stability model assessment, first six natural frequencies $\hat{\omega} = \omega/100$ with ED theories for the simply-supported hybrid sandwich plate with $a/h = 4$ and $N_\phi = 4$

$N_\phi = 4$								
	$\hat{\omega}_1$	$\hat{\omega}_2$	$\hat{\omega}_3$	$\hat{\omega}_4$	$\hat{\omega}_5$	$\hat{\omega}_6$	Ave. $\Delta\%$	Max $\Delta\%$
Exact [16]	57074.5	191301	250769	274941	362492	381036		
ED^4_{111}	74117.2611	196021.4358	266337.8024	375609.4465	479236.8289	700388.2760	31.86	83.81
ED^4_{221}	74117.2611	195859.5904	262204.0404	375609.4465	479236.8289	698489.6390	31.49	83.31
ED^4_{331}	61479.6131	195859.5904	262204.0404	286260.0233	393504.8144	698489.6390	18.44	83.31
ED^4_{441}	61472.0527	194604.1729	258178.7135	286469.3870	393326.4392	503761.3867	9.55	32.21
ED^4_{112}	69413.6742	196021.4358	266337.8024	373493.1295	459959.7522	700388.2760	29.47	83.81
ED^4_{222}	69413.6742	195859.5904	262204.0404	373493.1295	459959.7522	698489.6390	29.10	83.31
ED^4_{332}	58818.5899	195859.5904	262204.0404	282241.6256	371905.6530	698489.6390	16.43	83.31
ED^4_{442}	58818.4271	194608.0532	258103.3332	282262.5139	371901.9605	503050.1049	7.50	32.02
ED^4_{113}	69413.6742	196019.8645	265917.9172	373493.1295	413043.4039	459959.7522	16.77	35.84
ED^4_{223}	69413.6742	195825.4056	259586.1198	373493.1295	392801.9334	459959.7522	15.40	35.84
ED^4_{333}	58818.5898	195825.4056	259586.1199	282244.1899	371904.9274	392802.0161	2.88	3.52
ED^4_{443}	58818.1897	194478.4420	253960.8373	282250.9660	371899.1560	390383.6447	2.28	3.05
ED^4_{114}	69373.9556	196019.8645	265917.9117	373492.5650	413042.0284	459580.2205	16.74	35.84
ED^4_{224}	69373.8900	195825.4056	259586.1200	373492.5652	392802.0094	459580.7565	15.37	35.84
ED^4_{334}	58713.8241	195825.4056	259586.1194	281825.2319	371239.6178	392802.0522	2.79	3.52
ED^4_{444}	58713.9221	194592.1273	254739.3875	281830.2732	371143.8485	390960.9564	2.28	2.87

$\Delta\% = |\frac{\hat{\omega}_i - \hat{\omega}_{exact}}{\hat{\omega}_{exact}}| \times 100$

Table 5.6: Stability model assessment, first six natural frequencies $\hat{\omega} = \omega/100$ with EDZ theories for the simply-supported hybrid sandwich plate with $a/h = 4$ and $N_\phi = 1$

$N_\phi = 1$								
	$\hat{\omega}_1$	$\hat{\omega}_2$	$\hat{\omega}_3$	$\hat{\omega}_4$	$\hat{\omega}_5$	$\hat{\omega}_6$	Ave. $\Delta\%$	Max $\Delta\%$
Exact [16]	57074.5	191301	250769	274941	362492	381036		
EDZ^1_{111}	63198.5291	195965.2576	266195.2458	298704.5651	427699.8535	455511.7257	10.92	19.54
EDZ^1_{221}	63198.5291	195721.4541	260861.0564	298704.5651	427699.8535	436972.9467	9.73	17.99
EDZ^1_{331}	60049.1222	195721.4541	260861.0564	284231.2261	390425.7237	436972.9460	6.22	14.68
EDZ^1_{441}	60049.0768	202608.4421	205792.3973	284231.5013	332979.5044	390420.8769	7.17	17.93
EDZ^1_{112}	60591.7886	195965.2576	266195.2458	293425.3742	404981.6474	455511.7257	8.79	19.54
EDZ^1_{222}	60591.7886	195721.4541	260861.0564	293425.3743	404981.6473	436972.9452	7.60	14.68
EDZ^1_{332}	57643.9335	195721.4541	260861.0564	279710.7652	369966.1081	436972.9460	4.30	14.68
EDZ^1_{442}	57643.9194	202404.5353	239286.2874	279710.5512	329197.9991	369966.0809	4.20	9.18
EDZ^1_{113}	60591.7885	195924.5307	265890.1994	293425.3742	404981.6472	410256.8443	6.79	11.72
EDZ^1_{223}	60591.7886	195710.4249	259524.2996	293425.3743	389487.1322	404981.6474	5.40	7.45
EDZ^1_{333}	57643.9407	195710.4249	259524.3011	279710.8463	369965.9743	389487.1721	2.13	3.49
EDZ^1_{443}	57643.7109	186624.5173	229167.7980	279710.7703	321125.9438	369969.7271	4.68	11.41
EDZ^1_{114}	60582.5701	195924.5310	265890.1970	293311.1818	404964.3277	410256.7593	6.78	11.72
EDZ^1_{224}	60582.6543	195710.4248	259524.3024	293313.7372	389487.2534	404963.4363	5.39	7.45
EDZ^1_{334}	57547.0221	195710.4247	259524.3045	279394.9219	369075.9734	389487.2813	2.05	3.49
EDZ^1_{444}	57546.9234	194430.8380	254668.5904	279394.1024	369072.3898	387722.4067	1.53	1.81

$\Delta\% = |\frac{\hat{\omega}_i - \hat{\omega}_{exact}}{\hat{\omega}_{exact}}| \times 100$

Table 5.7: Stability model assessment, first six natural frequencies $\hat{\omega} = \omega/100$ with EDZ theories for the simply-supported hybrid sandwich plate with $a/h = 4$ and $N_\phi = 2$

$N_\phi = 2$								
	$\hat{\omega}_1$	$\hat{\omega}_2$	$\hat{\omega}_3$	$\hat{\omega}_4$	$\hat{\omega}_5$	$\hat{\omega}_6$	Ave. $\Delta\%$	Max $\Delta\%$
Exact [16]	57074.5	191301	250769	274941	362492	381036		
EDZ^2_{111}	63204.7359	195965.3819	266196.0204	298704.5654	427700.5059	455520.7908	10.92	19.55
EDZ^2_{221}	63204.7359	195721.4997	260861.0674	298704.5654	427700.5059	436974.2763	9.73	17.99
EDZ^2_{331}	60054.8821	195721.4997	260861.0675	284231.2898	390426.3398	436974.2756	6.22	14.68
EDZ^2_{441}	60054.8289	202611.3453	205847.9858	284231.5106	332987.2083	390421.0486	7.17	17.91
EDZ^2_{112}	60605.4801	195965.3819	266196.0204	293428.0734	404987.5286	455520.7908	8.79	19.55
EDZ^2_{222}	60605.4801	195710.5641	259570.1587	293428.0734	390745.7346	404987.5286	5.47	7.79
EDZ^2_{332}	57656.7080	195721.4997	260861.0675	279713.5755	369974.2544	436974.2756	4.31	14.68
EDZ^2_{442}	57656.6920	202403.1940	239231.9800	279713.3359	329132.9448	369974.2345	4.21	9.20
EDZ^2_{113}	60605.4801	195925.1060	265906.4529	293428.0734	404987.5285	411606.5170	6.85	11.72
EDZ^2_{223}	60605.4801	195710.5641	259570.1587	293428.0734	390745.7346	404987.5286	5.47	7.79
EDZ^2_{333}	57656.7119	195710.5644	259570.1716	279713.7020	369974.0847	390745.7781	2.20	3.51
EDZ^2_{443}	57656.5413	186460.7373	229279.0195	279713.5419	320665.3670	369976.9736	4.72	11.54
EDZ^2_{114}	60600.9666	195925.1063	265906.4508	293314.4798	404965.1564	411606.4323	6.84	11.72
EDZ^2_{224}	60600.9641	195710.5638	259570.1639	293314.4619	390745.9090	404965.1731	5.46	7.79
EDZ^2_{334}	57578.6073	195710.5637	259570.1682	279410.3753	369095.5061	390745.9692	2.11	3.51
EDZ^2_{444}	57575.1159	194443.5566	254739.4685	279394.6321	369163.4800	389191.1643	1.62	2.14

$$\Delta\% = \left|\frac{\hat{\omega}_i - \hat{\omega}_{exact}}{\hat{\omega}_{exact}}\right| \times 100$$

Table 5.8: Stability model assessment, first six natural frequencies $\hat{\omega} = \omega/100$ with EDZ theories for the simply-supported hybrid sandwich plate with $a/h = 4$ and $N_\phi = 3$

$N_\phi = 3$								
	$\hat{\omega}_1$	$\hat{\omega}_2$	$\hat{\omega}_3$	$\hat{\omega}_4$	$\hat{\omega}_5$	$\hat{\omega}_6$	Ave. $\Delta\%$	Max $\Delta\%$
Exact [16]	57074.5	191301	250769	274941	362492	381036		
EDZ^3_{111}	63204.7360	195965.3820	266196.0209	298704.5655	427700.5062	455520.7908	10.92	19.55
EDZ^3_{221}	63204.7360	195721.4999	260861.0697	298704.5655	427700.5062	436974.2785	9.73	17.99
EDZ^3_{331}	60054.8901	195721.4999	260861.0698	284231.3643	390427.2029	436974.2778	6.22	14.68
EDZ^3_{441}	60054.8459	202616.6481	205908.3947	284231.5074	332985.4968	390421.0449	7.17	17.89
EDZ^3_{112}	60605.4803	195965.3820	266196.0209	293428.0736	404987.5293	455520.7908	8.79	19.55
EDZ^3_{222}	60605.4803	195721.4999	260861.0698	293428.0736	404987.5293	436974.2770	7.61	14.68
EDZ^3_{332}	57656.7144	195721.4999	260861.0698	279713.5753	369974.4015	436974.2778	4.31	14.68
EDZ^3_{442}	57656.7007	202402.9022	239167.0428	279713.3526	329143.8457	369974.3774	4.21	9.20
EDZ^3_{113}	60605.4803	195925.1076	265906.4573	293428.0736	404987.5294	411607.4504	6.85	11.72
EDZ^3_{223}	60605.4803	195710.5650	259570.1776	293428.0736	390746.6096	404987.5293	5.47	7.79
EDZ^3_{333}	57656.7172	195710.5652	259570.1855	279713.6605	369974.2928	390746.6533	2.20	3.51
EDZ^3_{443}	57656.4366	186532.8123	229423.8995	279713.5894	320900.5197	369978.9103	4.69	11.47
EDZ^3_{114}	60600.9666	195925.1078	265906.4552	293314.4996	404965.1782	411607.3658	6.84	11.72
EDZ^3_{224}	60600.9666	195710.5648	259570.1827	293314.4997	390746.7843	404965.1782	5.46	7.79
EDZ^3_{334}	57578.6037	195710.5647	259570.1870	279410.6729	369096.1536	390746.8441	2.11	3.51
EDZ^3_{444}	57575.2686	194436.0311	254739.5909	279395.0747	369160.6618	389064.1778	1.61	2.11

$$\Delta\% = \left|\frac{\hat{\omega}_i - \hat{\omega}_{exact}}{\hat{\omega}_{exact}}\right| \times 100$$

Table 5.9: Stability model assessment, first six natural frequencies $\hat{\omega} = \omega/100$ with EDZ theories for the simply-supported hybrid sandwich plate with $a/h = 4$ and $N_\phi = 4$

$N_\phi = 4$								
	$\hat{\omega}_1$	$\hat{\omega}_2$	$\hat{\omega}_3$	$\hat{\omega}_4$	$\hat{\omega}_5$	$\hat{\omega}_6$	Ave. $\Delta\%$	Max $\Delta\%$
Exact [16]	57074.5	191301	250769	274941	362492	381036		
EDZ^4_{111}	63204.7360	195965.3820	266196.0209	298704.5655	427700.5062	455520.7908	10.92	19.55
EDZ^4_{221}	63204.7360	195721.4999	260861.0701	298704.5655	427700.5062	436974.2781	9.73	17.99
EDZ^4_{331}	60054.8908	195721.4999	260861.0698	284231.1063	390423.9537	436974.2778	6.22	14.68
EDZ^4_{441}	60054.8423	202613.3991	205870.8197	284231.5196	332986.8395	390421.1122	7.17	17.90
EDZ^4_{112}	60605.4803	195965.3820	266196.0209	293428.0737	404987.5293	455520.7908	8.80	19.55
EDZ^4_{222}	60605.4803	195721.4999	260861.0698	293428.0736	404987.5293	436974.2770	7.61	14.68
EDZ^4_{332}	57656.7131	195721.4999	260861.0698	279713.5712	369974.4119	436974.2778	4.31	14.68
EDZ^4_{442}	57656.7007	202402.8893	239164.4901	279713.3750	329144.3645	369974.3799	4.21	9.20
EDZ^4_{113}	60605.4803	195925.1076	265906.4573	293428.0735	404987.5293	411607.4504	6.85	11.72
EDZ^4_{223}	60605.4803	195710.5650	259570.1759	293428.0736	390746.6014	404987.5293	5.47	7.79
EDZ^4_{333}	57656.7404	195710.5650	259570.1772	279713.6958	369974.0861	390746.6387	2.20	3.51
EDZ^4_{443}	57656.6295	186434.9267	229117.2884	279713.5351	320894.6944	369975.7981	4.72	11.47
EDZ^4_{114}	60600.9666	195925.1078	265906.4546	293314.4996	404965.1782	411607.3653	6.84	11.72
EDZ^4_{224}	60600.9666	195710.5648	259570.1830	293314.4998	390746.7873	404965.1782	5.46	7.79
EDZ^4_{334}	57579.0674	195710.5647	259570.1870	279403.9498	369093.0186	390746.8445	2.11	3.51
EDZ^4_{444}	57585.0247	194140.7846	254705.2324	279406.4871	368997.2431	386098.4398	1.45	1.79

$\Delta\% = \left|\frac{\hat{\omega}_i - \hat{\omega}_{exact}}{\hat{\omega}_{exact}}\right| \times 100$

Table 5.10: Stability model assessment, first six natural frequencies $\hat{\omega} = \omega/100$ with LD theories for the simply-supported hybrid sandwich plate with $a/h = 4$ and $N_\phi = 1$

$N_\phi = 1$								
	$\hat{\omega}_1$	$\hat{\omega}_2$	$\hat{\omega}_3$	$\hat{\omega}_4$	$\hat{\omega}_5$	$\hat{\omega}_6$	Ave. $\Delta\%$	Max $\Delta\%$
Exact [16]	57074.5	191301	250769	274941	362492	381036		
LD^1_{111}	57252.4975	194839.5803	255646.0517	282167.4738	368457.5514	389524.3101	1.77	2.63
LD^1_{221}	57156.6815	191312.4884	251189.7673	275158.0023	363493.5452	388602.9383	0.44	1.98
LD^1_{331}	57148.0952	191312.2988	251187.8128	275060.6792	363174.3437	388536.3163	0.42	1.97
LD^1_{441}	57148.0859	191312.1664	251187.2555	275059.2913	363172.3735	388536.0079	0.42	1.97
LD^1_{112}	57142.9033	194837.8489	255228.3602	282071.2252	367800.0712	382131.0787	1.35	2.59
LD^1_{222}	57046.7419	191310.7556	250782.3884	275059.8011	362880.1710	381288.7025	0.04	0.10
LD^1_{332}	57039.0097	191310.5445	250779.0414	274958.3958	362519.6039	381132.9210	0.02	0.06
LD^1_{442}	57039.0004	191310.4121	250778.4901	274957.0105	362517.6721	381132.6921	0.02	0.06
LD^1_{113}	57142.9031	194837.7892	255225.7899	282070.9783	367797.1181	382025.4797	1.34	2.59
LD^1_{223}	57046.6011	191300.9933	250768.0852	275043.0068	362850.9094	381159.1647	0.03	0.10
LD^1_{333}	57038.8688	191300.7823	250764.7388	274941.6597	362490.5734	381004.1344	0.01	0.06
LD^1_{443}	57038.8610	191300.6427	250764.0240	274940.0088	362488.1424	381003.4674	0.01	0.06
LD^1_{114}	57142.9031	194837.7892	255225.7855	282070.9767	367797.0842	382025.0569	1.34	2.59
LD^1_{224}	57046.6011	191300.9933	250768.0812	275043.0054	362850.8795	381158.7507	0.03	0.10
LD^1_{334}	57038.8644	191300.7821	250764.7285	274941.5720	362490.0324	381003.0072	0.01	0.06
LD^1_{444}	57038.8566	191300.6425	250764.0138	274939.9212	362487.6015	381002.3402	0.01	0.06

$$\Delta\% = \left|\frac{\hat{\omega}_i - \hat{\omega}_{exact}}{\hat{\omega}_{exact}}\right| \times 100$$

Table 5.11: Stability model assessment, first six natural frequencies $\hat{\omega} = \omega/100$ with LD theories for the simply-supported hybrid sandwich plate with $a/h = 4$ and $N_\phi = 2$

$N_\phi = 2$								
	$\hat{\omega}_1$	$\hat{\omega}_2$	$\hat{\omega}_3$	$\hat{\omega}_4$	$\hat{\omega}_5$	$\hat{\omega}_6$	Ave. $\Delta\%$	Max $\Delta\%$
Exact [16]	57074.5	191301	250769	274941	362492	381036		
LD^2_{111}	57257.8737	194839.5924	255646.2597	282167.4983	368457.7395	389525.3819	1.77	2.63
LD^2_{221}	57162.0719	191312.5012	251189.9718	275158.0302	363493.7086	388603.9780	0.44	1.99
LD^2_{331}	57153.5020	191312.3117	251188.0178	275060.7071	363174.5061	388537.3527	0.42	1.97
LD^2_{441}	57153.4927	191312.1793	251187.4605	275059.3192	363172.5359	388537.0442	0.42	1.97
LD^2_{112}	57177.9321	194838.1450	255231.8726	282071.6137	367801.5462	382165.3086	1.36	2.59
LD^2_{222}	57081.8463	191311.0629	250785.8261	275060.2670	362881.5767	381322.1808	0.04	0.11
LD^2_{332}	57074.1045	191310.8517	250782.4797	274958.8614	362521.0086	381166.2336	0.01	0.03
LD^2_{442}	57074.0951	191310.7193	250781.9284	274957.4760	362519.0768	381166.0042	0.01	0.03
LD^2_{113}	57177.9320	194838.0854	255229.3031	282071.3669	367798.5938	382059.6572	1.35	2.59
LD^2_{223}	57081.7057	191301.3006	250771.5248	275043.4734	362852.3168	381192.5721	0.03	0.10
LD^2_{333}	57073.9637	191301.0895	250768.1790	274942.1259	362491.9799	381037.3774	0.00	0.00
LD^2_{443}	57073.9559	191300.9500	250767.4642	274940.4751	362489.5488	381036.7094	0.00	0.00
LD^2_{114}	57177.9320	194838.0854	255229.2987	282071.3653	367798.5599	382059.2341	1.35	2.59
LD^2_{224}	57081.7057	191301.3006	250771.5209	275043.4720	362852.2869	381192.1577	0.03	0.10
LD^2_{334}	57073.9593	191301.0894	250768.1688	274942.0383	362491.4390	381036.2491	0.00	0.00
LD^2_{444}	57073.9515	191300.9498	250767.4540	274940.3874	362489.0079	381035.5810	0.00	0.00

$\Delta\% = \left|\frac{\hat{\omega}_i - \hat{\omega}_{exact}}{\hat{\omega}_{exact}}\right| \times 100$

Table 5.12: Stability model assessment, first six natural frequencies $\hat{\omega} = \omega/100$ with LD theories for the simply-supported hybrid sandwich plate with $a/h = 4$ and $N_\phi = 3$

$N_\phi = 3$								
	$\hat{\omega}_1$	$\hat{\omega}_2$	$\hat{\omega}_3$	$\hat{\omega}_4$	$\hat{\omega}_5$	$\hat{\omega}_6$	Ave. $\Delta\%$	Max $\Delta\%$
Exact [16]	57074.5	191301	250769	274941	362492	381036		
LD^3_{111}	57257.8738	194839.5925	255646.2600	282167.4984	368457.7401	389525.3820	1.77	2.63
LD^3_{221}	57162.0723	191312.5013	251189.9718	275158.0303	363493.7106	388603.9787	0.44	1.99
LD^3_{331}	57153.5023	191312.3118	251188.0178	275060.7071	363174.5081	388537.3533	0.42	1.97
LD^3_{441}	57153.4930	191312.1794	251187.4605	275059.3192	363172.5379	388537.0449	0.42	1.97
LD^3_{112}	57177.9322	194838.1451	255231.8729	282071.6139	367801.5468	382165.3088	1.36	2.59
LD^3_{222}	57081.8466	191311.0629	250785.8261	275060.2670	362881.5787	381322.1814	0.04	0.11
LD^3_{332}	57074.1048	191310.8517	250782.4797	274958.8614	362521.0106	381166.2342	0.01	0.03
LD^3_{442}	57074.0955	191310.7193	250781.9284	274957.4760	362519.0788	381166.0048	0.01	0.03
LD^3_{113}	57177.9321	194838.0856	255229.3034	282071.3670	367798.5939	382059.6573	1.35	2.59
LD^3_{223}	57081.7067	191301.3011	250771.5256	275043.4736	362852.3168	381192.5721	0.03	0.10
LD^3_{333}	57073.9648	191301.0900	250768.1797	274942.1262	362491.9799	381037.3775	0.00	0.00
LD^3_{443}	57073.9570	191300.9505	250767.4650	274940.4753	362489.5488	381036.7094	0.00	0.00
LD^3_{114}	57177.9321	194838.0856	255229.2990	282071.3654	367798.5600	382059.2341	1.35	2.59
LD^3_{224}	57081.7067	191301.3011	250771.5216	275043.4722	362852.2869	381192.1577	0.0319	0.10
LD^3_{334}	57073.9604	191301.0898	250768.1695	274942.0385	362491.4390	381036.2491	0.00	0.00
LD^3_{444}	57073.9526	191300.9503	250767.4547	274940.3877	362489.0079	381035.5811	0.00	0.00

$$\Delta\% = \left|\frac{\hat{\omega}_i - \hat{\omega}_{exact}}{\hat{\omega}_{exact}}\right| \times 100$$

Table 5.13: Stability model assessment, first six natural frequencies $\hat{\omega} = \omega/100$ with LD theories for the simply-supported hybrid sandwich plate with $a/h = 4$ and $N_\phi = 4$

$N_\phi = 4$	$\hat{\omega}_1$	$\hat{\omega}_2$	$\hat{\omega}_3$	$\hat{\omega}_4$	$\hat{\omega}_5$	$\hat{\omega}_6$	Ave. $\Delta\%$	Max $\Delta\%$
Exact [16]	57074.5	191301	250769	274941	362492	381036		
LD^4_{111}	57257.8738	194839.5925	255646.2600	282167.4984	368457.7401	389525.3820	1.77	2.62
LD^4_{221}	57162.0723	191312.5013	251189.9718	275158.0303	363493.7106	388603.9787	0.44	1.99
LD^4_{331}	57153.5023	191312.3118	251188.0178	275060.7071	363174.5081	388537.3533	0.42	1.97
LD^4_{441}	57153.4930	191312.1794	251187.4605	275059.3192	363172.5379	388537.0449	0.42	1.97
LD^4_{112}	57177.9322	194838.1451	255231.8729	282071.6139	367801.5468	382165.3088	1.36	2.59
LD^4_{222}	57081.8466	191311.0629	250785.8261	275060.2670	362881.5787	381322.1814	0.04	0.11
LD^4_{332}	57074.1048	191310.8517	250782.4797	274958.8614	362521.0106	381166.2342	0.01	0.03
LD^4_{442}	57074.0955	191310.7193	250781.9284	274957.4760	362519.0788	381166.0048	0.01	0.03
LD^4_{113}	57177.9321	194838.0856	255229.3034	282071.3670	367798.5939	382059.6573	1.35	2.59
LD^4_{223}	57081.7067	191301.3011	250771.5256	275043.4736	362852.3168	381192.5721	0.03	0.10
LD^4_{333}	57073.9648	191301.0900	250768.1797	274942.1262	362491.9799	381037.3775	0.00	0.00
LD^4_{443}	57073.9570	191300.9505	250767.4650	274940.4753	362489.5488	381036.7094	0.00	0.00
LD^4_{114}	57177.9321	194838.0856	255229.2990	282071.3654	367798.5600	382059.2341	1.35	2.59
LD^4_{224}	57081.7067	191301.3011	250771.5216	275043.4722	362852.2869	381192.1577	0.03	0.10
LD^4_{334}	57073.9604	191301.0898	250768.1695	274942.0385	362491.4390	381036.2491	0.00	0.00
LD^4_{444}	57073.9526	191300.9503	250767.4547	274940.3877	362489.0079	381035.5811	0.00	0.00

$$\Delta\% = \left|\frac{\hat{\omega}_i - \hat{\omega}_{exact}}{\hat{\omega}_{exact}}\right| \times 100$$

Table 5.14: Convergence study on the first six natural frequencies $\hat{\omega} = \omega/100$ for the simply-supported hybrid Sandwich plate with $a/h = 4$

$a/h = 4$								
	$\hat{\omega}_1$	$\hat{\omega}_2$	$\hat{\omega}_3$	$\hat{\omega}_4$	$\hat{\omega}_5$	$\hat{\omega}_6$	Ave. $\Delta\%$	Max $\Delta\%$
Exact [16]	57074.5	191301	250769	274941	362492	381036		
LD4	57073.9526	191300.9503	250767.4547	274940.3877	362489.0079	381035.5811	0.00	0.00
LD3	57073.9648	191301.0900	250768.1797	274942.1262	362491.9799	381037.3775	0.00	0.00
LD2	57081.8463	191311.0629	250785.8261	275060.2670	362881.5767	381322.1808	0.04	0.11
LD1	57252.4975	194839.5803	255646.0517	282167.4738	368457.5514	389524.3101	1.77	2.63
EDZ3	57656.7172	195710.5652	259570.1855	279713.6605	369974.2928	390746.6533	2.20	3.51
EDZ2	60605.4801	195710.5641	259570.1587	293428.0734	390745.7346	404987.5286	5.47	7.79
EDZ1	63198.5291	195965.2576	266195.2458	298704.5651	427699.8535	455511.7257	10.92	19.54
ED4	58713.9221	194592.1273	254739.3875	281830.2732	371143.8485	390960.9564	2.28	2.87
ED3	58818.5898	195825.4056	259586.1199	282244.1329	371905.1891	392802.0161	2.88	3.52
ED2	69413.6740	195859.5902	262204.0384	373493.1294	459959.7518	698489.6372	29.10	83.31
ED1	74105.8979	196021.3374	266337.1465	375608.2780	479222.7800	700380.4385	31.85	83.81

$$\Delta\% = \left|\frac{\hat{\omega}_i - \hat{\omega}_{exact}}{\hat{\omega}_{exact}}\right| \times 100$$

Table 5.15: Convergence study on the first six natural frequencies $\hat{\omega} = \omega/100$ for the simply-supported hybrid sandwich plate with $a/h = 50$

$a/h = 50$								
	$\hat{\omega}_1$	$\hat{\omega}_2$	$\hat{\omega}_3$	$\hat{\omega}_4$	$\hat{\omega}_5$	$\hat{\omega}_6$	Ave. $\Delta\%$	Max $\Delta\%$
Exact [16]	618.118	15681.6	21492.8	209704	210522	378104		
LD4	618.1043	15681.5458	21492.5789	209704.0828	210522.2329	378104.4048	0.00	0.00
LD3	618.1043	15681.5458	21492.5789	209704.2461	210522.5579	378104.9863	0.00	0.00
LD2	618.1053	15681.5458	21492.5790	209788.3688	210605.3868	378278.3540	0.02	0.05
LD1	619.0220	15683.4178	21494.4314	212810.9560	214690.3703	384953.0613	0.91	1.98
EDZ3	618.3814	15687.0501	21496.5094	212012.8112	216749.3787	386101.5399	1.04	2.96
EDZ2	619.0455	15693.5478	21496.5144	222042.1743	262302.7327	429559.1567	7.39	24.60
EDZ1	688.0640	15693.6372	21498.4563	222201.5611	262434.3395	429719.3585	9.28	24.66
ED4	618.4637	15693.5245	21497.7823	218019.2079	218997.3898	385648.9017	1.69	4.02
ED3	618.5502	15694.2317	21500.0619	218018.3434	219002.5507	388109.7374	1.80	4.03
ED2	620.2993	15694.8760	21505.2370	320858.9291	331281.1194	679987.9466	31.78	79.84
ED1	689.8670	15694.9515	21507.4033	320954.6225	331380.8063	680009.5086	33.68	79.85

$$\Delta\% = \left|\frac{\hat{\omega}_i - \hat{\omega}_{exact}}{\hat{\omega}_{exact}}\right| \times 100$$

Table 5.16: Coupling effect on the first six natural frequencies $\hat{\omega} = \omega/100$ with ED theories for the simply-supported hybrid sandwich plate with $a/h = 4$ and $a/h = 100$

		$a/h = 4$			$a/h = 100$		
		coupled (SC)	uncoupled	$\Delta\%$	coupled (SC)	uncoupled	$\Delta\%$
ED4	$\hat{\omega}_1$	58713.9221	56939.2867	3.12	155.3185	146.8253	5.78
	$\hat{\omega}_2$	194592.1273	193118.9470	0.76	7847.0781	7800.0647	0.60
	$\hat{\omega}_3$	254739.3875	250329.3699	1.76	10750.8523	10484.9161	2.54
	$\hat{\omega}_4$	281830.2732	279663.2320	0.77	217208.5781	217196.7310	0.00
	$\hat{\omega}_5$	371143.8485	362994.4955	2.24	218408.7479	218393.1767	0.01
	$\hat{\omega}_6$	390960.9564	388144.2091	0.72	385725.9000	386390.7652	0.17
ED3	$\hat{\omega}_1$	58818.5898	57163.1434	2.90	155.3392	147.0295	5.65
	$\hat{\omega}_2$	195825.4056	194618.3471	0.62	7847.1666	7800.1711	0.60
	$\hat{\omega}_3$	259586.1199	254169.1651	2.13	10751.1371	10485.1325	2.54
	$\hat{\omega}_4$	282244.1329	279977.6950	0.81	217208.7749	217196.7545	0.00
	$\hat{\omega}_5$	371905.1891	363372.5578	2.35	218409.7552	218393.6229	0.01
	$\hat{\omega}_6$	392802.0161	390534.8377	0.58	388129.6691	386420.8898	0.44
ED2	$\hat{\omega}_1$	69413.6740	66641.6628	4.16	155.4498	147.1240	5.66
	$\hat{\omega}_2$	195859.5902	194618.5553	0.64	7847.4964	7804.4665	0.55
	$\hat{\omega}_3$	262204.0384	255320.1774	2.70	10753.8682	10508.7944	2.33
	$\hat{\omega}_4$	373493.1294	372521.4827	0.26	320462.8873	320453.8215	0.00
	$\hat{\omega}_5$	459959.7518	453187.4552	1.49	330617.3938	330608.7186	0.00
	$\hat{\omega}_6$	698489.6372	668362.3884	4.51	679909.3135	644125.8394	5.55
ED1	$\hat{\omega}_1$	74105.8979	73720.9288	0.52	172.9563	171.8841	0.62
	$\hat{\omega}_2$	196021.3374	194876.7410	0.59	7847.5058	7804.4814	0.55
	$\hat{\omega}_3$	266337.1465	259635.8978	2.58	10754.1390	10509.0805	2.33
	$\hat{\omega}_4$	375608.2780	375555.5069	0.01	320488.1367	320487.2236	0.00
	$\hat{\omega}_5$	479222.7800	478536.3310	0.14	330641.1352	330640.2137	0.00
	$\hat{\omega}_6$	700380.4385	669973.6977	4.54	679914.7177	644130.7562	5.55

$\Delta\% = |\frac{\hat{\omega}_{coupled} - \hat{\omega}_{uncoupled}}{\hat{\omega}_{uncoupled}}| \times 100$

Table 5.17: Coupling effect on the first six natural frequencies $\hat{\omega} = \omega/100$ with EDZ theories for the simply-supported hybrid sandwich plate with $a/h = 4$ and $a/h = 100$

		$a/h = 4$			$a/h = 100$		
		coupled (SC)	uncoupled	$\Delta\%$	coupled (SC)	uncoupled	$\Delta\%$
EDZ4	$\hat{\omega}_1$	57585.0247	56004.1835	2.82	155.3103	146.8172	5.78
	$\hat{\omega}_2$	194140.7846	193045.5801	0.57	9028.1864	7798.5358	15.77
	$\hat{\omega}_3$	254705.2324	250278.9961	1.77	11422.7968	10476.8747	9.03
	$\hat{\omega}_4$	279406.4871	276872.5801	0.91	99733.4355	211511.4983	52.85
	$\hat{\omega}_5$	368997.2431	361485.9774	2.08	99733.4355	215775.6740	53.78
	$\hat{\omega}_6$	386098.4398	386590.2057	0.13	211527.0479	384883.3594	45.04
EDZ3	$\hat{\omega}_1$	57656.7172	56185.1779	2.62	155.3285	147.0212	5.65
	$\hat{\omega}_2$	195710.5652	194566.6773	0.59	7843.5789	7798.6434	0.58
	$\hat{\omega}_3$	259570.1855	254146.8380	2.13	10749.3416	10477.0948	2.60
	$\hat{\omega}_4$	279713.6605	277078.0626	0.95	211527.6590	211511.6725	0.01
	$\hat{\omega}_5$	369974.2928	361938.8579	2.22	215791.9741	215775.7522	0.01
	$\hat{\omega}_6$	390746.6533	388737.7370	0.52	386107.4111	384911.6749	0.31
EDZ2	$\hat{\omega}_1$	60605.4801	59073.6908	2.59	155.3707	147.0597	5.65
	$\hat{\omega}_2$	195965.3819	194594.9664	0.70	7846.8424	7803.9407	0.55
	$\hat{\omega}_3$	266196.0204	254975.9700	4.40	10749.3468	10478.3042	2.59
	$\hat{\omega}_4$	293428.0734	290390.6244	1.05	221516.9683	221499.8172	0.01
	$\hat{\omega}_5$	404987.5286	395729.7279	2.34	261492.5647	261478.8186	0.00
	$\hat{\omega}_6$	455520.7908	436929.2236	4.25	429558.9614	428945.3271	0.14
EDZ1	$\hat{\omega}_1$	63198.5291	63030.6094	0.27	172.8467	171.7729	0.62
	$\hat{\omega}_2$	195965.2576	194876.7406	0.56	7846.8536	7803.9538	0.55
	$\hat{\omega}_3$	266195.2458	259606.4802	2.54	10749.5892	10478.5173	2.59
	$\hat{\omega}_4$	298704.5651	298461.1021	0.08	221557.5866	221555.2405	0.00
	$\hat{\omega}_5$	427699.8535	426409.5804	0.30	261525.0359	261523.1462	0.00
	$\hat{\omega}_6$	455511.7257	455468.4938	0.01	429599.0590	428984.4909	0.14

$\Delta\% = |\frac{\hat{\omega}_{coupled} - \hat{\omega}_{uncoupled}}{\hat{\omega}_{uncoupled}}| \times 100$

Table 5.18: Coupling effect on the first six natural frequencies $\hat{\omega} = \omega/100$ with LD theories for the simply-supported hybrid sandwich plate with $a/h = 4$ and $a/h = 100$

		$a/h = 4$			$a/h = 100$		
		coupled (SC)	uncoupled	$\Delta\%$	coupled (SC)	uncoupled	$\Delta\%$
LD4	$\hat{\omega}_1$	57073.9526	55514.7764	2.81	155.2848	146.6802	5.87
	$\hat{\omega}_2$	191300.9503	189939.4848	0.72	7841.7120	7795.9804	0.59
	$\hat{\omega}_3$	250767.4547	246834.0821	1.59	10748.8484	10476.1621	2.60
	$\hat{\omega}_4$	274940.3877	272676.7516	0.83	208921.5919	208910.6773	0.00
	$\hat{\omega}_5$	362489.0079	355350.7482	2.01	209855.3115	209837.2685	0.01
	$\hat{\omega}_6$	381035.5811	379190.1485	0.49	378390.2280	378350.7473	0.01
LD3	$\hat{\omega}_1$	57073.9648	55514.7915	2.81	155.2848	146.6801	5.87
	$\hat{\omega}_2$	191301.0900	189939.6207	0.72	7841.7120	7795.9804	0.59
	$\hat{\omega}_3$	250768.1797	246834.6942	1.59	10748.8484	10476.1621	2.60
	$\hat{\omega}_4$	274942.1262	272678.4240	0.83	208921.6976	208910.7823	0.00
	$\hat{\omega}_5$	362491.9799	355352.7720	2.01	209855.6885	209837.6459	0.01
	$\hat{\omega}_6$	381037.3775	379192.1675	0.49	378390.6738	378351.1914	0.01
LD2	$\hat{\omega}_1$	57081.8463	55523.8953	2.80	155.2849	146.6802	5.87
	$\hat{\omega}_2$	191311.0629	189949.2767	0.72	7841.7120	7795.9804	0.59
	$\hat{\omega}_3$	250785.8261	246848.8669	1.59	10748.8484	10476.1621	2.60
	$\hat{\omega}_4$	275060.2670	272794.5064	0.83	209006.0233	208995.1025	0.00
	$\hat{\omega}_5$	362881.5767	355708.8005	2.02	209937.3849	209919.3148	0.01
	$\hat{\omega}_6$	381322.1808	379503.0350	0.48	378532.6039	378492.6851	0.01
LD1	$\hat{\omega}_1$	57252.4975	55754.8334	2.69	155.5084	146.9533	5.82
	$\hat{\omega}_2$	194839.5803	193420.5759	0.73	7841.9461	7796.2128	0.59
	$\hat{\omega}_3$	255646.0517	251327.1948	1.72	10749.0796	10476.3759	2.60
	$\hat{\omega}_4$	282167.4738	279928.7532	0.80	211932.0962	211919.3192	0.01
	$\hat{\omega}_5$	368457.5514	359977.4902	2.35	214106.0242	214088.2300	0.01
	$\hat{\omega}_6$	389524.3101	388091.4042	0.37	385093.0154	385058.8333	0.01

$\Delta\% = \left|\frac{\hat{\omega}_{coupled} - \hat{\omega}_{uncoupled}}{\hat{\omega}_{uncoupled}}\right| \times 100$

5.2 Sandwich Hybrid CNT-RC piezoelectric plate

In this section free vibration analysis of square simply supported CNT-RC plate, embedded with piezoelectric layers (PZT-4) at the top and bottom of free surfaces, is carried out. Short-circuit surface conditions are considered for the potential in the electro-mechanical case ($\Phi_t = \Phi_b = 0$). Four different types of uniaxially aligned reinforcements are investigated in the analysis, including uniformly distributed UD-CNT and functinally graded (FG-X, FG-O and FG-V). Properties of single costituents of the composite CNT-RC plate are reported in Table 5.1. For all of the numerical examples proposed the material properties of the CNT-RC are those given by the extended Voigt's rule of mixtures Eq. 2.16 for the room temperature T = 300K, with the efficiency parameters η_1, η_2 and η_3 related to the CNT volume fraction indices V^*_{CNT} involved in the analysis [5]. Tables from 5.19 to 5.22 show solutions for the fundamental frequency parameter of simply supported and short-circuited hybrid CNT-RC piezoelectric plate by considering all the CNT distribution through the thickness and several values of the volume fraction indices $V^*_{CNT} = 0.11$, $V^*_{CNT} = 0.14$ and $V^*_{CNT} = 0.17$. The dimensionless eigen-frequency parameter is defined as $\hat{\omega} = (\omega a^2/h)\sqrt{\rho_m/E_m}$. The length to thickness ratio of the plate is set to $a/h = 20$ and two different thickness configurations are considered in the analysis $h_p : h_c : h_p = 0.1h : 0.8h : 0.1h$ and $h_p : h_c : h_p = 0.2h : 0.6h : 0.2h$, where h_p and h_c denote the thickness of piezoelectric layer and the thickness of CNT-RC core layer, respectively. Frequency parameters are computed by using different theories (ED and LD). The convergence study is carried out by comparing frequencies with respect to the results of Wu and Lin [17] and the relative errors are reported. Table 5.23 show the electro-mechanical coupling effect on the frequency parameters.

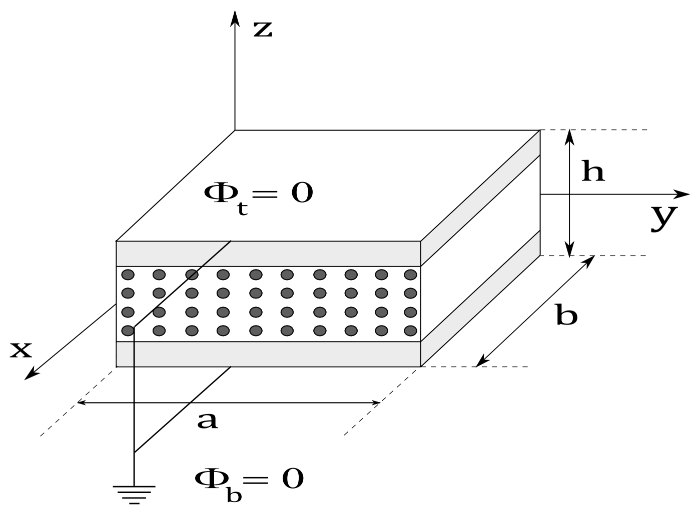

Figure 5.2: Hybrid sandwich plate [PZT-4/CNT-RC/PZT-4]

Table 5.19: ED solutions of frequency parameters for the simply supported sandwich [PZT-4/CNTRC/PZT-4] plates with different CNTs types, CNT voulme fraction V^*_{CNT}, length to thickness ratio $a/h = 20$, and $0.1\ h : 0.8\ h : 0.1\ h$

V^*_{CNT}	Theories	UD	FG-V	FG-O	FG-X
0.11	ED1	23.366974 (25.1284 %)	23.098914 (25.4892 %)	23.024593 (26.9160 %)	23.708535 (23.9954 %)
	ED2	21.1304 (13.1519 %)	20.8268 (13.1459 %)	20.7457 (14.3544 %)	21.5108 (12.5014 %)
	ED3	19.2028 (2.8299 %)	19.0302 (3.3447 %)	19.0227 (4.8985 %)	19.3658 (1.2833 %)
	ED4	19.1963 (2.7950 %)	19.0240 (3.3517 %)	19.0159 (4.8198 %)	19.3590 (1.2476 %)
	Wu and Lin [17]	18.6744	18.4071	18.1416	19.1205
0.14	ED1	23.7892 (25.0181 %)	23.4381 (25.4036 %)	23.3613 (27.0842 %)	24.2135 (23.8733 %)
	ED2	21.6113 (13.5732 %)	21.2157 (13.5129 %)	21.1327 (14.9604 %)	22.0823 (12.9703 %)
	ED3	19.5490 (2.7353 %)	19.3541 (3.5522 %)	19.3211 (5.1056 %)	19.7319 (0.9463 %)
	ED4	19.5422 (2.6991 %)	19.3475 (3.5173 %)	19.3136 (5.0651 %)	19.7246 (0.9091 %)
	Wu and Lin [17]	19.0286	18.6902	18.3826	19.5470
0.17	ED1	24.2837 (19.7350 %)	23.8597 (20.5411 %)	23.7786 (22.7416 %)	24.7839 (17.8885 %)
	ED2	22.1474 (9.2019 %)	21.6711 (9.4840 %)	21.5832 (11.4095 %)	22.7017 (7.9845 %)
	ED3	20.5786 (1.4665 %)	20.2963 (2.5386 %)	20.2620 (4.5897 %)	20.8453 (0.8461 %)
	ED4	20.5705 (1.4265 %)	20.2887 (2.5002 %)	20.2531 (4.5436 %)	20.8365 (0.8876 %)
	Wu and Lin [17]	20.2812	19.7939	19.3729	21.0232

$\Delta\% = |\frac{\hat{\omega}_i - \hat{\omega}_{Wu}}{\hat{\omega}_{Wu}}| \times 100$

Table 5.20: LD solutions of frequency parameters for the simply supported sandwich [PZT-4/CNTRC/PZT-4] plates with different CNTs types, length to thickness ratio $a/h = 20$, and CNT volume fraction $V^*_{CNT} = 0.11$

$V^*_{CNT} = 0.11$					
$h_p : h_c : h_p$	Theories	UD	FG-V	FG-O	FG-X
0.1 h : 0.8 h : 0.1 h	LD1	18.7800 (0.5660 %)	18.5255 (0.6434 %)	18.3132 (0.9461 %)	19.2095 (0.4655 %)
	LD2	18.7684 (0.5038 %)	18.5138 (0.5798 %)	18.3015 (0.8814 %)	19.1879 (0.3528 %)
	LD3	18.7684 (0.5038 %)	18.5076 (0.5461 %)	18.3015 (0.8814 %)	19.1879 (0.3528 %)
	LD4	18.7684 (0.5038 %)	18.5076 (0.5461 %)	18.3015 (0.8814%)	19.1879 (0.3528 %)
	Wu and Lin [17]	18.6744	18.4071	18.1416	19.1205
0.2 h : 0.6 h : 0.2 h	LD1	17.4244 (0.7285 %)	17.3847 (0.7611 %)	17.3135 (0.7403 %)	17.5347 (0.7824 %)
	LD2	17.3967 (0.5685 %)	17.3715 (0.6802 %)	17.3057 (0.6952 %)	17.4952 (0.5555 %)
	LD3	17.3967 (0.5685 %)	17.3607 (0.6225 %)	17.3001 (0.6626 %)	17.4902 (0.5269 %)
	LD4	17.3967 (0.5685 %)	17.3607 (0.6222 %)	17.3001 (0.6626 %)	17.4902 (0.5269 %)
	Wu and Lin [17]	17.2984	17.2534	17.1863	17.3986

$\Delta\% = |\frac{\hat{\omega}_i - \hat{\omega}_{Wu}}{\hat{\omega}_{Wu}}| \times 100$

Table 5.21: LD solutions of frequency parameters for the simply supported sandwich [PZT-4/CNTRC/PZT-4] plates with different CNTs types, length to thickness ratio $a/h = 20$, and CNT volume fraction $V^*_{CNT} = 0.14$

$V^*_{CNT} = 0.14$					
$h_p : h_c : h_p$	Theories	UD	FG-V	FG-O	FG-X
$0.1\ h : 0.8\ h : 0.1\ h$	LD1	19.1325 (0.5464 %)	18.8235 (0.7133 %)	18.5602 (0.9665 %)	19.6429 (0.4910 %)
	LD2	19.1159 (0.4590 %)	18.8009 (0.5925 %)	18.5549 (0.9374 %)	19.6234 (0.3913 %)
	LD3	19.1159 (0.4590 %)	18.8006 (0.5908 %)	18.5549 (0.9374 %)	19.6234 (0.3912 %)
	LD4	19.1159 (0.4590 %)	18.8006 (0.5908 %)	18.5549 (0.9374 %)	19.6234 (0.3912 %)
	Wu and Lin [17]	19.0286	18.6902	18.3826	19.5470
$0.2\ h : 0.6\ h : 0.2\ h$	LD1	17.5809 (0.7091 %)	17.5342 (0.7980 %)	17.4694 (0.8837 %)	17.7099 (0.7430 %)
	LD2	17.5622 (0.6019 %)	17.5122 (0.6717 %)	17.4574 (0.8144 %)	17.6808 (0.5779 %)
	LD3	17.5622 (0.6019 %)	17.5048 (0.6294 %)	17.4523 (0.7852 %)	17.6808 (0.5779 %)
	LD4	17.5622 (0.6019 %)	17.5048 (0.6291 %)	17.4523 (0.7852 %)	17.6808 (0.5779 %)
	Wu and Lin [17]	17.4572	17.3954	17.3164	17.5793

$\Delta\% = |\frac{\hat{\omega}_i - \hat{\omega}_{Wu}}{\hat{\omega}_{Wu}}| \times 100$

Table 5.22: LD solutions of frequency parameters for the simply supported sandwich [PZT-4/CNTRC/PZT-4] plates with different CNTs types, length to thickness ratio $a/h = 20$, and CNT volume fraction $V^*_{CNT} = 0.17$

$V^*_{CNT} = 0.17$					
$h_p : h_c : h_p$	Theories	UD	FG-V	FG-O	FG-X
0.1 h : 0.8 h : 0.1 h	LD1	20.3409 (0.2945 %)	19.8762 (0.4162 %)	19.5019 (0.6661 %)	21.1202 (0.4616 %)
	LD2	20.3301 (0.2414 %)	19.8664 (0.3664 %)	19.4977 (0.6446 %)	21.1052 (0.3903 %)
	LD3	20.3301 (0.2414 %)	19.8662 (0.3656 %)	19.4977 (0.6446 %)	21.1052 (0.3903 %)
	LD4	20.3301 (0.2414 %)	19.8662 (0.3656 %)	19.4977 (0.6446 %)	21.1052 (0.3903 %)
	Wu and Lin [17]	20.2812	19.7939	19.3729	21.0232
0.2 h : 0.6 h : 0.2 h	LD1	18.5712 (0.5495 %)	18.4709 (0.5628 %)	18.3973 (0.8308 %)	18.7701 (0.5472 %)
	LD2	18.5537 (0.4545 %)	18.4549 (0.4754 %)	18.3895 (0.7877 %)	18.7412 (0.3926 %)
	LD3	18.5537 (0.4545 %)	18.4427 (0.4090 %)	18.3857 (0.7668 %)	18.7412 (0.3925 %)
	LD4	18.5537 (0.4545 %)	18.4426 (0.4088 %)	18.3857 (0.7668 %)	18.7412 (0.3925 %)
	Wu and Lin [17]	18.4698	18.3676	18.2458	18.6680

$\Delta\% = |\frac{\hat{\omega}_i - \hat{\omega}_{Wu}}{\hat{\omega}_{Wu}}| \times 100$

Table 5.23: Coupled and Uncoupled solutions of frequency parameters for the simply supported sandwich [PZT-4/CNTRC/PZT-4] plates with different CNTs types, length to thickness ratio $a/h = 20$, and CNT volume fraction

V^*_{CNT}	$h_p : h_c : h_p$	CNTs Type	coupled (SC)	uncoupled	Δ%
0.11	0.1 h : 0.8 h : 0.1 h	UD	18.7684	17.8517	5.1351
		FG-V	18.5076	17.5742	5.3110
		FG-O	18.3015	17.3465	5.5053
		FG-X	19.1879	18.3183	4.7472
0.11	0.2 h : 0.6 h : 0.2 h	UD	17.396744	16.440726	5.8149
		FG-V	17.3607	16.3729	6.0329
		FG-O	17.3001	16.2853	6.2313
		FG-X	17.4902	16.6123	5.2848
0.14	0.1 h : 0.8 h : 0.1 h	UD	19.1159	18.2192	4.9217
		FG-V	18.8006	17.8870	5.1072
		FG-O	18.5549	17.6215	5.2967
		FG-X	19.6234	18.7721	4.5351
0.14	0.2 h : 0.6 h : 0.2 h	UD	17.5622	16.6302	5.6042
		FG-V	17.5048	16.5428	5.8156
		FG-O	17.4523	16.4622	6.0142
		FG-X	17.6808	16.8286	5.0642
0.17	0.1 h : 0.8 h : 0.1 h	UD	20.3302	19.4142	4.7177
		FG-V	19.8663	18.9353	4.9167
		FG-O	19.4978	18.5507	5.1055
		FG-X	21.1053	20.2249	4.3527
0.17	0.2 h : 0.6 h : 0.2 h	UD	18.5537	17.6029	5.4012
		FG-V	18.4426	17.4633	5.6082
		FG-O	18.3857	17.3770	5.8048
		FG-X	18.7412	17.8743	4.8503

$\Delta\% = |\frac{\hat{\omega}_{coupled}-\hat{\omega}_{uncoupled}}{\hat{\omega}_{uncoupled}}| \times 100$

Chapter 6

Results: Dynamic Response and Active Control

6.1 Dynamic Response and Active Control

In this section the dynamic response of a simply supported piezoelectric FG-CNTRC square plate with $a = b = 20\,m$, is analyzed. The thickness of CNT-RC core layer is $h_c = 0.8\,m$, while the thickness for each piezoceramic layer is $h_p = 0.1\,m$. The material properties of the plate are given the same as those in Table 5.1. Piezoelectric sensors and actuators are used to investigate the active vibration control of the plate. In vibration control analysis, the upper piezoelectric layer acts as actuators, while the lower one acts as sensors. The response of the plate is controlled using the dynamic velocity feedback control algorithm and a close loop. Four different types of uniaxially aligned reinforcements are investigated in the analysis, including uniformly distributed UD-CNT and functinally graded (FG-X, FG-O and FG-V). Two load cases are considered in this work. The plate is subjected to an harmonic load $F = F_0 \sin(\Omega t)$ and to an impulsive load F_0 which is suddenly removed, placed in the mid-point. The structural damping ratio for each mode is assumed to be 0.8 % according with [19]. The mechanical deflection u_z is evaluated in the mid-point of the plate.

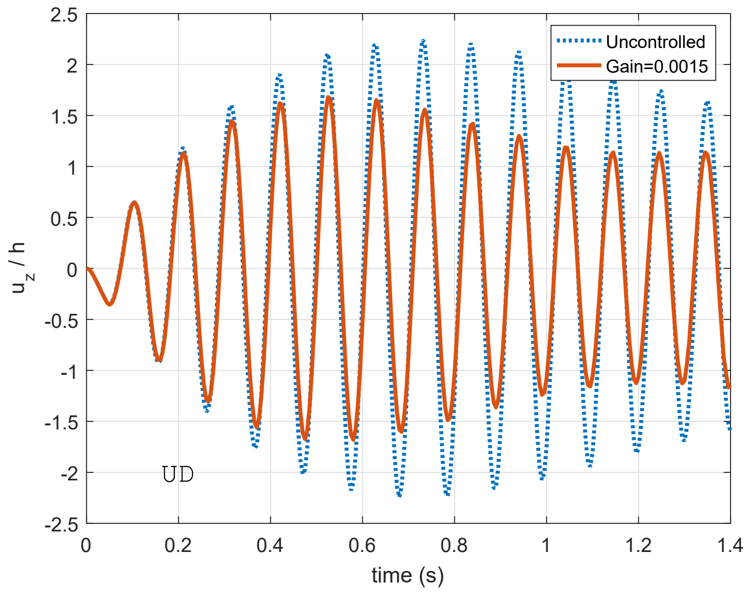

Figure 6.1: Forced response of the piezoelectric laminated UD-CNTRC plate with $G_v = 1.5 \times 10^{-3}$ for the case $V^*_{CNT} = 0.11$

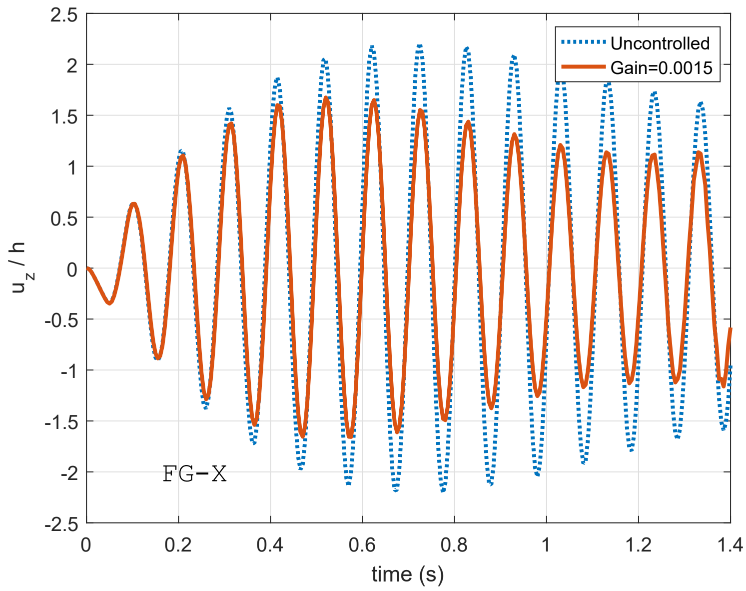

Figure 6.2: Forced response of the piezoelectric laminated FG-X plate with $G_v = 1.5 \times 10^{-3}$ for the case $V^*_{CNT} = 0.11$

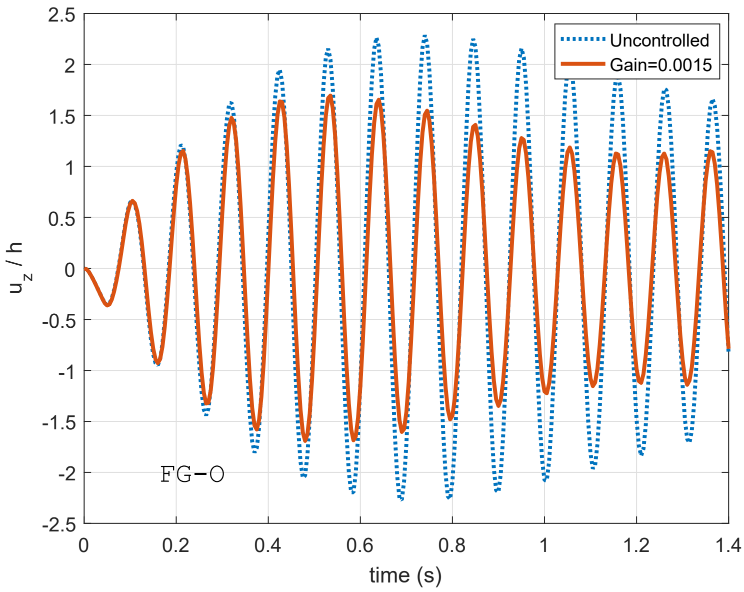

Figure 6.3: Forced response of the piezoelectric laminated FG-O plate with $G_v = 1.5 \times 10^{-3}$ for the case $V^*_{CNT} = 0.11$

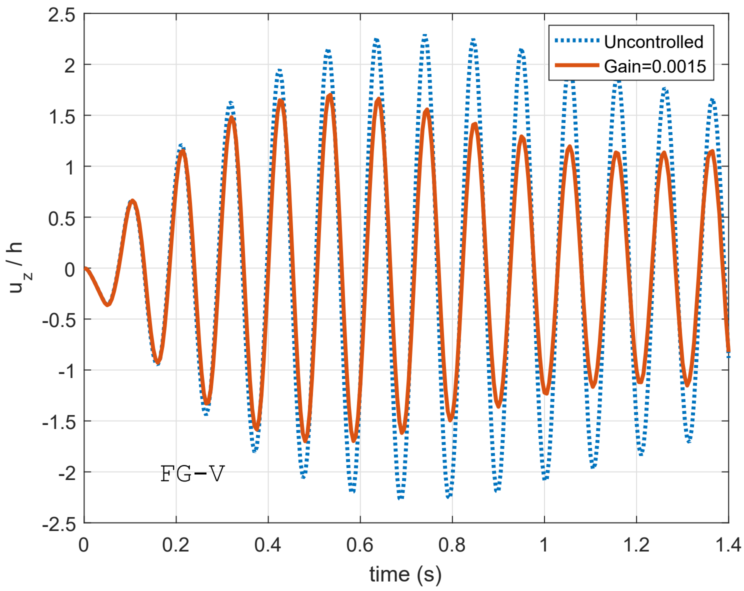

Figure 6.4: Forced response of the piezoelectric laminated FG-V plate with $G_v = 1.5 \times 10^{-3}$ for the case $V^*_{CNT} = 0.11$

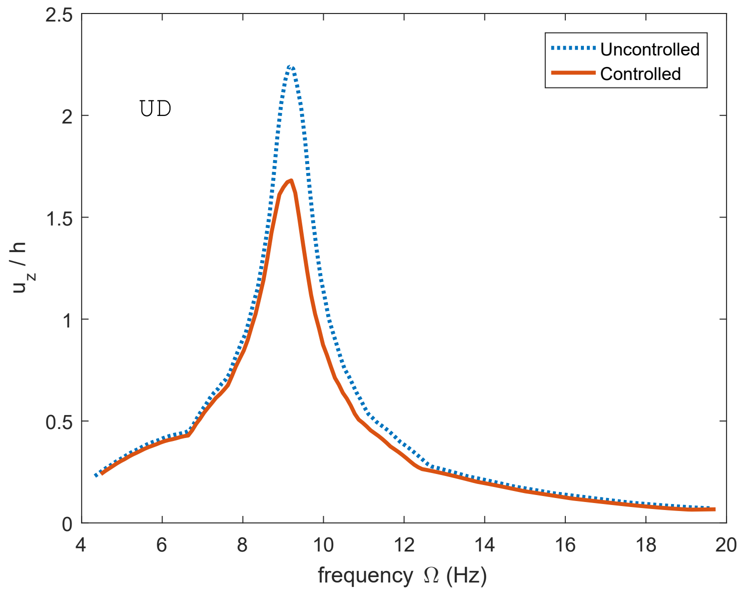

Figure 6.5: Dynamic deflection of the piezoelectric laminated UD-CNTRC plate for the case $V^*_{CNT} = 0.11$

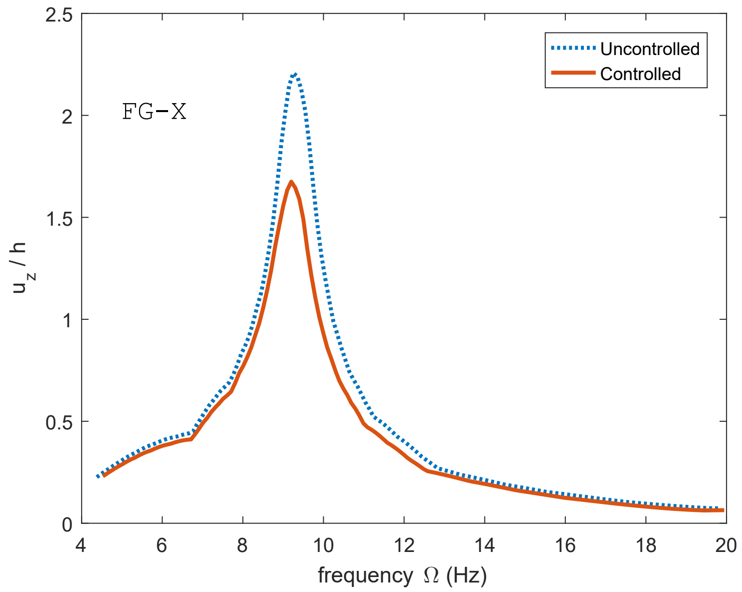

Figure 6.6: Dynamic deflection of the piezoelectric laminated FG-X plate for the case $V^*_{CNT} = 0.11$

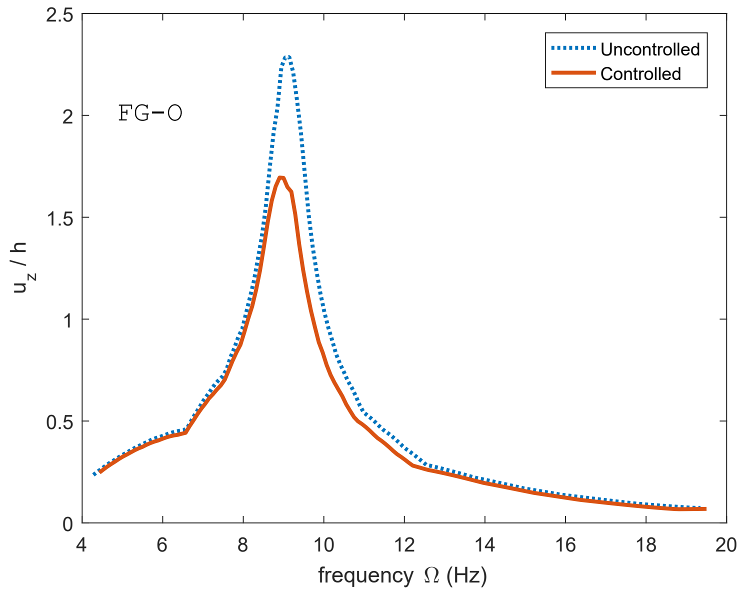

Figure 6.7: Dynamic deflection of the piezoelectric laminated FG-O plate for the case $V^*_{CNT} = 0.11$

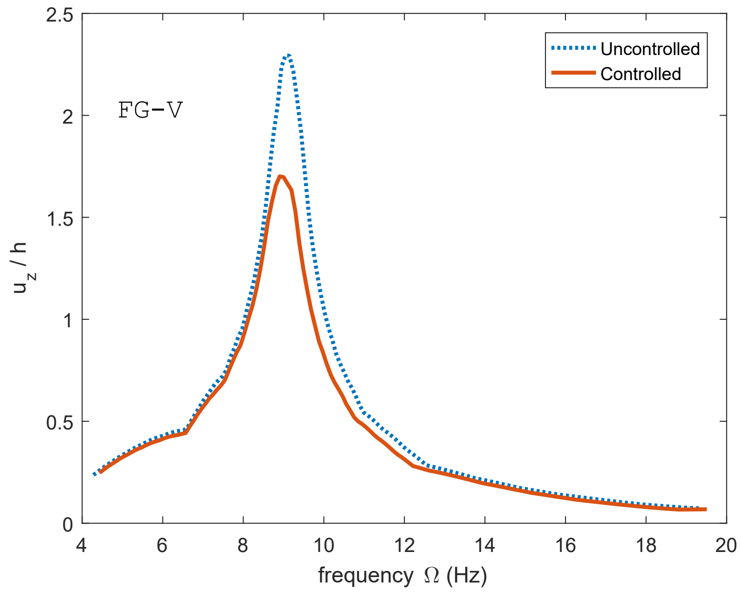

Figure 6.8: Dynamic deflection of the piezoelectric laminated FG-V plate for the case $V^*_{CNT} = 0.11$

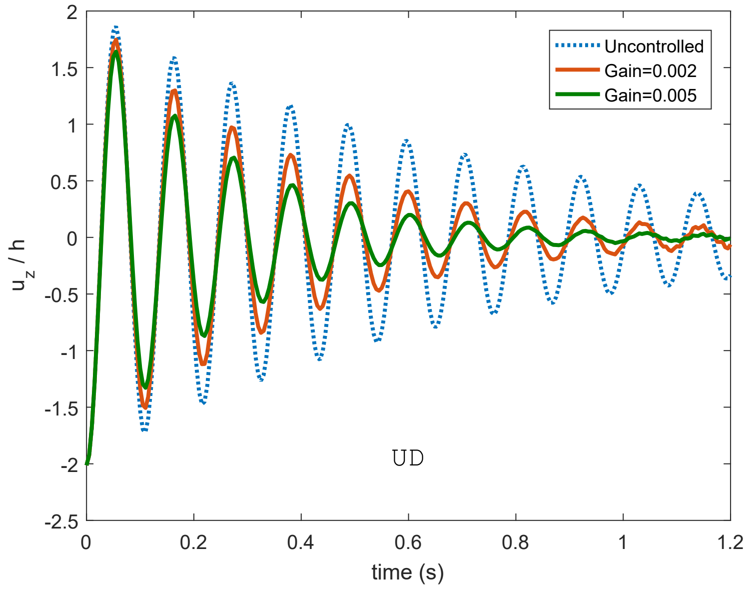

Figure 6.9: Effect of the velocity feedback control gain G_v on the dynamic response of the simply supported UD-CNTRC plate

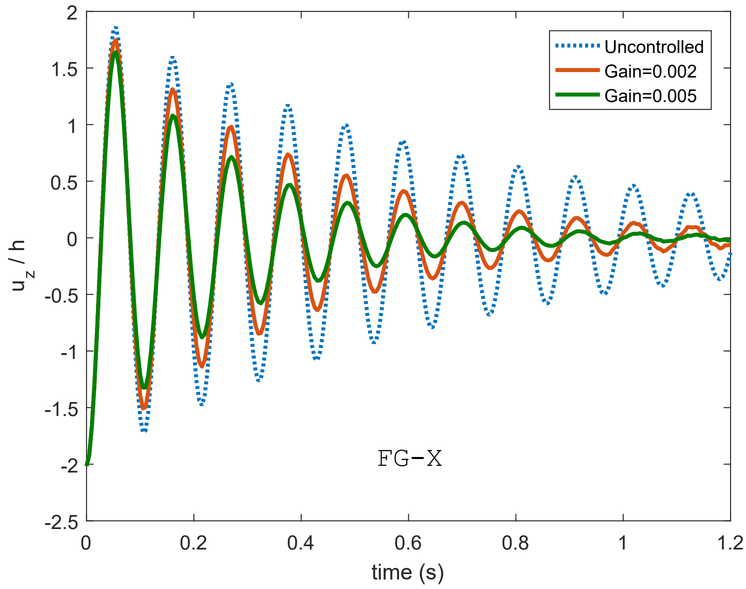

Figure 6.10: Effect of the velocity feedback control gain G_v on the dynamic response of the simply supported FG-X plate

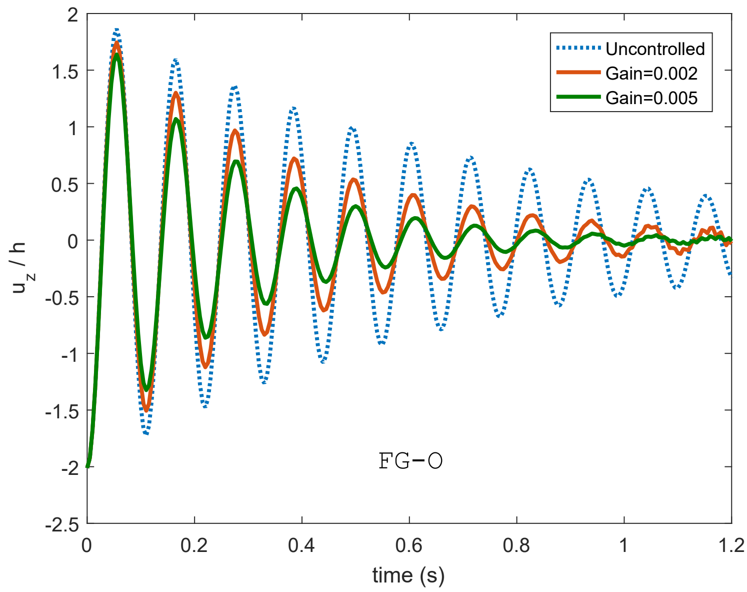

Figure 6.11: Effect of the velocity feedback control gain G_v on the dynamic response of the simply supported FG-O plate

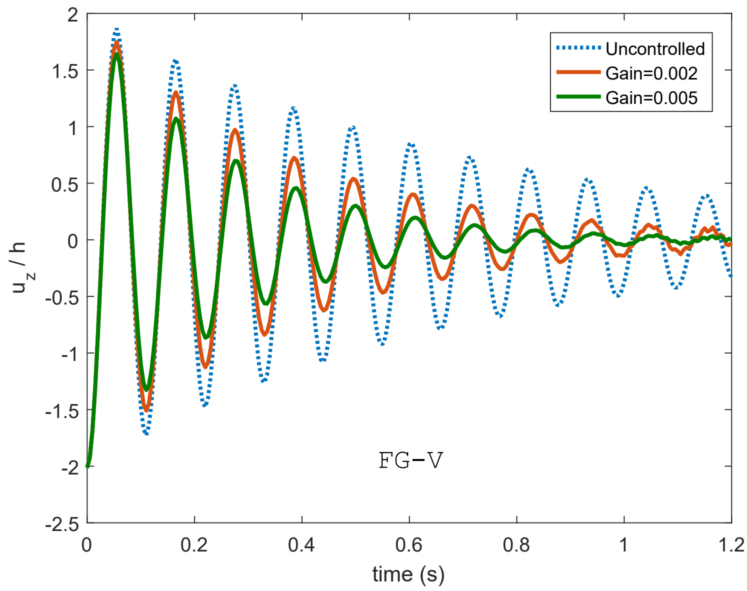

Figure 6.12: Effect of the velocity feedback control gain G_v on the dynamic response of the simply supported FG-V plate

Chapter 7

Conclusions: Numerical Results and Discussion

7.1 Free Vibration Results

7.1.1 Laminated Orthotropic plate

Tables 5.2-5.10 show the first six natural frequencies of a square laminated orthotropic piezoelectric plate, as discussed in section 5.1. The analysis are performed with all the thoeries. The expansion orders N_ϕ, N_{u_z} and N_{u_x} are consider totally indipendent in order to investigate the convergence to the exact solution. As can be observed, N_ϕ do not affect the rate of convergence to the exact solutions. Besides, dealing with ED theories, when the expansion order N_u overcomes the potential expansion order $N_\phi = 4$ the solution stability is compromised. Tables 5.14-5.15 provide a convergence study on the first six natural frequencies with length to thickness ratios $a/h = 4, 50$. As expected, the LDN theories produce the best results. The ESL models with imposed zig-zag form EDZN lead in the most cases to a slight improvement compared to the EDN theories. More specifically, LD3 and LD4 theories lead to the exact solutions while ED4 and EDZ3 lead to an Average error $\Delta\%$ of less than 2.5 % when the plate is thick ($a/h = 4$). Furthermore for LD theories, an increase of the expansion order has a very small effect. On the contrary ED theories are more sensible to the expansion order, especially when the plate is thick.

7.1.2 FG-CNTRC Piezoelectric plate

Convergence assessment and validation

As widely introduced in section 5.2, a convergence assessment of the models for the free vibration of a simply supported square CNT-RC piezoelectric plate is presented in Tables 5.19-5.22. It is clear that the LDN theories achieve the best level of accurancy and are in excellent agreement with the results of [17]. More specifically, the analysis performed with the LD4 theory leads to an error $\Delta\%$ on natural frequency parameter of less than 1%. On the other hand, the analysis performed with the ED4 theory leads to an average error of 3 %.

Parametric study

Table 5.23 provides the parametric study, carried out to evaluate the influences of distribution pattern of CNT reinforcements, volume fraction of CNT and thickness configurations of the sandwich CNT-RC piezoelectric plate as well as the electro-mechanical coupling effect. The parametric study is performed by using the LD4 theory. As can be seen by comparing the four different types of CNT distributions through the thickness, the magnitude order of the frequency parameters is: FG-X > UD > FG-V > FG-O-type. This order highlights the fact that the CNT reinforcements are more efficient when are distributed far from the mid-surface, enanching the overall stiffness of the CNT-RC plate. In all the cases, increasing the CNT volume fraction V^*_{CNT} results in higher frequency parameter due to the enanchement of the stiffness of the plate. On the contrary, reducing the core thickness of the CNT-RC leads to a lower value of the frequency parameter, as expected. It is worth mentioning the electro-mechanical coupling effect by comparing the frequency parameter for the electro-mechanical case with the pure mechanical case. In general, the frequency parameters, which is a flexural mode, for the coupled case result higher than those of the uncoupled case. This phenomenon is compatible with all the results obtained in literature [18], [19] and [14]. In fact for the coupled case, due to the direct piezoelectric effect, when the plate oscillates, the electrical energy is converted to mechanical energy and the piezoelectric coupling matrix can be consider as an additional stiffness for the plate. Besides, when the mechanical stiffness of the plate is higher, the direct piezoelectric effect results in a lower electro-mechanical coupling in accordance with [14]. This trend can be seen by comparing the two thickness configurations of the sandwich plate. Increasing the thickness of the piezoelectric layers results in decreasing of the overall stiffness of the plate. Then, the natural frequency increment Δ, due to the direct piezoelectric effect, is more evident in thicker piezoelectric layers (case $h_p : h_c : h_p = 0.2h : 0.6h : 0.2h$). Instead it is observed that the higher CNT volume fraction leads to an higher stifness of the plate which results in lower value of the increment Δ. In particular, the FG-X CNT-RC plate with $V^*_{CNT} = 0.17$ which results the stiffest plate, shows the lowest value of Δ.

7.2 Dynamic vibration control of FG-CNTRC Piezoelectric plate

Figures from 6.9 to 6.12, show the effect of the velocity feedback gain G_v on the transient response of the mid-point for all CNT distributions. As can be seen, when the control system is inoperative ($G_v = 0$), the response decreases with respect to time due to the only structural damping effect. The decay of the response is faster when the Gain factor G_v increases and the control system results stable, as expected. In fact, the stability of the system is ensured by the active damping matrix which results always definite positive. Figures from 6.1 to 6.8, show dynamic forced response of the mid-point of the plate. It can be seen that the amplitude of the center point deflection of the plate is reduced due to the active damping effect. Furthermore the graphs reflect the resonance phenomena of the plate, as expected when the plate is subjected to an armonic load.

Overall the vibration of the plate can be properly controlled and suppressed by using the velocity feedback control algorithm based on a closed loop and the Gain factor can be adeguately designed in order to satisfy constrains on the dynamic oscillations.

7.3 Future works

Dynamic analysis of CNT-Reinforced composite plate embedded with single piezoelectric patches at the top and bottom of free surfaces could be consider as a possible extension of this work. The analysis could be carried out in order to investigate how the placement of the patches affects the vibration control results and to find the optimal positions to suppress and control the first modes of the structure. A further possible extension could be place the piezoelectric sensor and actuator layers at the same side of the plate in order to evaluate the stability and the effectiveness of the control system [14]. FKurtheremore two additional layers of FGMs (Al/Al_2O_3) could be integrated at the top and bottom of the plate to enanche thermal resistance of the structure.

Bibliography

[1] C. Soutis. *Fibre reinforced composites in aircraft construction*, Progress in Aerospace Sciences 41 (2005) 143–151.

[2] J.N. Reddy. *Mechanics of laminated composite plates and shells*, CRC press (2004) Chapter 1.

[3] Erasmo Carrera, Salvatore Brischetto and Pietro Nali. *Plates and Shells for Smart Structures Classical and Advanced Theories for Modeling and Analysis*, Chapter 1.

[4] A.Y.N. Sofla, S.A. Meguid, K.T. Tan, W.K. Yeo. *Shape morphing of aircraft wing: Status and challenges*, Materials and Design 31 (2010) 1284–1292.

[5] Fiorenzo A. Fazzolari. *Thermoelastic Vibration and Stability of Temperature-Dependent Carbon Nanotube-Reinforced Composite Plates*, Composite structures (2018).

[6] Min-Feng Yu1, Oleg Lourie1, Mark J. Dyer, Katerina Moloni, Thomas F. Kelly, Rodney S. Ruoff1. *Strength and Breaking Mechanism of Multiwalled Carbon Nanotubes Under Tensile Load*, Science 28 Jan 2000: Vol. 287, Issue 5453, pp. 637-640.

[7] Gururaja Udupa,S.Shrikantha Rao, S.V. Gangadharan. *Functionally graded Composite materials: An overview*, Procedia Materials Science 5 (2014) 1291 – 1299.

[8] Fiorenzo A.Fazzolari. *Sandwich Structures*, Stability and Vibrations of Thin Walled Composite Structures 2017, Pages 49-90.

[9] M.M. Shahzamanian, B.B. Sahari, M. Bayat, F. Mustapha and Z. N. Ismarrubie1. *Elastic Contact Analysis of Functionally Graded Brake Disks Subjected to Thermal and Mechanical Loads*, International Journal for Computational Methods in Engineering Science and Mechanics, 14:10–23, 2013.

[10] Farhad Abad, Jafar Rouzegar.*An exact spectral element method for free vibration analysis of FG plate integrated with piezoelectric layers*, Composite Structures 180 (2017) 696–708.

[11] Fayaz R. Rofooei Ali Nikkhoo. *Application of active piezoelectric patches in controlling the dynamic response of a thin rectangular plate under a moving mass*, International Journal of Solids and Structures 46 (2009) 2429–2443.

[12] F. Moleiroa, A.L. Araújoa, J.N. Reddy. *Benchmark exact free vibration solutions for multilayered piezoelectric composite plates*, Composite Structures 182 (2017) 598–605.

[13] Zhu Su, Guoyong Jin, Tiangui Ye. *Electro-mechanical vibration characteristics of functionally graded piezoelectric plates with general boundary conditions*, International Journal of Mechanical Sciences, (2018) 42-53.

[14] B.A. Selim, L.W. Zhang and K.M. Liew. *Active vibration control of CNT-reinforced composite plates with piezoelectric layers based on Reddy's higher-order shear deformation theory*, Composite Structures 163 (2017) 350-364.

[15] A. Robaldo, E. Carrera and A. Benjeddou. *A unified formulation for finite element analysis of piezoelectric adaptive plates*,Computers and Structures 84 (2006) 1494–1505.

[16] D. Ballhause, M. D'Ottavio, B. Kroplin, E. Carrera. *A unified formulation to assess multilayered theories for piezoelectric plates*, Computers and Structures 83 (2005) 1217–1235.

[17] Chih-Ping, Wu and Hong-Ru Lin. *Three-dimensional dynamic responses of carbon nanotube–reinforced composite plates with surface-bonded piezoelectric layers using Reissner's mixed variational theorem–based finite layer methods*, Journal of Intelligent Material Systems and Structures 2015, Vol. 26(3) 260–279.

[18] *Free vibration of functionally graded carbon nanotube reinforced composite plates integrated with piezoelectric layers*, Computers and Mathematics with Applications 72 (2016) 2433–2449.

[19] K. Nguyen-Quang, T. Vo-Duy, H. Dang-Trung, T. Nguyen-Thoi. *An isogeometric approach for dynamic response of laminated FG-CNT reinforced composite plates integrated with piezoelectric layers*, Comput. Methods Appl. Mech. Engrg. 332 (2018) 25–46.

[20] S. Y. Wang, S. T. Quek, K. K. Ang. *Vibration control of smart piezoelectric composite plates*, Smart Mater. Struct. 10 (2001) 637–644.

[21] X.Q. He, T.Y. Ng, S. Sivashanker, K.M. Liew. *Active control of FGM plates with integrated piezoelectric sensors and actuators*, International Journal of Solids and Structures 38 (2001) 1641-1655.

[22] Erasmo Carrera, Fiorenzo A. Fazzolari, Maria Cinefra. *Thermal stress analysis of composite beams, plates and shells*, cap.6, page 221.

[23] Hui-Shen Shen Zhen-Xin Wang. *Assessment of Voigt and Mori–Tanaka models for vibration analysis of functionally graded plates*, Composite Structures 94 (2012) 2197–2208

[24] Y.M. Ghugal and R.P. Shimpi.
A Review of Refined Shear Deformation Theories of Isotropic and Anisotropic Laminated Plates, Journal of Reinforced Plastics and Composites, Vol. 21, No. 9/2002.

[25] Erasmo Carrera, Fiorenzo A. Fazzolari, Maria Cinefra. *Thermal stress analysis of composite beams, plates and shells*, cap.4, page 97.

[26] J.N. Reddy. *Mechanics of laminated composite plates and shells*, CRC press (2004) Chapter 11 pag. 271.

[27] E. Carrera. *Historical review of Zig-Zag theories for multilayered plates and shells*, Appl Mech Rev 2003 56(3) 287–308.

[28] H. Murakami. *Laminated composite plate theory with improved in-plane responses*, Journal of Applied Mechanics, 53, 661-666, 1986.

[29] J.N. Reddy. *Mechanics of laminated composite plates and shells*, CRC press (2004) Chapter 12 pag. 730.

[30] Fiorenzo A. Fazzolari, Erasmo Carrera. *Accurate free vibration analysis of thermo-mechanically pre/post-buckled anisotropic multilayered plates based on a refined hierarchical trigonometric Ritz formulation*, Composite Structures 95 (2013) 381–402.

[31] Fiorenzo A. Fazzolari. *Natural frequencies and critical temperatures of functionally graded sandwich plates subjected to uniform and non-uniform temperature distributions*, Composite Structures Volume 121, March 2015, Pages 197-210.

[32] Fiorenzo A. Fazzolari, Erasmo Carrera. *Coupled thermoelastic effect in free vibration analysis of anisotropic multilayered plates and FGM plates by using a variable-kinematics Ritz formulation*, European Journal of Mechanics A/Solids 44 (2014) 157-174.

[33] Fiorenzo A. Fazzolari. *A refined dynamic stiffness element for free vibration analysis of cross-ply laminated composite cylindrical and spherical shallow shells*, Composites Part B: Engineering Volume 62, June 2014, Pages 143-158.

[34] Fiorenzo A. Fazzolari, Erasmo Carrera. *Free vibration analysis of sandwich plates with anisotropic face sheets in thermal environment by using the hierarchical trigonometric Ritz formulation*, Composites Part B: Engineering Volume 50, July 2013, Pages 67-81.

[35] I. Chowdhury, S.P. Dasgupta. *Computation of Rayleigh damping coefficients for large systems*, Electron, J. Geotech. Eng. 8 (2003).